# EXPERIMENTAL AND NUMERICAL STUDIES IN SELF-COMPACTING CONCRETE

Firas Badry

Ph.D. 2015

# EXPERIMENTAL AND NUMERICAL STUDIES IN SELF-COMPACTING CONCRETE

Firas Badry

B.Sc., M.Sc.

Submitted for the degree of

Doctor of Philosophy


School of Engineering

Cardiff University, UK

October 2015

*In the Name of God*

*The Most Compassionate and the Most Merciful*

# DECLARATION

This work has not previously been accepted in substance for any degree and is not concurrently submitted in candidature for any degree.

Signed…… (candidate)

Date……

## STATEMENT 1

This thesis is being submitted in partial fulfilment of the requirements for the degree of Doctor of Philosophy.

Signed……(candidate)

Date……

## STATEMENT 2

This thesis is the result of my own independent work/investigations, except where otherwise stated. Other sources are acknowledged by explicit references.

Signed……(candidate)

Date……

## STATEMENT 3

I hereby give consent for my thesis, if accepted, to be made available for photocopying and for inter-library loan, and for the title and summary to be made available to outside organisations.

Signed……(candidate)

Date……

# ACKNOWLEDGEMENT

I want to take this opportunity to express my immeasurable appreciation and deepest gratitude for the help and support extended to me by all those who gave me the chance to accomplish this thesis.

My deepest gratitude is to my supervisor, Professor B.L. Karihaloo. It has been an honour to be his Ph.D. student. I appreciate his support, advice, guidance, valuable comments, suggestions and provisions that benefited me much in completion and success of this study. Sharing his knowledge helped in numerical computations and analysis of the results. Without his help I could not have finished my dissertation successfully.

Also I would like to thank my co-supervisor Dr S. Kulasegaram who has been always helpful. I am deeply grateful to him for valuable discussions we had during my research project.

Further gratitude and appreciation is expressed to my country, **Iraq** (Ministry of Higher Education and Scientific Research/Ministry of Construction and Housing) for funding my study and giving me this opportunity.

Warm and special thanks are expressed to my parents and my wife for their support and patience during the preparation of this research.

## SYNOPSIS

This thesis describes the steps taken to develop normal strength (30-80 MPa) self-compacting concrete mixes with 20mm maximum size aggregate. For the self-compacting concrete mixes with 20mm maximum size of aggregate fulfilment of the flow and cohesiveness criteria are found insufficient for the mix design. It is found that they must additionally meet the passing ability criterion.

A Lagrangian particle based method, the smooth particle hydrodynamics (SPH), is used to simulate the flow of SCC mixes. An incompressible SPH method is employed to simulate the flow of such non-Newtonian fluids whose behaviour is described by a Bingham-type model, in which the kink in the shear stress versus shear strain rate diagram is first appropriately smoothed out. The basic equations solved in the SPH are the incompressible mass conservation and Navier-Stokes equations.

The yield stress of SCC mixes is predicted in an inverse manner using the SPH simulation methodology and matching the measured and simulated $t_{500}$, $t_{stop}$ and the final spread of the cone flow test. It is found that the yield stress of SCC mixes varies only slightly with an increase in the characteristic compressive strength of the mix. The plastic viscosity on the other hand shows a marked increase. The latter was estimated by a micromechanical procedure proposed by Ghanbari & Karihaloo (2009) based on the measured viscosity of the cement paste alone and on the volume fractions of the mix constituents.

The SPH simulation methodology was also used for predicting the distribution of large coarse aggregates in the cone spread. This distribution was found to be indeed very similar to that revealed in the cut sections of the hardened test cone spread. These large coarse aggregates had been painted with non-toxic non-water soluble paints prior to being used in the test mix.

The simulation of SCC mixes revealed that the cone lift rate in the slump flow test has a significant effect on the flow pattern and the measured $t_{500}$. The latter decreases as the cone lift rate increases from 0.1 to 1 m/s. The effect on the spread (i.e. $t_{stop}$) is, however, insignificant.

# TABLE OF CONTENTS

# LIST OF FIGURES

# LIST OF TABLES

# Chapter 1

# Introduction

## 1.1. Scope of the research

Concrete has achieved great importance as structural material in the last century; it has been widely used as a construction material with the advantages of strength, durability, resistance to fire, cost-effectiveness and on-site fabrication. The properties of hardened concrete depend on its properties in the fresh state. In practice, concrete that can be readily placed into formwork is referred to as workable. Among the most important properties of fresh concrete is ‘‘workability’’; it generally refers to the consistency, flow-ability, pump-ability, compact-ability, and passing-ability of a mix. However, the required external energy (i.e. vibration) to compact the mix depends on the workability of the mix. With the increased use of heavily reinforced and/or complex shaped concrete elements there is a growing need for decrease in production time with no increase in man power, providing adequate compaction of such abnormal elements can be difficult with the restricted access for vibrators. For that reason self-compacting concrete (SCC) was developed.

Self-compacting concrete, a new category of high-performance concrete with excellent deformability and segregation resistance, was first developed in Japan in 1988. The necessity of this type of concrete was proposed by Okamura in 1986. Self-Compacting Concrete (SCC), also referred to as ‘‘Self-Consolidating Concrete’’, has recently been one of the most important developments in the building industry because of its very attractive properties in the fresh state as well as after hardening. The use of SCC will lead to a more industrialised production, reduce the technical costs of in-situ cast concrete construction, improve the quality, durability and reliability of concrete structures and eliminate some of the potential for human error.

Self-compacting concrete should flow through and fill the gaps in heavy reinforcement and corners of formwork without any need for vibration and compaction. In addition, it

should have the ability to flow around obstacles while maintaining good suspension of coarse particles in the matrix (no segregation), thus avoiding arching near obstacles and blockage during flow. In other words, self-compacting concrete mixes should have high fluidity, passing ability and appropriate level of homogeneity (segregation resistance). Self-compacting concrete, just as normal concrete, contains particles of different sizes and specific gravity (heterogeneous). The high fluidity of SCC mixes can cause instability of its constituents, if the mixes do not have enough cohesiveness. Therefore it is important to control the volume fractions of the constituents. In the last two decades, self-compacting concrete with its special properties is becoming an attractive alternative to normal vibrated concrete.

Cement paste characteristics and the volume fractions of the mix constituents have a major influence on the properties of the SCC in both the fresh and hardened states, for instance on workability, strength and durability. Because flow-ability is a main attribute of SCC, the accurate prediction and control of its rheology is crucial for its successful production.

The accurate prediction of the essential rheological characteristics of SCC provides a useful tool to model the flow and to understand the flow behaviour in the fresh state. The flow of SCC is best described by a Bingham-type constitutive model. This model contains two material properties, namely the yield stress ($\tau_y$) and plastic viscosity ($\eta$). The yield stress of all SCC mixes is low in comparison with normal vibrated concrete and changes only marginally over a wide range of plastic viscosities. The plastic viscosity of a homogeneous cement paste can be measured accurately by using viscometers but after adding coarse aggregate to the paste the results obtained by using rheometers usually fluctuate and do not follow any trend due to the heterogeneous

nature of the mix. It is thus necessary to use alternative theoretical methods to predict the plastic viscosity of a heterogeneous SCC mix.

The accurate prediction and control of the flowing behaviour, and the homogeneity (coarse aggregate distribution) of an SCC mix are very important to ensure the quality of the final product. The most cost-effective way to fully understand and assess this behaviour is by carrying out numerical simulations, and comparing them with experiments. The plastic viscosity of an SCC mix is first predicted accurately by a micromechanical procedure, whereas its yield stress is back calculated by matching simulations with experiments. The numerical simulation of the flow is also used to track the distribution of coarse aggregate particles during flow and to assess the effect of cone lift rate (CLR) on the flow pattern and the results recorded in the slump flow test.

## 1.2. Research objectives

- To produce a wide range of normal strength self-compacting concrete (SCC) mixes with a maximum aggregate size (g) of 20 mm ranging in cube compressive strength from 30 to 80 MPa .The mixes should have good flow-ability, passing ability and cohesiveness without segregation.
- To record accurately the time $t_{500}$ (the time when the mix spread reaches 500mm), and spread of each mix in the slump flow test.
- To predict the plastic viscosity of the developed SCC mixes using the micromechanical procedure depending on the plastic viscosity of the paste and the volume fractions of the ingredients.
- To simulate the entire cone flow test from the moment the cone was lifted until the mix stopped to flow using the three dimensional mesh-less Smoothed Particle Hydrodynamics (SPH) computational approach, treating the SCC mix as a non-Newtonian Bingham fluid.

- To investigate whether the yield stress $\tau_y$ of the mix can be accurately estimated from the measured $t_{500}$ and spread knowing the plastic viscosity of the mix.
- To compare the distribution of coarse aggregate particles in the cone spread after it stopped to flow as revealed by the numerical simulation with the distribution of the coarse aggregate particles of the corresponding sizes in the cut sections of the cured test cone spread.
- To investigate the effect of the cone lift rate (CLR) on the flow pattern and $t_{500}$ in the slump flow test.

## 1.3. Research methodology

To achieve the above objectives research was undertaken in five stages:

- Firstly, self-compacting concrete (SCC) mixes with a maximum size of aggregate 20 mm of varying strengths are developed to meet the flow-ability, passing ability and segregation resistance criteria. The design of SCC mixes followed the mix proportioning method proposed by Deeb and Karihaloo (2013) and the traditional trial-and-error approach, starting from vibrated concrete mixes that had been tested in the same laboratory. The flow-ability, passing ability and segregation resistance for each mix were checked using the slump cone, J-Ring and L-box tests. All mixes had no visible signs of segregation. In the slump cone test times ($t_{500}$, $t_{stop}$), spread and cone lift rate (CLR) for each mix were recorded for later use.
- Secondly, the plastic viscosity of the SCC mixes is estimated from the known plastic viscosity of the cement paste. For this, concrete was regarded as a two-phase suspension of solid and liquid phases. The liquid matrix phase consisted of cement paste i.e. cement and cement replacement material, water and super-plasticiser or viscosity modifying agent (VMA) if it was used. The plastic

viscosity of the homogeneous paste can be accurately measured. The increase in the plastic viscosity of the paste due to the addition of a solid phase (filler, fine and coarse aggregates) to this paste is predicted from a two-phase model. The model is applied in several stages until all ingredients of SCC have been accounted for.

- Thirdly, the entire cone flow test is then simulated from the moment the cone was lifted until the mix stopped to flow using the three dimensional Lagrangian particle-based technique, the so-called smoothed particle hydrodynamics (SPH) computational approach, treating the SCC mix as a non-Newtonian Bingham fluid. The basic equations solved in the SPH are the incompressible mass conservation and Navier-Stokes equations. The yield stress $\tau_y$ of the mix is accurately estimated from the measured $t_{500}$ time and spread knowing the plastic viscosity of the mix. The plastic viscosity of the SCC needed for this simulation is predicted by a micromechanical procedure, as mentioned above.
- Fourthly, the 3D simulations of SCC are focused on tracking the distribution of large aggregates ($8 \leq g < 12$, $12 \leq g < 16$, $16 \leq g < 20$ and $g \geq 20$ mm) during the flow. This distribution was found indeed to be very similar to that revealed in the cut sections of the hardened test cone spread. The large coarse aggregates had been painted with non-toxic non-water soluble paints prior to being used in the test mix.
- Fifthly, the SPH simulation technique is used to investigate the effect of the cone lift rate on the flow pattern and $t_{500}$ in slump flow test.

## 1.4. Outline of the thesis

The contents of this thesis are organised into eight chapters, followed by bibliographical references. For clarity of presentation, each chapter is divided into sections and sub-sections, as required. A brief overview of the contents of various chapters follows.

**Chapter 2** gives a general overview of SCC for instance its basic properties, materials used in its production with their influence on its characteristics in the fresh and hardened states and a review of workability tests on the fresh SCC. Also some practical examples of structures made with SCC are presented.

**Chapter 3** gives a brief review of the rheology of self-compacting concrete. Different methods used for simulating the flow of SCC which are available in the literature are reviewed. An overview of smooth particle hydrodynamic approach, its concept, particle interpolation, kernel functions, density and gradient evaluation are presented together with a corrected particle interpolation formulation. The three-dimensional Lagrangian form of the governing equations of flow used to model the flow of SCC namely, the mass and momentum conservation equations are described in the same chapter. Next to that the formulations relating to incompressible SPH and coupling of SPH formulation with a suitable Bingham-type model to represent the rheological behaviour of SCC are also presented in this Chapter.

**Chapter 4** describes the steps taken to develop self-compacting concrete mixes of varying strengths. In the design of such mixes, the flow-ability, good cohesiveness and passing ability criteria must be met. Times $t_{500}$, $t_{stop}$ and average spread diameter have been recorded in slump flow test for all developed mixes. The plastic viscosities of the SCC mixes so developed are then estimated by the micromechanical procedure.

**Chapter 5** describes the three-dimensional incompressible Lagrangian SPH method used to model all the developed mixes from the moment the cone is lifted until the mix stops to flow. This chapter is dedicated to investigating whether the yield stress $\tau_y$ of the mixes can be accurately back calculated from the measured $t_{500}$ and spread knowing the plastic viscosity of the mix.

**Chapter 6** describes the simulations of SCC mixes focussing on the distribution of large aggregates ($8 \leq g < 12$, $12 \leq g < 16$, $16 \leq g < 20$ and $g \geq 20$ mm) during the flow. The numerical results are shown to be in very good agreement with experimental results made in the laboratory with the corresponding sizes of colour coded coarse aggregate.

**Chapter 7** describes the simulation of the flow of self-compacting concrete mixes for different cone lift rates (CLR) ranging from 0.1 to 1.0 m/s to investigate the effect of the cone lift rate (CLR) on the flow pattern and $t_{500}$.

**Chapter 8** summarises the main conclusions on the basis of the research work embodied in Chapters 4 to 7. Recommendations for future research will be also made.

The thesis concludes with an alphabetical list of references to the works in the literature, cited in the text, and several appendices. Some of the work described in this thesis has been published or is in the process of publication, and has been presented at two Conferences. For easy reference, these publications are listed below.

1- Badry F, Kulasegaram S and Karihaloo B L, (2015). Estimation of the yield stress and distribution of large aggregates from slump flow test of self-compacting concrete mixes using smooth particle hydrodynamics simulation", *J Sustainable Cement-based Materials,* doi:10.1080/21650373.2014.979266 (in press)

2- Badry F, Kulasegaram S and Karihaloo B L, (2015). Effect of cone lift rate on the flow time of self-compacting concrete, *Magazine of Concrete Research*, doi:10.1680/macr.14.00379 (in press)

3- Karihaloo B L, Kulasegaram S and Badry F, (2015). On the accurate estimation of the rheological properties of self-compacting concrete, *J Chinese Ceramic Society,* 43(10), pp.1396-1400. doi: 10.14062/j.issn.0454-5648.2015.10.09 (in press)

4- Badry F, Karihaloo B L, Kulasegaram S, (2015). Simulation of the flow of non-Newtonian self-compacting concrete. The 23rd UK Conference of the Association for Computational Mechanics in Engineering 8 – 10 April 2015, Swansea University, Swansea,(ACME UK 2015).

5- Badry F, Karihaloo B L, Kulasegaram S, (2015). Simulation of the Flow of Non-Newtonian Self-Compacting Concrete. IV International conference on Particles-Based methods, Fundamentals and Applications, 28-30 September 2015, Barcelona, Spain, (PARTICLES 2015).

# Chapter 2

# Self-compacting concrete

## 2.1. Introduction

Concrete is one of the most important structural materials, and today it is difficult to find constructional design without using concrete. In the last two decades, concrete has no longer remained a material just consisting of cement, aggregates, and water, but it has become an engineered customised material with several new constituents to meet many varied requirements of the construction industry. Increasing population and modern cities demand new aspirant structural design ideas and increase the demands on reinforced concrete structures. The shapes and sections of elements are becoming more complex as is the reinforcement which is becoming denser and clustered. The complex section shapes i.e. irregular or slender architectural members, heavy and closely spaced reinforcement raise problems of casting, compacting and filling the concrete element. Therefore, concrete produced for such members should be able to pass the dense rebar net without blocking or segregating. The design, production and quality control of such concrete is a big challenge. An inability to completely fill the formwork and non-efficient vibratory compaction (i.e. inclusion of irregularly distributed pockets of entrapped air voids or segregation) tends to cause durability issues for the concrete in the hardened state, and if this leads to chemical corrosion of reinforcement, can compromise strength, on top of the obvious aesthetic problems. This problem has been facing engineers for many years.

Self-compacting or self-consolidating concrete (SCC), a latest innovation in concrete technology is being regarded as one of the most promising developments in the construction industry due to its numerous advantages over conventional vibrated concrete. Self-compacting concrete is a modern concrete technology developed in Japan; it falls into the category of high performance concrete. It is getting more technical and economic attention due to the following advantages: assuring the project

quality, reducing noise, accelerating construction progress, improving construction environment and reducing project total cost. Self-compacting concrete in its fresh state exhibits a low resistance to flow to ensure high flow-ability, and a moderate viscosity to maintain a homogeneous deformation through restricted sections. Also, SCC can pass through congested reinforcing steel bars while compacting under its own weight without any external vibration. Such concrete can improve the homogeneity necessary to ensure good bond development with reinforcing steel, adequate structural performance, and improved durability.

Architectural designers have a good opportunity to show their creativity by exploiting the properties of SCC. In the past, they did not have such a freedom to select the shapes and sizes of elements. Complex shapes, larger span bridges, underwater structures, congested reinforced and slender members can be built with this highly promising material for the future of in-situ and pre-cast construction industries.

The SCC is a breakthrough in concrete technology and is now regarded as a good alternative to normal vibrated concrete. SCC was first used in Japan and made its European debut in Sweden in the 1990s. Now nearly all the countries in Europe conduct some form of research and development into this material. However the applications are still few and vibrated concrete is still considered as the standard concrete. As extensive research into SCC continues to gain a complete picture of its characteristics the confidence in using such concrete will undoubtedly increase.

In this Chapter, a general overview of the properties and applications of SCC will be given, highlighting the influence of materials used on its characteristics in both fresh and hardened states. Finally, the rheological properties and testing methods in the fresh state will be discussed.

## 2.2. History of development

In the eighties of the last century, the durability of concrete structures was a major topic of interest in Japan. Another topic worldwide was underwater concrete construction. Research in Japan, the UK, and North America led to the production of new concrete mixes with a high degree of washout resistance. Strength, durability and aesthetics of concrete elements after hardening still depended on the quantity and quality of vibration to which the mix was subjected to get adequate compaction by skilled workers. However, at the same time lack of the skilled construction workers required for standard vibrated concrete in Japan was leading to a reduction in the quality of construction work and durability. This, in turn, led to the development of SCC with the concept being first tried in Japan in the mid-1980s (Gaimster and Dixon, 2003; Okamura and Ouchi, 2003).

The first SCC mix was proposed by Okamura (1986) at Tokyo University, who also conducted a fundamental study on the workability of SCC. The first prototype of proportioning for SCC was completed in 1988, using the same constituent materials as used in standard vibrated concrete, the main purpose of SCC was to avoid vibrating the unreachable zones and to eliminate noise caused by vibration, besides shortening the construction time (Okamura and Ouchi, 2003).

This technology spread to Europe starting from Sweden to other Scandinavian countries at the end of the 1990s (Billberg, 1999). In Denmark, SCC has been used in significant amounts with an annual production reaching approximately 20% and 30% of the total concrete production in ready-mix and pre-cast industries, respectively (Thrane et al., 2004). Other countries, such as the UK, France and Germany, have also been developing and using the material. Moreover, in the beginning of the 21st century, the SCC started to be of interest in the USA (Ouchi et al., 2003). The ways of producing SCC are quite different in different countries depending on the traditions and available

materials. However, the current annual production of SCC indicates that challenges still need to be overcome, as SCC has a lower stability (segregation resistance) compared with vibrated concrete (Thrane et al., 2004).

Recently SCC has seen a spurt in its development as a result of the use of various materials such as pulverized-fuel ash (PFA), ground granulated blast furnace slag (GGBS), condensed silica fume (CSF), and fillers (e.g. limestone powder) but the main reason has been the development of new types of chemical additives (super-plasticizer, SP and viscosity modifying agents, VMA). Although the current overall production of SCC is still relatively small compared to conventional concrete (Gaimster and Dixon, 2003), the global gap is narrowing indicating that in the future there is likely to be an even greater demand for all types of SCC.

## 2.3. Self-compacting concrete: Definition

The British Standard (BS EN 206-9 2010) defines "SCC is the concrete that is able to flow and compact under its own weight, fill the formwork with its reinforcement, ducts, box-outs etc., whilst maintaining homogeneity".

Other researchers (Khayat et al., 1999; Bartos and Marrs, 1999) have defined SCC in almost the same terms as a highly flow-able concrete that should meet the following requirements:

- **Flow-ability**: SCC should have the ability to completely flow (horizontally and vertically upwards, if necessary) and fill all spaces in formwork without any external compaction.

- **Passing ability**: SCC should pass through heavy reinforcing steel bars without any blockage or/ nesting.

- **Segregation resistance:** SCC should remain homogeneous and cohesive without any separation of its heavy components (aggregates or/and fibres), throughout the entire construction process (mixing, transporting, handling, placing, casting, etc.).

## 2.4. Advantages and disadvantages of using SCC

The use of SCC on site offers many advantages (Naik et al., 2004):

- **Eliminating vibration and lower noise level:** There are environmental advantages as well, among these being the removal of noise from vibration, Figure 2.1. This is particularly relevant for the precast industry where for larger factories noise can be a considerable problem.

**Figure 2.1: Filling by SCC without vibration (www.concreteconstruction.net)**

- **Easy placement and filling:** The impressive filling ability, flow-ability and passing ability of SCC eases placement significantly even with very complex formwork shape and/or heavy reinforcement and eliminates honeycombing, blow holes and grout loss.

- **Better surface finish:** Better visual appearance, surfaces mostly free of voids, and lower variation of strength, Figure 2.2.

**Figure 2.2: Surface finish of Perham, MN tower using SCC with no repairs**

- **Reduced cost of skilled labour and construction time:** SCC can be placed at a faster rate without vibration resulting in reducing manpower and saving construction time.

- **Improved durability:** The structural durability is improved by using dense matrix of SCC that also improves bond with reinforcement.

- **Environmentally friendly production:** Fillers can be waste or recycled materials.

- **Safety of formwork:** With no vibrators used in casting, the loads imposed on the formworks are reduced.

Domone (2006) reviewed sixty-eight case studies of using self-compacting concrete (SCC) from 1993 to 2003, focussing on the reasons for using SCC instead of vibrated concrete VC. The result of this review was that:

- In 67% of the case studies, SCC was used because of its technical advantages in situations where vibration was either difficult or impossible due to the heavy reinforcement or inaccessibility;

- In 14% of the case studies, SCC was used for economic reasons as it saved costs on skilled labour and reduced construction time;

- In 10% of the case studies, SCC was used for new types of structure such as thin sections, pre-cast units and steel/concrete composites;

- In the remaining case studies, SCC was used to improve working conditions by reducing noise levels.

A possible disadvantage of using SCC compared with vibrated concrete is the unavoidable fluctuations in the property of raw materials. If the mix proportions cannot be adjusted in time, it is difficult to guarantee the quality of SCC (Ji et al., 2008). Moreover, due to the nature of SCC and high fluidity, handling and transporting of SCC become sensitive operations. In addition the high cost of some materials such as super-plasticiser which is only partly compensated by the low cost of labour.

Another major disadvantage of SCC is that there is a lack of globally agreed test standards and mix designs (Douglas, 2004). However, recent research results overcome this disadvantage, as will be described below.

## 2.5. Properties of self-compacting concrete in fresh state

### 2.5.1. Workability (flow ability and filling ability)

Workability is a way of describing the performance of concrete in the plastic state and for SCC it is refers to the ability of the mix to deform and undergo changes in shape with completely filling all areas and corners of the formwork horizontally and vertically, if needed while maintaining its homogeneity. Often workability is characterized by the following properties: filling ability, passing ability, and stability (segregation resistance). The workability of SCC is characterized by the fluidity and

cohesion of the mix, and is mainly assessed using the slump flow test described later in this chapter.

Kennedy (1940) proposed the 'Excess Paste Theory' to explain the mechanism governing the workability of concrete. He reported that the mixes should have enough paste to cover the surface area of the aggregate and excess paste to minimize the internal friction among the aggregates and to give better flow-ability. Without the paste layer, friction and interlock between the aggregates would be increase dramatically, and it would be impossible to achieve workability.

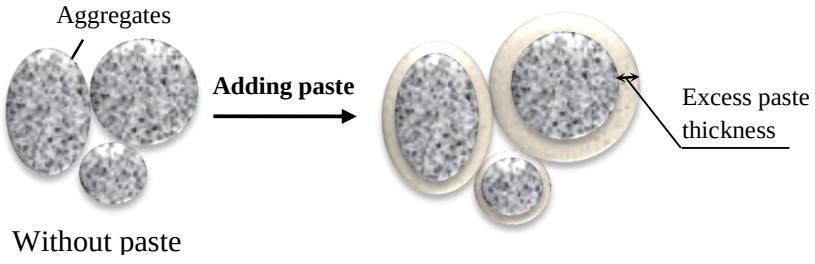


**Figure 2.3: Excess paste layer around aggregates (After: Oh et al., 1997)**

Figure 2.3 illustrates the action of layers of cement past around aggregates. Okamura recommends that the aggregate content should be reduced in order to avoid blockage (Okamura and Ouchi, 1999). The thickness of the paste layer would be best related to the diameter of the aggregates (Oh et al., 1997).

### 2.5.2. Passing ability

Passing ability refers to the ability of SCC mix to deform and pass through closely spaced reinforcement or obstacles without blocking, whilst maintaining good homogeneity, thus avoiding coarse aggregate arching, blockage and segregation during flow. The J-ring and L-box tests are the most common methods used to assess the passing ability of a SCC mix.

With an increase in the volume fraction, maximum size and irregularity in the shape of coarse aggregates, the expectation of blocking would increase. Moreover, the presence of fibres in self-compacting fibre reinforced concrete would make it more difficult to pass through gaps in the reinforcement.

Okamura and Ouchi (2003) reported that during flow of SCC the potential of collision and contact between particles increases as the distance between the particles decreases, resulting in an increase in the internal stresses when concrete is deformed, particularly near obstacles causing blockage. Research shows that the energy required for flowing is consumed by the increase of internal stresses. Limiting the coarse aggregate content whose energy consumption is high can effectively reduce the risk of blockage. Figure 2.4 shows how the normal stress could be generated due to the approach of coarse aggregate particles near obstacles.

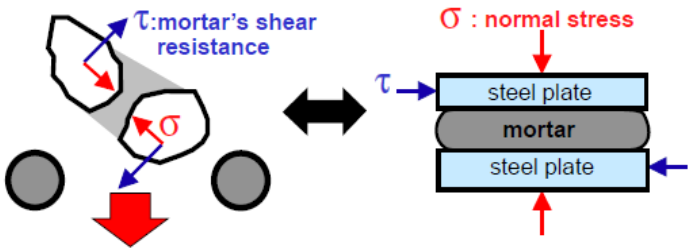


**Figure 2.4: Normal stress generated in mortar due to approaching coarse aggregate particles (After: Okamura and Ouchi, 2003)**

Using a highly viscous paste is another way to avoid the blockage of coarse aggregates during SCC flow throw obstacles by preventing localized increases in internal stress due to the approach of coarse aggregate particles, thus increasing the SCC passing ability (Okamura and Ouchi, 2003). Roussel et al. (2009) stated that a low viscosity cement paste and thus a very fluid SCC might be more prone to have its coarsest particles blocked in closely spaced reinforced zones. This is related to the instability of the material, and to the increase in the local volume fraction of coarse aggregates near an

obstacle because the material is not stable as shown in Figure 2.5; in this case, the material is too fluid to carry its own particles during the flow.

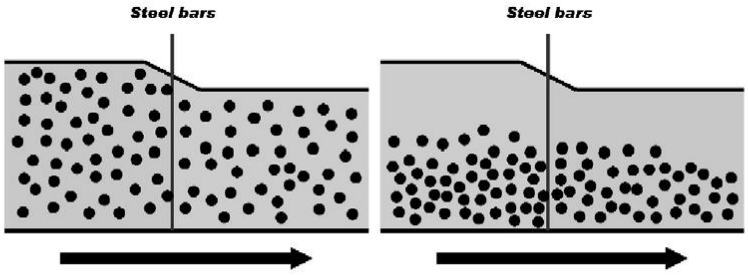


**Figure 2.5: Local increase of the aggregate volume fraction due to dynamic segregation. A low viscosity cement paste could increase the risk of blocking by allowing for a strong segregation within the material (After: Roussel et al., 2009)**

With reducing gaps between steel bars blocking possibility can be further increased. The spacing between bars is typically recommended to be 3 times the maximum aggregate size (EFNARC, 2005).

### 2.5.3. Segregation and bleeding resistance (homogeneity/cohesiveness)

Segregation resistance is the ability of SCC to remain uniform and cohesive throughout the entire construction process (mixing, transporting, handling, placing, casting and etc.). In other words, the coarse aggregates are suspended in the matrix and distributed homogeneously. Stability of a SCC is controlled by the cohesiveness of the mix and the viscosity of the concrete mix which can be increased by reducing the free water content and increasing the volume fraction of fines (Khayat et al., 1999).

Viscosity is the main factor controlling the segregation resistance and bleeding, therefore increasing the viscosity of a SCC mix could prevent segregation and/or bleeding. Bleeding is a special case of segregation due to the settlement of solid particles in which water moves upwards by capillary action and separates from the mix. A little bleeding is acceptable for concrete, but excessive bleeding can lead to a

decrease in strength, high porosity, and poor durability particularly at the surface (Douglas, 2004).

In order to prevent concrete bleeding or segregation, two simple methods can ensure adequate stability; the first tactic is based on using low w/c, high powder content, mineral admixtures, and low aggregate volume fraction and adjusting the workability by adding adequate amount of super-plasticiser (SP). The second approach involves a viscosity-modifying admixture (VMA), low or moderate powder content and super-plasticiser (Bonen et al., 2004). The first approach will used in Chapter 4 to optimise SCC mixes

## 2.6. Main differences between SCC and normal vibrated concrete

The composition of SCC is quite similar to conventional vibrated concrete. It consists of cement, aggregates, water and admixtures. However, the aggregate volume fractions are different. Coarse aggregate is less in content, and fine materials are large in content. Figure 2.6 shows visually the typical differences between the volume fractions of ingredients in self-compacting concrete (SCC) and standard vibrated concrete (VC).

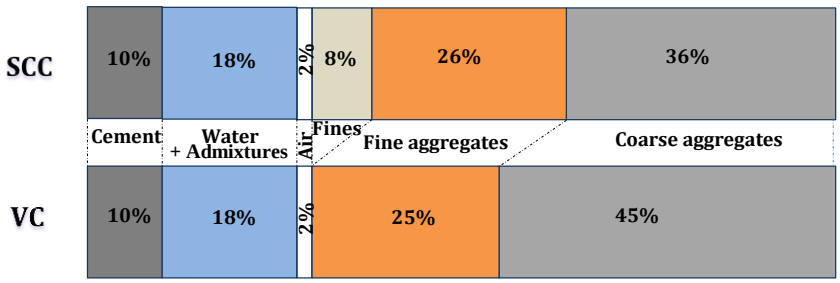


**Figure 2.6: Comparison between VC and SCC mixes (After: Okamura and Ouchi, 2003)**

Due to the material properties and the proportion of the dense matrix of SCC, the internal air bubbles liberate to the surface without any external vibration. High fluidity and moderate viscosity give the SCC its distinctive characteristics, passing ability

through and around heavy rebars without blockage and filling ability of any corners in the formwork without any segregation or bleeding. The impressive properties of SCC in the fresh state mostly lead to high strength, better bond with rebars and enhance the durability of concrete in the hardened state (Looney et al., 2012).

## 2.7. Proportioning of SCC mixes

In order to produce a SCC, concrete should have high fluidity and good cohesiveness without segregation or bleeding, in other words it must be as fluid as possible to fill areas and corners of the formwork, under its own weight and pass through closely spaced reinforcement without blockage or segregation. The method of proportioning the amounts of materials and admixtures is crucial to achieve these objectives. Okamura and Ouchi (2003) suggested three main rules to select SCC ingredients:

- Limiting aggregate content;
- Using super-plasticizer;
- Reducing water-powder ratio.

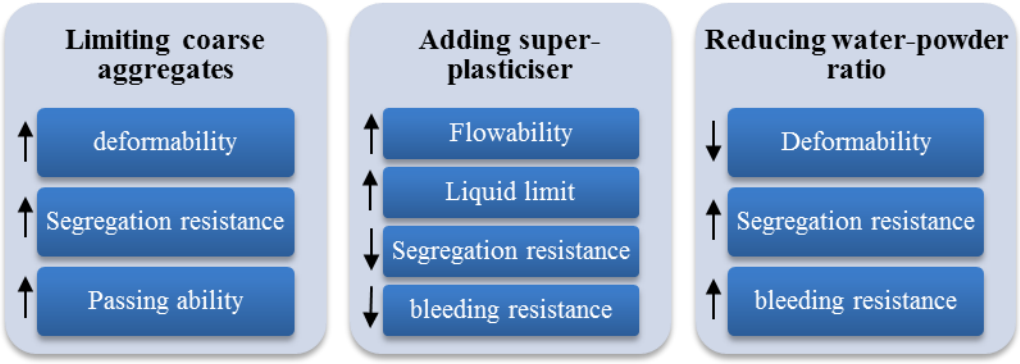


**Figure 2.7: Effect of each parameter on the SCC properties. ↑ Increases, ↓ decreases**

Figure 2.7 illustrates the influence of each parameter on the mechanism of achieving self-compatibility.

**Limiting aggregate content:** The flowing ability, the filling ability and passing ability of SCC mixes are restricted by the friction between the aggregates. By reducing the volume fraction and maximum size of coarse aggregates, and using smooth rounded aggregates instead of crushed ones, the above properties would be enhanced, thus improving the workability and optimizing the packing density of the skeleton. Rounded particles have been shown to achieve higher packing densities than crushed particles (Douglas, 2004). The effect of coarse aggregate on the rheology of SCC will be explained in section 2.14.2.

**High amount of super-plasticiser (SP)**: Using the optimum dose of SP gives the SCC mix high flow-ability and passing ability while maintaining the homogeneity at an acceptable level. The super-plasticiser disperses flocculated cement particles, by reducing the attractive forces and increasing the repulsion forces among them. A high amount of SP would result in segregation and a low amount would limit the fluidity. The overall performance of SCC is improved with a good degree of cohesiveness (Kwan and Ng, 2010). The effect of SP on the rheology of SCC will be explained in section 2.14.2.

**High paste volume:** the distinct property of SCC mixes compared with VC mixes is that they contain a high volume of paste to ensure aggregate separation (Tviksta, 2000). Okamura and Ouchi (2003) reported that the deformation of SCC during flow can increase the internal stresses, particularly near obstacles. The energy required for flowing is consumed by these excess internal stresses, which may cause blockage. However, a high viscosity paste prevents localized increases in internal stresses due to the approach of coarse aggregate particles. A high amount of fine particles leads to an increase in the workability and cohesiveness thus reducing the possibility of the interlocking of coarse particles which could result in a blocking behaviour (Khayat,

2000). Due to the necessity of a large amount of fine materials, cement replacement materials such as GGBS, silica fume, fly ash, etc. are usually used to increase the amount of fines, in order to avoid excessive heat generation. The effect of paste content on the rheology of SCC will be explained in section 2.14.2.

**Using Viscosity modifying agents (VMA):** These products are generally cellulose derivatives, polysaccharides or colloidal suspensions. The use of VMA gives the same effect as the fine particles in minimising bleeding and coarse aggregate segregation by thickening the paste and retaining the water in the skeleton. For normal strength SCC with high water to binder content, the introduction of such products seems to be justified. On the other hand, they may be less useful for high performance SCC with low water to binder ratio. Viscosity agents are assumed to make SCC less sensitive to water variations. Because of the small quantities of viscosity agents required, however, it may be difficult to achieve accuracy of dosage (Tviksta, 2000). VMA is used generally to enhance the stability of fluid concrete and to facilitate the casting of congested or restricted areas. The enhanced cohesiveness of such concrete can reduce structural defects resulting from increased porosity under aggregates and embedded reinforcement. This can lead to improved tensile strength, impermeability, and bond strength with reinforcement (Khayat, 1998).

## 2.8. SCC Mix design

There is no unique mix design solution for the production of SCC and a wide variety of methods have been used (Domone et al., 1999). Extensive research has been dedicated to achieve self-compatibility. Three methodologies of mix proportioning can be distinguished depending on the method of providing viscosity : "Powder- type" by increasing the powder content, "VMA-type" using viscosity modifying admixture (VMA) and "Combined- type" with a balance between increasing powder content and

using a viscosity agent depending on the constructional conditions, material availability, limitations of concrete production plant.

### 2.8.1. Powder-type SCC

This was the first proposed prototype. It is characterized by a high powder content and low water to powder ratio, in other words, improving the plastic viscosity by limiting the free water content and using a superplasticiser to provide flow-ability. Mixes in this type are sensitive to changes in the constituent materials because of high powder content. Okamura and Ozawa (1995) suggested a simple mix proportioning methodology for SCC mixes (Figure 2.8):

- Fix the coarse aggregate content at 50% of solid volume and the fine aggregate content at 40% of mortar volume;
- Depending on the properties of mortar, choose the water to powder ratio in the range of 0.9-1;
- The self compactability is achieved by adjusting the super-plasticiser dosage and the final water to powder ratio.

This Japanese method with a high paste content and relatively independent consideration of gravel and sand has been adopted and used in many European countries as a starting point for the development of SCC (Brouwers and Radix, 2005).

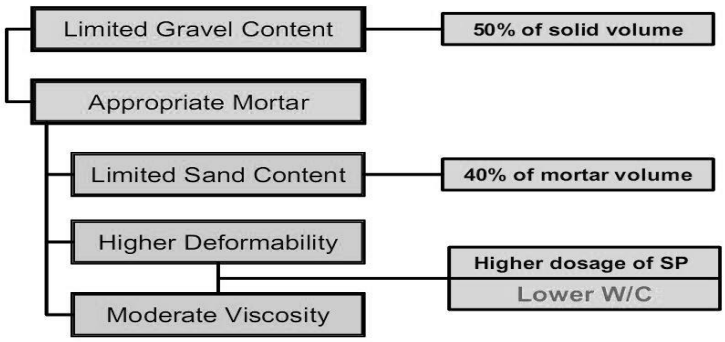


**Figure 2.8: A typical mix design of SCC (After: Ouchi et al., 1996)**

'The Chinese method' is an alternative method developed by Su and Miao (2003). This method can result in less paste and hence saving the most expensive constituents, namely cement and filler. Proportioning in this method starts with packing all coarse and fine aggregates, and then filling of the aggregate voids with paste. Concrete with normal strength can be obtained with this method, while in Japanese method a higher strength concrete can be attained (Brouwers and Radix, 2005).

### 2.8.2. VMA-type SCC

A high dosage of VMA is added to the mix of SCC to control and increase the plastic viscosity without increasing the powder content. A higher amount of super-plasticiser or higher water-powder ratio is required to achieve flow-ability compared with the powder-type method.

### 2.8.3. Combined-type SCC

A small amount of VMA is added to the powder-type SCC to develop and improve the robustness of the mix. In this type of mix proportioning, the VMA used is less compared with VMA-type SCC and the powder content and water to powder ratio are less than those in the powder-type SCC. The viscosity is provided by the VMA along with the powder. This type of SCC was reported to have high filling ability, high segregation resistance and improved robustness (Rozière et al., 2007).

### 2.8.4. Cardiff method of SCC mix proportioning

Recently a rigorous method for proportioning normal and high strength SCC mixes based on their plastic viscosity has been proposed by Karihaloo and Ghanbari (2012) and Deeb and Karihaloo (2013). It exploits the expression for the plastic viscosity of an SCC mix developed by Ghanbari and Karihaloo (2009) using micro-mechanical principles. This method produces a bewildering array of mixes that reach the target plastic viscosity, but does not give any practical guidelines on how to choose the most

appropriate mix, Moreover, the method was developed on the basis of reference mixes of a range of known cube compressive strength, but the latter was not explicitly imposed as a design criterion. Abo Dhaheer et al. (2015a, b) have overcome the above shortcomings of this method. Practical guidelines in the form of design charts have been provided for choosing the mix proportions that achieve the target plastic viscosity in the range of 3–15 Pa s, and the target cube compressive strength in the range of 30–80 MPa. This method will be explained in Chapter 4.

## 2.9. Cement replacement materials (CRMs)

High flow-ability and stability (segregation resistance) are the main distinct characteristics of SCC. They are attained by limiting the coarse aggregate volume fraction, the maximum aggregate size and reducing water-powder ratio together with the addition of super-plasticiser (SP) (Ouchi et al., 1998). However, for such a concrete to remain cohesive during the flow (mixing, transporting and placing), special attention has to be paid to mix proportioning. The increased flow-ability may cause segregation and bleeding which can be overcome usually by enhancing the viscosity of concrete mix. This is usually done by increasing the volume fraction of paste, by reducing the maximum aggregate size or by using viscosity modifying admixtures (VMA) (Khayat et al., 1999). However, chemical admixtures are expensive and may contribute to increasing the cost of concrete. On the other hand, including high powder content in a mix by using a high volume of cement has the disadvantage related to a higher temperature rise and shrinkage during hydration in addition to increase in SCC cost. Alternatively, a replacement of a proportion of cement with other materials is in certain circumstances desirable. Cement replacement materials (CRMs) are a better way to impart high workability to the mix by enhancement of particle distribution, cohesiveness and improvement of certain mechanical and rheological properties, as well

as reduction of the risk of thermal cracking, in addition to a reduction in the total cost of SCC. The CRMs or mineral admixtures as they are called are generally industrial by-products and have therefore economic and environmental benefits.

All CRMs have physical and chemical advantages; physical is the particle size is same or smaller than Portland cement particle and the chemical is their ability to exhibit pozzolanic behaviour and become a part in the hydration reactions. The main component of Pozzolans is silica ($SiO_2$) in a reactive form, which on its own has little or no cementitious value. However, using fine CRMs in the presence of moisture they will chemically react with calcium hydroxide at ordinary temperatures to form cementitious compounds (Domone and Illston, 2010; Lewis et al., 2003). The most common CRMs used are ground granulated blast furnace slag (GGBS), micro-silica or silica fume (SF) and pulverised fuel ash or fly ash (FA).

### 2.9.1. Ground granulated blast furnace slag (GGBS)

Ground granulated blast-furnace slag (Figure 2.9) is a by-product from the blast-furnaces for iron production. It is classified by EN 15167-1 and EN 15167-2 (or BS 6699) according to its level of reactivity. Many countries around the world have successfully used GGBS in many applications as a cement replacement material. As well as the obvious economic and environmental advantages of using what is essentially a recycled material, GGBS has appreciable advantages in terms of the hardened concrete finish and durability (Uysal and Yilmaz, 2011; Boukendakdji et al., 2012; Dinakar et al., 2013).

Using GGBS as a part of cement content in self-compacting concrete has many advantages related to increasing its compatibility, workability and durability, besides an increase in the resistance to sulphate and chloride attack (Roussel, 2007). The powder of GGBS has lower density than Portland cement; therefore replacing a part of cement by

GGBS will increase the paste volume, which subsequently increases the cohesiveness, deformability and segregation resistance.

**Figure 2.9: Ground granulated blast-furnace slag (GGBS)**

The smoother surface texture of the slag particles and slow rate of hydration compared to cement tend to lower the water demand in mixes having blended cement and GGBS than in mixes having cement only (Lewis et al., 2003). For SCC mixes GGBS has a positive effect on the workability, and from extensive experimental work, the results indicate that for SCC mixes containing GGBS, as GGBS content increases, water-to-binder ratio decreases for the same workability (Oner and Akyuz, 2007). GGBS blended concrete has lower strength at an early age but the strength increases as the curing period is extended, so that GGBS blended concrete will get to a higher strength than cement concrete only, the reason being that the slow pozzolanic reaction and that the formation of calcium hydroxide requires time (Figure 2.10).

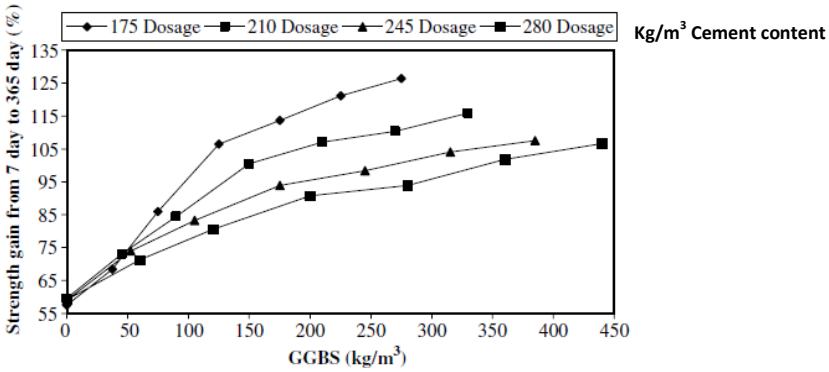


**Figure 2.10: Strength gain from 7 to 365 days in concrete containing GGBS (After: Oner and Akyuz, 2007)**

Depending on the desired properties, 50 per cent of cement mass in the mix can be replaced by GGBS (Ramachandran et al., 1981). Oner and Akyuz (2007) reported that the compressive strength of concrete mixes containing GGBS increases as the amount of GGBS increases, till an optimum limit at around 55% of the total binder content, the compressive strength does not improve with adding more of GGBS (Figure 2.11), which can be explained by the presence of unreacted GGBS, acting as a filler material in the paste. A high volume fraction of GGBS may affect the stability of SCC resulting in reduced robustness with problems of consistence control, while slower setting can also increase the risk of segregation (EFNARC, 2005).

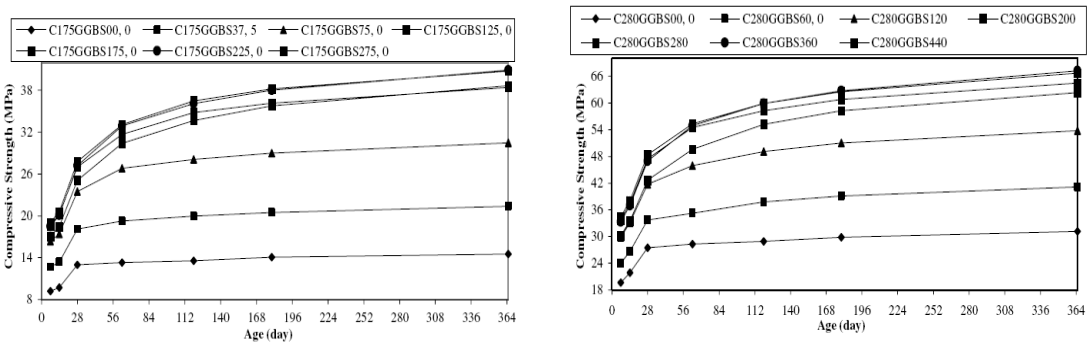


**Figure 2.11: Compressive strength development of 175 dosage cement (left) and 280 dosage (right) (After:Oner and Akyuz , 2007)**

### 2.9.2. Micro-silica or condensed silica fume (SF)

The general term micro-silica or trade names condensed silica fume and silica fume are often used to describe by-products extracted from the exhaust gases of ferrosilicon, silicon, and other metal alloy smelting furnaces. It is almost pure silica consisting primarily of amorphous (non-crystalline) silicon dioxide ($SiO_2$) powder. The very fine spherical particles or microspheres have a mean diameter about 0.15 microns. It is an additive that has become a feature of mix design for both high strength, and self-compacting concrete (Mehta, 1986).

Due to its significant fineness (Figure 2.12) when micro-silica is added to Portland cement concrete it improves its compressive strength, bond strength and abrasion resistance. It also significantly reduces the concrete permeability by blocking the capillary channels. Each microsphere is on average 100 times smaller than an average cement grain. Silica fume is a highly reactive pozzolan when used in concrete because of its fine particles, large surface area, and the high $SiO_2$ content. Standard specifications for micro-silica used in cementitious mixtures are given in ASTM C1240 and EN 13263.

**Figure 2.12: Micro-silica**

Silica fume performs two roles in concrete (Siddique and Khan, 2011) :

- **Pore-size refinement and matrix densification**: The presence of silica fume in the Portland cement concrete mixes causes considerable reduction in the volume of large pores at all ages. It basically acts as filler due to its fineness because of which it fits into the spaces between grains.

- **Pozzolanic reaction**: When Portland cement in concrete begins to react chemically, it releases calcium hydroxide (CH); these CH crystals are a source of weakness because cracks can easily propagate through or within these crystals without any significant resistance affecting the strength, durability and other properties of concrete. Silica fume reacts with this CH to form additional binder material called Calcium Silicate Hydrate (C-S-H) which is very similar to the Calcium Silicate Hydrate formed from Portland cement and water and therefore reduces the CH content.

Adding silica fume to concrete increases the cohesion and the yield stress (explained later) of a SCC mix, thus decreasing the slump flow in fresh state (Carlsward et al., 2003). As a result SCC containing silica fume is less prone to segregation and bleeding than concrete without silica fume. Rao (2003) reported that the workability of mortar slightly decreases as the silica fume content is increased. This is due to the higher specific surface of silica fume, which increases the water demand to complete hydration.

In the case of Portland cement, 18% micro-silica (by weight of cement) is theoretically enough for the total consumption of calcium hydroxide produced during the primary reaction of cement with water (Papadakis, 1999). However, as the small micro-silica particles also physically fill the pores, more than 25% micro-silica should be added to concrete to get the densest granular mixture (Richard and Cheyrezy, 1995).

Duval and Kadri (1998) have studied the influence of micro-silica blended with cement on some of the properties of fresh and hardened concretes. It was found that micro-silica increased the compressive strength at most by 25%, but the workability of concretes was best when its content was between 4 and 8%.

### 2.9.3. Fly ash (FA)

Fly ash (or pulverised fuel ash) is a by-product of coal-fired electricity generating plants. Fly ash (Figure 2.13) has pozzolanic properties; therefore, it can be used as a partial cement replacement in SCC.

According to the type of coal used in the power stations, there are two classes of fly ash, i.e. class C fly ash and class F fly ash.

The class C fly ash is produced from the burning of younger lignite or sub-bituminous coal. This class generally contains more than 20% lime (CaO). Conversely, the class F fly ash is obtained from the burning of harder, older anthracite and bituminous coal. This fly ash is pozzolanic in nature and contains less than 20% lime (CaO). The use of fly ash as a partial replacement for Portland cement is generally limited to Class F fly ash.

Fresh and hardened properties are generally improved when fly ash is used in SCC mixtures. It can replace up to 30% by mass of Portland cement increasing the strength, chemical resistance and durability of SCC. However, the rate of strength gain in concrete mixes containing fly ash is slower than in concretes made with only Portland cement.

**Figure 2.13: Fly ash (lab photograph)**

FA particles are mostly spherical in shape, therefore replacing a part of cement in SCC mix can improve its workability while reducing water demand (Koehler, 2007). Lachemi (2001) found that the use of fly ash and GGBS in SCC reduces the amount of super-plasticiser needed to obtain slump flow spread as compared with concrete made with Portland cement only. Shah and Modhera (2014) stated that an increase in fly ash from 30% to 70% leads to a high slump spread from 730 to 780 mm.

FA increases the compressive strength, improves durability and reduces drying and autogenous shrinkage of SCC (Obla et al., 2003).

Sonebi (2004) stated that the use of fly ash reduced the rheological properties of SCC, both the yield stress and plastic viscosity. However, Park et al. (2005) found that fly ash slightly reduced yield stress but increased the plastic viscosity of super-plasticised pastes.

## 2.10. Using limestone powder in SCC

Fillers such as limestone powder (referred to hereafter as LP) are usually by-products or cheap materials (Figure 2.14) and are often used as a bulk constituent in self-compacting concretes to enhance certain properties of SCC, where a low proportion of coarse aggregate may be desirable.

**Figure 2.14: Limestone Filler (< 2mm)**

The use of LP particularly in self-compacting concrete is widespread in the World today. The principal recognised advantages of using limestone powder as a mineral additive are associated with its effect on cost and workability, and not for its effect on strength (Şahmaran et al., 2006). Natural limestone is not a pozzolanic material. However the effect of LP on workability can be attributed to its physical and not its chemical properties, although the shape and size of limestone particles varies widely depending on the type of LP used (Yahia et al., 2005). Its action can be related to a change in the microstructure of the cement matrix associated with the small size of the particles, showing an enhancement in the packing density of powder, increasing the stability and the cohesiveness of fresh SCC.

Surabhi et al. (2009) reported that replacing up to 20% of cement with limestone powder can enhance fresh and hardened properties of SCC with same water to binder ratio. Figure 2.15 shows that replacing cement with 20% of limestone powder can increase the slump flow spread and can result in a moderate flow time $t_{500}$.

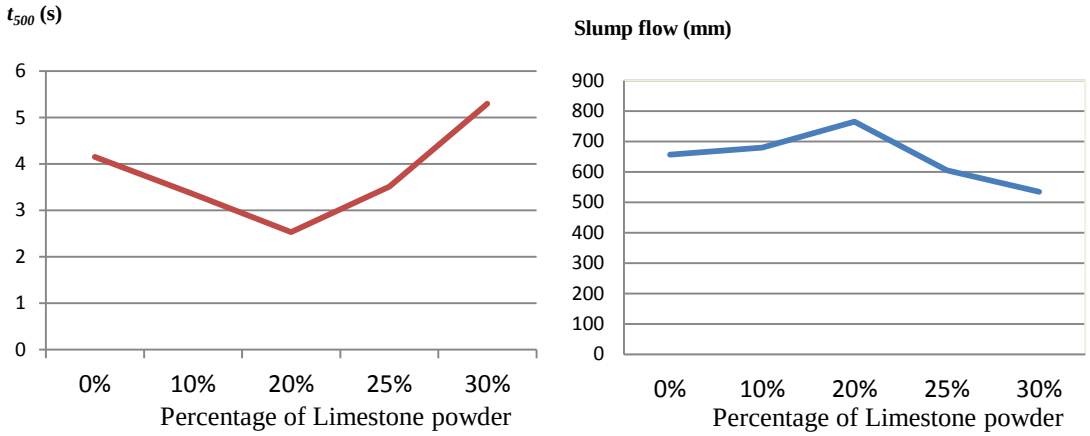


**Figure 2.15: Fresh properties of SCC using limestone powder (After: Surabhi et al., 2009)**

However, Yahia et al. (2005) reported that excessive amounts of fine particles mean a significant rise in the surface area of powder and an increase in inter-particle friction, due to solid-solid contact, which may cause a substantial rise in the viscosity, affecting the ability of the mixture to deform under its own weight and pass through obstacles.

## 2.11. Effect of super-plasticiser (SP) on SCC

The fresh behaviour and flow pattern of self-compacting concrete affect the hardened properties of concrete which is dominated primarily by the dispersing of its components. When cement particles contact with water, particles have different charges (positive and negative) which lead to them grouping together to form flocks. The flocks also trap the free water (Figure 2.17) which is necessary to lubricate the particles during the flow. As a result internal friction occurs within the mix, restricting its flow-ability as the particles will not be able to flow pass each other with ease. The demand for a high level of workability, together with good stability of the mix for SCC has led to the use a number of chemical admixtures. Super-plasticisers or high-range water-reducing admixtures (HRWRAs) contribute to the achievement of denser packing and lower porosity in concrete by increasing the flow-ability (without increasing water content).

Moreover the hydration of the cement particles is improved by greater dispersion and this is necessary in producing SCCs of high strength and good durability.

**Figure 2.16: Polycarboxylate-based super-plasticiser**

HRWRAs (Figure 2.16) have been used to improve the flow-ability of concrete with low water to binder ratio (w/b). The particles of superplasticiser, which are generally in the form of long molecules, contain a small negative charge; they will tend to repel each other. When these long molecules become associated with the individual cement particles, the particles of cement are repulsed from each other. SP adsorb onto the cement particle surfaces and break up the flocks, leaving individual cement grains, which can pass each other easily, making the mix more fluid.

Figure 2.17 illustrates the deflocculating of cement particles and freeing of the trapped water through the dispersing action of SP. However, a high amount could cause segregation and bleeding.

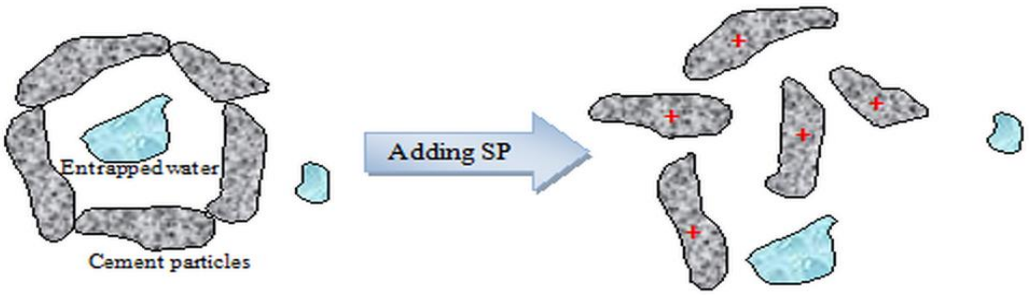


**Figure 2.17: Method of de-flocculation and water liberation with use of super-plasticiser.**

There are mainly four categories of superplasticiser, namely the sulfonated melamine formaldehyde condensates (plasticiser), sulfonated naphthalene formaldehyde condensates, modified lignosulfonates, and carboxylated acrylic ester co-polymers or poly-carboxylic ethers (Kong et al., 2003). Figure 2.18 shows the progression in the development of admixture technology.

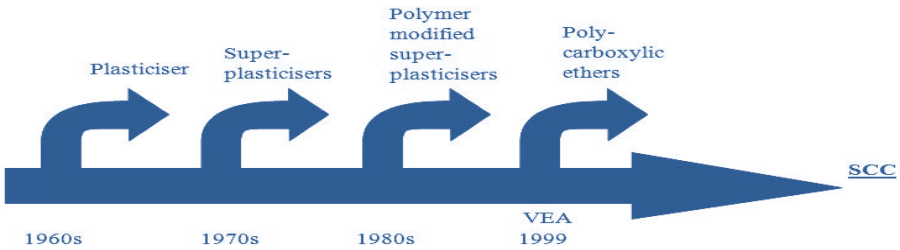


**Figure 2.18: Development in admixture technology (After: Dransfield, 2003)**

Polycarboxylate-based HRWRAs with their different structures and modes of action play a very vital role in self-compacting concrete and are an essential component in SCC production.

Old types of SP namely Sulfonate-based HRWRAs consist of anionic polymers that adsorb onto the cement particles and impart a negative charge, resulting in electrostatic repulsion.

Figure 2.19 illustrates the effect of sulfonate-based polymer on the dispersion of cement paste by electrostatic repulsion.

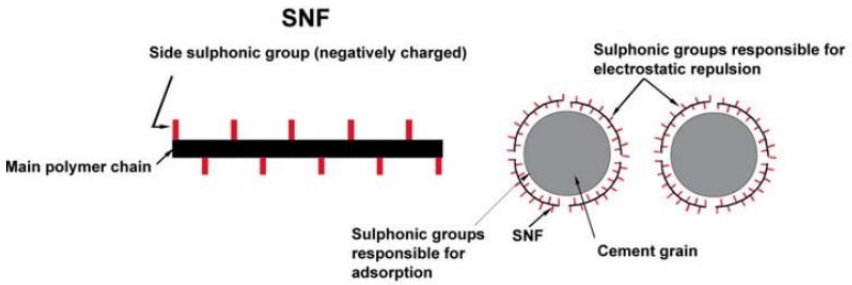


**Figure 2.19: Schematic picture of sulfonate-based HRWRAs and the related electrostatic repulsion effect on the dispersion of cement particles (After: Collepardi, 2005)**

On the other hand, polycarboxylate-based HRWRAs consist of flexible, comb-like polymers with a main polycarboxylic backbone and grafted polyethylene oxide side chains. The physical effects of superplasticizer molecules can be considered being of the following three types: physical adsorption under the effect of Van der Waals and electrostatic forces, Long-range repulsive forces due to a reconfiguration of the superficial charges, and steric repulsive forces among adjacent superplasticizer molecules and adjacent cement particles (Aïtcin et al., 2008). The backbone, which includes ionic carboxylic or sulfonic groups, adsorbs onto a cement particle and the non-ionic side chains extend outward from the cement particle. The side chains physically separate cement particles, which is referred to as steric hindrance as illustrated in Figure 2.20 (Koehler, 2007). Polycarboxylate-based HRWRAs may function by both electrostatic repulsion and steric hindrance (Li et al., 2005) or only by steric hindrance (Blask and Honert, 2003; Li et al., 2005) depending on the structure of the polymer.

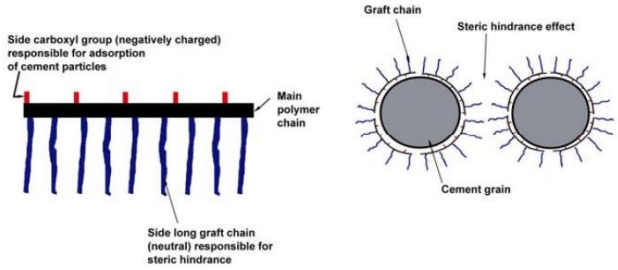


**Figure 2.20: Schematic picture of the polycarboxylate-based super-plasticiser and its steric hindrance effect on the dispersion of cement particles (After: (Collepardi 2005)**

Polycarboxylate-based super-plasticisers are more sensitive than sulfonate-based super-plasticiser to the amount of mixing energy (Koehler and Fowler, 2007).

## 2.12. Viscosity modifying agents (VMA)

VMAs, also known as anti-washout admixtures have been in use for a long time. They were mainly used for underwater concreting in the past, but are now also used in self-compacting concrete. VMA can be added to the concrete mixes to improve segregation resistance, cohesiveness and reduce bleeding. In general these admixtures increase yield stress and plastic viscosity. They may be also used as an alternative to increasing the powder content or reducing the water content of a concrete mixture (Koehler et al., 2007).

Acrylic- or cellulose- based water-soluble polymers or polysaccharides of microbial sources, such as welan gum are the commonly used viscosity-modifying agents in concrete. Water-soluble polymers can imbibe some of the free water in the system, thus increasing the viscosity of the cement paste which, in turn, enables the paste to hold aggregate particles in a stable suspension.

When using a VMA in SCC mixes it is necessary to take into account its compatibility with the super-plasticiser used. For instance, cellulose derivatives are incompatible with a naphthalene-based super-plasticiser, whereas welan gum is compatible (Khayat, 1995). Adding VMAs to SCC mixes can alter cement hydration, resulting generally in a

decrease in the compressive strength, flexural strength and modulus of elasticity of hardened concrete (Khayat, 1995).

## 2.13. Testing self-compacting concrete in fresh state

Workability is a way of describing the performance of concrete in the plastic state and for SCC, workability is often characterized by the following properties: filling ability, passing ability, and stability (segregation resistance) (PCI, 2003).

Assessing the workability of SCC mix can be divided into three categories as proposed by (Tattersall, 2003):

- Qualitative assessment; it is a general description of concrete behaviour such as workability, flow-ability, stability, compatibility, pump-ability…etc. without any attempt to quantify. This was discussed previously in this Chapter.

- Quantitative empirical assessment to be used as a simple description of quantitative behaviour such as slump flow test, L-box test…etc.

- Quantitative fundamental assessment; it is a description related to rheological terms of concrete, e.g. plastic viscosity, fluidity and yield value.

The most important way to understand the flow behaviour of SCC is the quantitative fundamentals. Different types of rheometers can be using to test the rheological properties of SCC mixes. However, these tests are sensitive, expensive and they can be rather time-consuming, therefore they are not suited for use at the working site, (Utsi et al., 2003). Therefore, it is important to find suitable workability test methods easy to use inside as well as outside the laboratory, and to calibrate them with the rheological parameters. Researchers studying the use self-compacting concrete have developed laboratory tests to understand more fully the movement and consolidation of self-

compacting concrete and successfully implementing in practice, for instance slump flow test, J-ring test, L-box test, U-box test, V-funnel test and wet sieve stability…etc. The workability tests recommended by British standard (BS EN 206-9 2010) are the slump flow test for flowing ability, L-box and J-ring tests for passing-ability and filling-ability, and visual inspection or sieve stability test can be used for segregation resistance. The next sections will be devoted to explain these tests.

### 2.13.1. Flow-ability test (slump flow test)

This inexpensive test is a modified version of slump test (ASTM C143). Slump test is used to assess the horizontal flow of SCC mainly when there are no obstacles. The test measures three different aspects, the filling ability by measuring the horizontal flow diameter SF, $t_{500}$ the time needed SCC to reach 500 mm which indicates the viscosity of concrete and the segregation can be visually inspected. Because it is a very simple test, the slump test can be done either on site or in the laboratory with inverted or upright Abram's cone. It is usually the test that accepts or rejects a mix at the working site (Utsi et al., 2003). The occurrence of unevenly distributed coarse aggregate is considered as an indication of segregation, which demonstrates that the concrete segregates during the test and may segregate after placing.

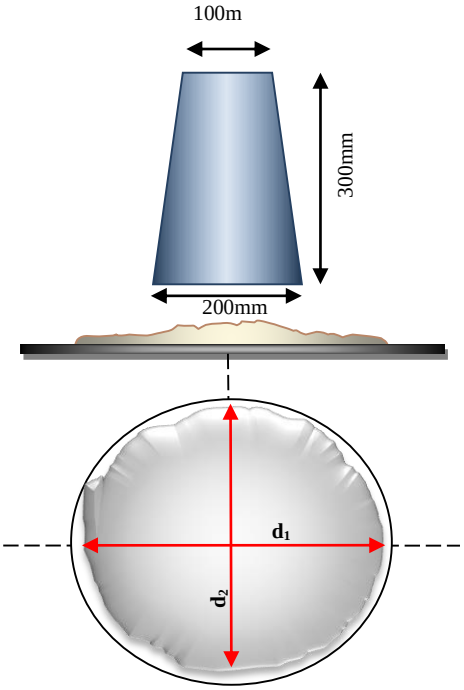


**Figure 2.21: Slump test apparatus with upright cone.**

The cone is placed on a firm non-absorbing levelled flat steel surface with a plane area of at least 900 mm x 900 mm, filled with SCC. The guidelines for slump test of conventional vibrated concrete recommend that the cone be lifted vertically slowly and carefully to ensure a correct result, with the lifting operation taking approximately 3 to 7 seconds, however for SCC cone should be lifted in 1 to 3 sec in one movement (0.1- 0.3 m/s) (BS EN12350-8:2010) or lift the cone in 3±1 second to a height of 230±75 mm (≤ 0.1 m/s) (C1611 ASTM, 2011). SCC flows out under its own weight. Two horizontal perpendicular diameters $d_1$ and $d_2$ as illustrated in Figure 2.21 are recorded and the average flow spread diameter *SF* calculated using Equation (2.1)

$$SF = (d_1+d_2)/2 \qquad (2.1)$$

**Criteria of acceptance** (BS EN12350-8 2010)

- Achieving a large diameter with no segregation indicates a good deformability and a low yield stress.

- This test is not acceptable when the largest aggregate size in more than 40mm.

- The difference between $d_1$ and $d_2$ should be less than 50mm otherwise the test should be repeated.

- Segregation can be detected by visually inspecting a ring of cement paste/mortar in the edge of flow, and /or ensuring that no coarse aggregates and fibres have lifted in the centre of flow.

- According to the latest mix design guidelines for self-compacting concretes (BS EN 206-9 2010) two viscosity classes are introduced: viscosity class 1 (VS1) and viscosity class 2 (VS2) depending on whether $t_{500}$ < 2 s or ≥ 2 s.

Long et al. (2014) report that, for pre-stressed precast SCC should have slump flow spread values of 635–760 mm.

Here it should be mentioned that this test is affected by different parameters, such as the moisture of the apparatus, different testing person and the speed of lifting the cone (Cattaneo and Mola, 2012). The friction can play a role in slightly increasing $t_{500}$ only when using large aggregates.

### 2.13.2. Passing ability tests

#### 2.13.2.1. J-ring test

This test is intended to assess the passing ability of the concrete through gaps typically between rebars. If the concrete flow is blocked then the aggregate size could be too large for the particular application (BS EN12350-10: 2010). J-ring is a test used usually with a slump test to evaluate the flow through tight openings including spaces between reinforcing bars and other obstructions without segregation or blocking. For this test, the slump test apparatus is used with an open steel rectangular section ring with 10 (or

16 in some cases to represent light or dense reinforcement ) steel rods (ϕ16mm) and 100 mm height, as shown in the Figure 2. 22. The gap between the bars is 78 mm ± 1 in case of 10 bars.

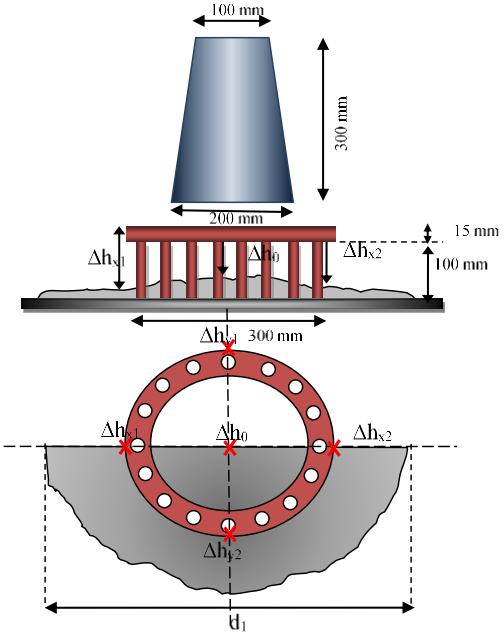


**Figure 2.22: J-ring test apparatus**

After filling the cone with concrete without using any vibration or rodding, the slump cone is lifted vertically allowing the concrete to flow freely through the bars. The time needed for the flow to reach 500 mm diameter is recorded as $t_{500J}$, and the flow allowed to stop before recording the average of two diameters measured in two perpendicular directions. Flow spread of the J-ring ($SF_J$) indicates the restricted deformability of SCC and can be expressed using Equation (2.2)

$$SF_J = (d_1+d_2)/2 \qquad (2.\ 2)$$

- Flow time $t_{500J}$ is recorded.

- Blocking step $P_J$ is calculated using Equation (2.3).

$$P_j = \frac{\Delta h_{x1} + \Delta h_{x2} + \Delta h_{y1} + \Delta h_{y2}}{4} - \Delta h_0 \qquad (2.\ 3)$$

where:

$\Delta h_{0:}$ is the height of concrete at the centre of flow.

$\Delta h_{x1}$, $\Delta h_{x2}$, $\Delta h_{y1}$, $\Delta h_{y2}$ are heights of concrete at positions just outside the J-ring.

**Criteria of acceptance**

- Chan et al. (2010), has defined a limitation to evaluate passing ability of SCC with or without steel fibres using the J-ring can be assessed relative to the flow spread (*SF*) of the same mix using the slump test as described in Table 2.1:

**Table 2.1: Passing ability criteria (ASTM C1621)**

| ($SF-SF_J$) | Passing ability rate | Notes |
|---|---|---|
| <25mm | **0** | **No visible blocking** |
| 25mm-50mm | **1** | **Minimal to noticeable blocking** |
| >50mm | **2** | **Noticeable to extreme blocking** |

- The blocking step $P_J$ should be less than 10mm based on EFNARC (2005).

- This test is not acceptable when the maximum aggregate size is more than 40mm.

- The difference between $d_1$ and $d_2$ should be less than 50mm otherwise the test should be repeated.

- Segregation can be evaluated visually, a ring of cement paste/mortar in the edge of flow, and /or ensuring that no coarse aggregates have lifted in the centre.

Long et al. (2014) reported that for a pre-stressed precast SCC slump flow spread minus J-Ring flow diameter should be ≤75 mm.

#### 2.13.2.2. L-box test

The L-box test was also developed in Japan to test underwater concrete, and it has been adopted to test highly flow-able concretes. L-box test is used to assess the filling and passing ability of SCC in a confined space, or in other words the ability of concrete to pass though reinforced bars without blocking or segregation to fill a complex form. The apparatus (Figure 2.23) consists of a long rectangular trough with a vertical column/hopper at one end. A gate is fitted to the base of the column allowing discharge of SCC into the horizontal trough. Adjacent to the gate is an arrangement of bars which permits assessment of the blocking potential to be made. Concrete is poured into the vertical leg, and the sliding door is raised to allow the concrete to flow into the horizontal section. Typically, reinforcement bars are placed at the entrance of the horizontal section to gauge the passing ability of the concrete. ($H_1$, $H_2$) are the heights of concrete at the beginning and end of the horizontal section, respectively. The ratio $H_2/H_1$ represents the filling ability or levelling ability, and typically, this value should be 0.8~1, while the passing ability can be detected visually by inspecting the area around the rebars.

In L-box, 2 or 3 smooth steel bars with 12 mm diameter can be used to represent light or dense reinforcement with distance between them 59 and 41 mm, respectively. Generally, the spacing of the reinforcing bars should be at least three times the maximum aggregate size (Ferraris, 1999).

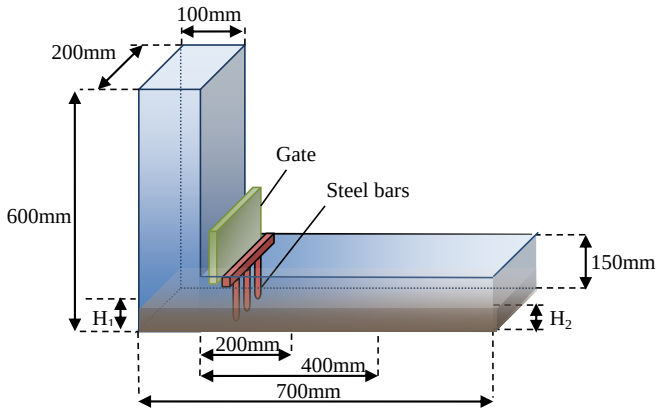


**Figure 2.23: L-box test apparatus**

The passing ability ratio PL should be calculated:

$$PL = \frac{H_2}{H_1} \qquad (2.\ 4)$$

$H_1$ is the mean depth of concrete in the vertical section of the box after the flow of SCC.

$H_2$ is the mean depth of concrete at the end of the horizontal section of the box.

Also the flow speed can be measured by the time taken to reach the distance of 200 mm ($t_{200}$) or 400 mm ($t_{400}$) from the gate.

**Criteria of acceptance**

- For this test, at least 14 liter of SCC should be prepared in accordance with (BS EN12350-10: 2010).
- No signs of segregation or bleeding.
- Passing ability ratio PL should be between 0.8 and 1
- There is no recommendation for $t_{200}$ and $t_{400}$ values, but longer values represent higher viscosity.

It should be mentioned that this test is very sensitive to the operators, for example, in regard to the lifting speed of the gate (Nguyen et al., 2006).

### 2.13.3. Segregation resistance tests

A number of empirical tests have been reported to evaluate SCC segregation.

#### 2.13.3.1. Visual examination

The visual examination method is carried out by inspecting the periphery of the concrete after measuring the slump flow spread and rating it from 0 to 3 (PCI, 2003). However it is an inadequate method because it depends on the experience of the individual and fails to evaluate segregation quantitatively.

#### 2.13.3.2. Sieve stability test

The dimensions used for the segregation column test are (500x150x100) mm. The test involves samples of concrete being taken from the top part and bottom part of a column shaped apparatus via doors after the apparatus has been jolted 20 times and allowed a static settlement period of 5 min. Those samples are washed out on a 5mm sieve and dried out to determine the proportion of coarse aggregate. Segregation resistance is expressed as the ratio between coarse aggregate mass in the top part and coarse aggregate mass in the bottom part.

## 2.14. Rheology of SCC: Quantitative fundamental study

Rheology is the study of the deformation and flow of matter under stress (Tattersall and Banfill, 1983), and knowing the rheological parameters (yield stress and plastic viscosity) of the fluid provides a quantitative fundamental way of characterizing the filling/passing ability and stability of SCC. Rheology has been studied for many years through the development of SCC. Self-compacting concrete is a viscous non-Newtonian fluid, described by a bi-linear Bingham-type rheological model (defined in Chapter 3) ,

in which the flow only starts once the shear stress has reached a critical value called the yield stress $\tau_y$. Bingham model contains two material properties, namely the yield stress $\tau_y$ and the plastic viscosity $\eta$ (Papanastasiou, 1987). The mix composition and the characteristics of self-compacting concrete constituents strongly affect the rheology and fresh state behaviour of SCC.

Understanding rheological parameters of SCC, namely the plastic viscosity and the yield stress, provides a quantitative and fundamental way of characterizing the deformability, passing ability and stability of SCC, which are critical for concrete industry as they affect all the mechanical properties in the hardened state.

### 2.14.1. Measuring the rheological parameters of Bingham model

Plastic viscosity $\eta$ is the measure of the resistance to flow due to internal friction. It can also be regarded as the ability of this fluid to resist shear or angular deformation, which is mainly due to the interaction between fluid particles. SCC should have a high viscosity in order to suspend aggregate particles in a homogenous manner within the concrete matrix without segregation, excessive bleeding, or paste separation. The yield stress is the measure of the minimum amount of energy required to make SCC initiate flow. Flow starts once the shear stress becomes higher than the yield stress. However, when its value becomes equal or lower than the yield stress, the flow stops. To be considered SCC, concrete must flow easily under its own weight, so its yield stress should be as low as possible.

It has generally been known that the slump property of a normal fresh cementitious mix is mainly governed by its yield stress (Kong et al., 2003). When the yield stress of a fresh concrete mix is greater than the gravitational stress, the fresh mix is prevented from completely collapsing to the plate surface. As the yield stress becomes less than the gravitation stress, the slump height decreases. In this process, the contribution of the

viscosity to the fresh properties is considered to be relatively small. Once the gravitational stress acting on the fresh mix is much greater than the yield stress, the fresh mix completely collapses onto the plate, followed by the spreading of the mix over the plate surface. The role of viscosity is more important during spreading. The flow stops when the gravitational stress is equal or less than the yield stress. This idea will be adopted numerically to estimate the yield stress in Chapter 6.

It is known from the literature that the yield stress of SCC mixes is very low (Dransfield et al., 2003), around 200 Pa (Deeb et al., 2014a,b) in comparison with normal concretes (thousands of Pa), and remains nearly constant over a large range of plastic viscosities as shown in Figure (2.24).

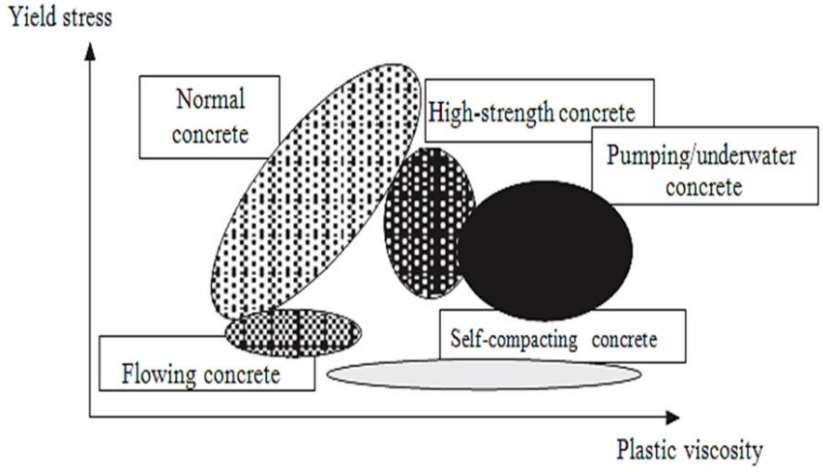


**Figure 2.24: Rheology of several types of concrete (After: Dransfield et al., 2003)**

Rheometers are used to measure the rheological parameters of general viscous liquids (such as cement pastes) and solid-liquid suspensions (such as self-compacting concretes). A wide range of rheometers is commercially available such as the coaxial cylinder rheometers, parallel plate rheometers and impeller rheometers (Domone, 2003).

Domone (2003) reported that for a given concrete mix, logically, any rheometer should give the same values of these two fundamental parameters $\tau_y$ and $\eta$. But in practice that

is not the case. Banfill et al. (2001) proved the difference between the values by using a series of comparative tests in which three instruments were taken to the same laboratory and used simultaneously to test a series of fresh concrete mixes with a wide different range of rheological characteristics. Figure 2.25 shows an example of how two different rheometers gave totally different responses for the same mix.

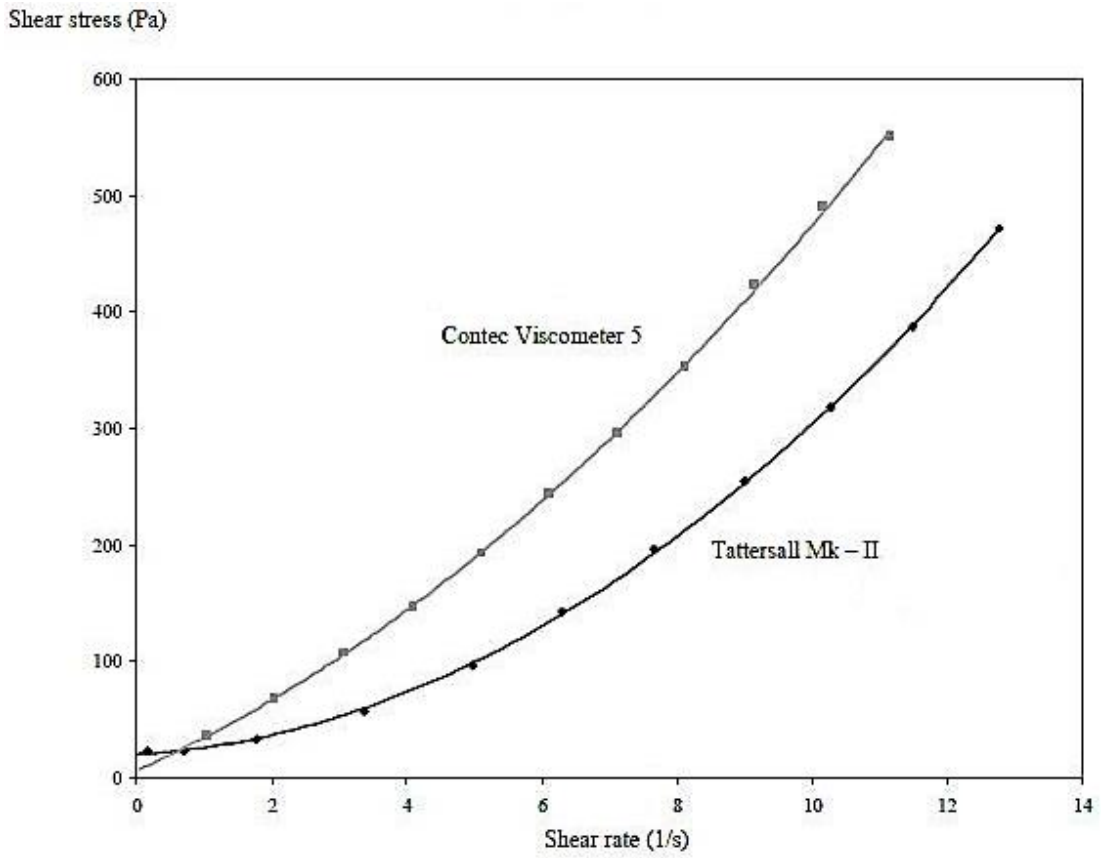


**Figure 2.25: Two different responses for a single SCC mix tested by two rheometers (After: Feys et al. 2007)**

In both cases the yield stress values were somewhat more consistent than those of plastic viscosity. These inaccurate results, which are often with a large scatter with mixes containing long fibres, have triggered research into alternative prediction techniques for plastic viscosity (Krieger, 1959; Struble and Sun, 1995).

Ghanbari and Karihaloo (2009) have proposed a micromechanical procedure for calculating the plastic viscosity of SCC with or without steel fibres. This procedure is

based on the rheology of concentrated suspensions and the knowledge of the plastic viscosity of cement paste alone or of the cement paste with SP and/or VMA. This procedure has been shown to predict the plastic viscosity of SCC mixes with or without fibres that agree very well with measured values. Details of this micromechanical procedure will be explained in Chapter 4.

Many researchers (Grünewald, 2004; Thrane et al., 2007; Tregger et al., 2007; Roussel, 2006) have found a relationship between the rheological characteristics (yield stress and plastic viscosity) of a self-compacting concrete mix and the measured parameters in the slump flow test (slump flow spread and $t_{500}$). Further, it is recognized that the plastic viscosity can be related to the time $t_{500}$ but that the slump flow spread is a function of both the yield stress $\tau_y$ and the density of SCC. In general, both the yield stress and the plastic viscosity increase with time, as the concrete hardens (Castro and Liborio, 2006).

### 2.14.2. Effect of materials and mix proportions on the Bingham constants

Rheological properties of SCC vary with different mix proportions and material components, and it is important to understand how the yield stress and the plastic viscosity of concrete mixes vary. There is a considerable amount of published information on this which can be summarised as follows:

- Both yield stress and the plastic viscosity decrease with an increase in the water to powder ratio (Ramachandran and Beaudoin, 2000; Banfill, 2006). Figure 2.26 shows the effect of water to cement ratio on both the plastic viscosity and yield stress of the paste.

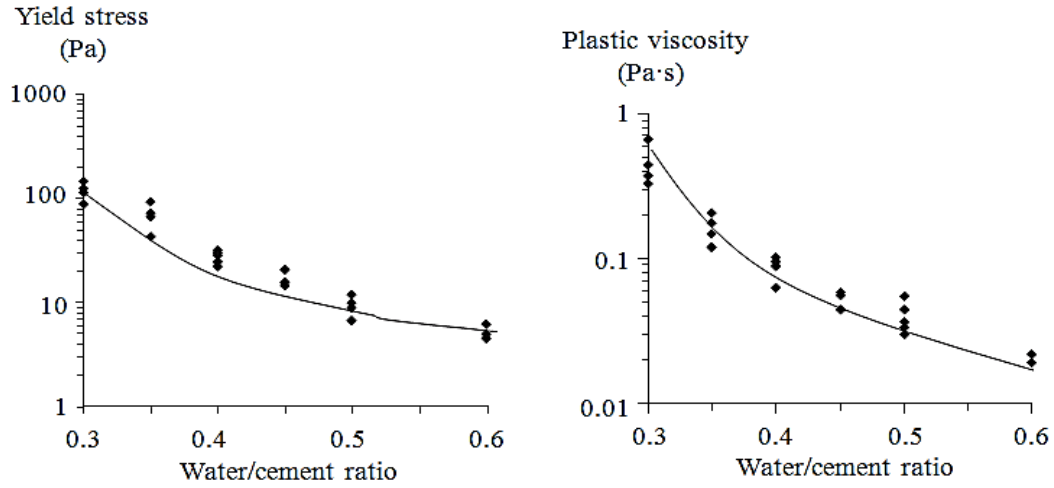


**Figure 2.26: Typical effect of water-cement ratio on Bingham constants for cement paste (After: Domone and Thurairatnam, 1988)**

– Domone and Thurairatnam (1988); Banfill (2006) have reported that the yield stress decreases with increasing super-plasticiser concentration as illustrated in Figure 2.27, while super-plasticiser has a different effect on the plastic viscosity depending on the type of super-plasticiser. For example, solid-based super-plasticisers like naphthalene-based, lead to an increase in the plastic viscosity, while the liquid-based super-plasticisers such as Gelenium ACE 333 have the opposite effect.

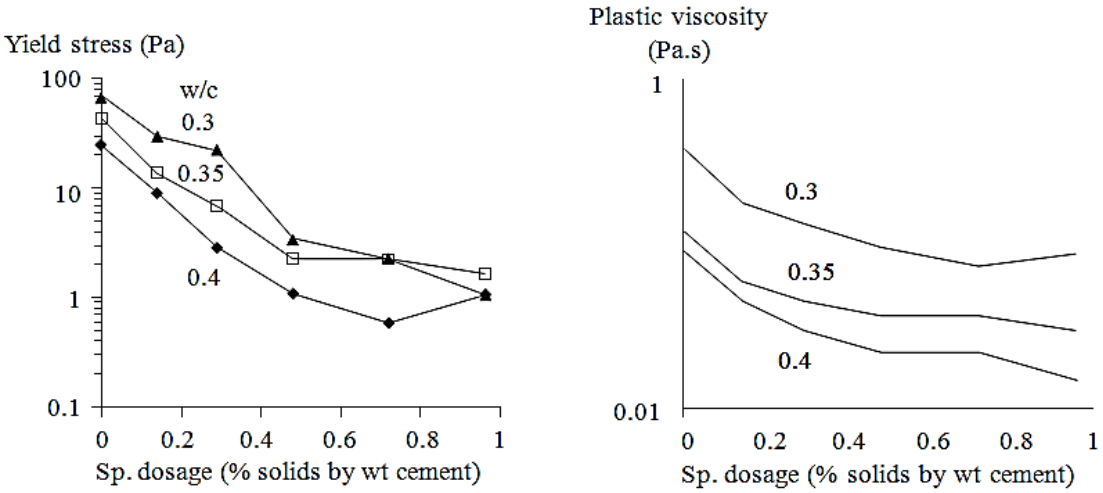


**Figure 2.27: Typical effect of superplasticiser on Bingham constants for cement paste (After: Domone and Thurairatnam, 1988).**

- Increasing the volume fraction of aggregate (with angularity) results in a high plastic viscosity and yield stress, however aggregate with round and smooth surface tends to have opposite effect on both the plastic viscosity and yield stress (Ramachandran and Beaudoin, 2000; Koehler and Fowler, 2007).

- There is contradictory evidence available in the literature on the effect of GGBS replacement on the viscosity of cement paste, depending on the type of viscometer used (Nehdi and Rahman, 2004). Some results show a slight decrease in viscosity, while others show the opposite trend.

- Ramachandran and Beaudoin (2000) report that yield stress increases with low fly ash contents and decreases with high contents of fly ash. Rahman et al. (2014) agreed that for various types of SCC, an increase in fly ash or limestone filler content leads to a decrease in the yield stress, while Banfill (2006) reached opposite conclusion that pulverized-fuel ash (PFA) reduces both the yield stress and plastic viscosity.

- Increasing the paste content reduces the yield stress, but has the opposite effect on the plastic viscosity.

- Silica fume considerably increases yield stress and initially reduces plastic viscosity (Ramachandran and Beaudoin, 2000). Small amounts of SF reduce the plastic viscosity, with almost no effect on the yield stress; however, above a threshold level of SF, which depends on the cement content, there is a substantial increase in the yield stress, followed by an increase in the plastic viscosity.

## 2.15. SCC applications

As of today, self-compacting concrete remains a nascent technology with limited use in comparison with that of vibrated concrete. However a lot of amazing structures have been built with SCC, for instance:

- **The Burj Khalifa Dubai** structure represents the state of-the-art in super high-rise buildings. During its construction the most recent accomplishments in all fields have been united, including concrete production technology. Several different concrete mixes were used in this project. It was necessary to place 230000$m^3$ of fresh concrete. That is the quantity that was built-in into tower, podium and office annex excluding foundations. SCC grade 50 was used in floor structures and C60 and C80 in vertical load-bearing members. The structure has sufficient rigidity, toughness and high load-bearing capacity. In the course of construction of the building the concrete was pumped to higher and higher heights so it was necessary to provide extraordinary flowing ability of concrete through pipes. A world record was achieved in November 2007 when concrete was pumped to a height of 601m. Everything in this fantastic project was carefully planned; for example the concrete mix for the piles which are 1.5m in diameter and 43 meters long with design capacity of 3000 tonnes each was a 60 MPa mix based on a triple blend with 25% fly ash, 7% silica fume, and a water to cement ratio of 0.32. A viscosity modifying admixture was used to obtain a slump flow of 675 +/- 75mm to limit the possibility of defects during construction. Total height, 818 m, was reached on 17 January, 2008.

**Figure 2.28: Burj Khalifa in Dubai**

– **Arlanda Airport Control Tower, Stockholm, Sweden**

The total height of the tower is 83m. The structure of the pillar consists of two shafts having different dimensions which is emphasised by two-colour design. There are several eccentrically placed circular floor structures at the top. Facade walls are parts of a cone. The tower was completed and opened in 2001. Today it represents a symbol of Stockholm. During the construction stage, the inner formwork was climbed by a crane while the outer scaffolding and formwork were self-climbing. SCC was used in order to achieve the concreting speed of a standard floor height h=3.27m in a 4 day climbing cycle of formwork and to ensue high-quality concrete placing without vibration. The decreased noise level during concrete placing enabled concreting during the night shift.

**Figure 2.29: Arlanda Airport Control Tower, Stockholm, Sweden**

- **Ušće Shopping Centre**

The Ušće Shopping Centre was designed by a company from Belgrade. The building work started in mid-2007. As many as 5000 people worked on the construction of the building at a particular moment. Upon opening on March 31, 2009, Belgrade gained the largest Shopping centre in the region with 130,000 $m^2$ in area. Concrete MB40 was specified for foundations, floor structures, columns, etc. to shorten the construction periods and to obtain high-quality visible part of the structure. Peripheral walls of underground structures were built with SCC. Fresh SCC reached flow-ability class SF3 (SF = 850mm). Hardened concrete was MB 40. Columns of underground floors were also made with SCC. Flow-ability of this fresh concrete was SF = 900mm, and class of hardened concrete was MB60. Concrete in foundation slabs was SCC, with flow-ability of fresh concrete SF = 900mm. Hardened concrete was MB40. Foundation slab thickness of 300 mm provided complete watertight concrete.


**Figure 2.30: Ušće Shopping Centre**

These are only some of the most recent and most modern architectural buildings in which SCC was used. It is expected that the implementation of SCC in the future will be more frequent and wider.

## 2.16. Concluding remarks

The majority of concrete cast relies on compaction to ensure that adequate strength and durability is achieved. Insufficient compaction will lead to the inclusion of voids, which not only lead to a reduction in compressive strength but strongly influence the natural physical and chemical protection of embedded steel reinforcement afforded by concrete. The self-compacting concrete is an advanced type of concrete that homogeneously fills formwork of different shapes and geometry under its own weight, without any additional compaction, passes through closely spaced reinforcement without showing any blockage or segregation. The use of self-compacting concrete changes the basic material technology concepts and transforms the concrete construction process. The unique properties of SCC open the possibilities for automation of concrete construction and concrete product manufacturing processes and allow building concrete structures in more efficient ways. The use of SCC has many advantages including increased construction productivity, improved jobsite safety, and enhanced concrete quality. These benefits, however, must be measured against the potentially higher material costs

and the need for greater technical expertise and quality control measures. It has been successfully used for a wide range of precast and ready mix concrete applications.

This chapter gave a general overview of SCC including:

- Properties, the basic principle of its mix design.
- The mechanism of achieving self-compacting ability.
- Influence of cement replacement materials and admixtures on the characteristics of SCC in the fresh state. It was concluded that in the fresh state, CRMs enhance self-compacting ability, fluidity and cohesiveness while improving its performance in the hardened state.
- The rheology of SCC was introduced, with an overview of the rheological parameters and the effects of materials and mix proportions on the Bingham constants. The most popular methods of testing SCC were introduced including the slump flow test, J-ring test, L-box test and sieve stability test.

There is however scope for a systematic development of SCC mixes and a need to understand the influence of rheological parameters on their flow characteristics. This will be undertaken in the present Thesis.

The next Chapter will give a brief review of how to model the flow of fresh self-compacting concrete.

# Chapter 3

# Rheology of SCC and methods of simulating fresh concrete flow – A brief summary

## 3.1. Introduction

This chapter gives a brief summary of the rheology of SCC and the methods of simulating its flow. Details may be found in the PhD thesis of Deeb (2014).

### 3.1.1. Rheology

Rheology is the science of flow and deformation of matter under stress (Tattersall and Banfill, 1983). From rheology point of view, self-compacting concrete is often modelled as a Bingham fluid (Vasilic et al., 2011). This model contains two parameters: 1. Yield stress $\tau_y$, which is the minimum shear stress that an SCC mix has to overcome to start flowing. 2. Plastic viscosity: The measure of the resistance of SCC to flow due to internal friction. Concrete with higher plastic viscosity takes longer to flow. It is closely related to $t_{500}$ and v-funnel time (the higher the plastic viscosity, the longer $t_{500}$ and v-funnel time).

Most numerical simulations consider only the steady-state of the flow while the thixotropic state i.e. the loss of workability of concrete during the flow is not been taken into account. However, SCC can exhibit shear thickening behaviour which means the plastic viscosity $\eta$ increases with the shear rate $\dot{\gamma}$ (e.g. in pumping and mixing); in this case, SCC can be modelled by the Herschel-Bulkley model (Vasilic et al., 2011).

The Bingham constitutive model is described by the equations

$$\tau = \tau_y + \eta\dot{\gamma} \qquad \tau > \tau_y \tag{3.1}$$

$$\dot{\gamma} = 0 \qquad \tau \leq \tau_y \tag{3.2}$$

From a computational point of view, it is expedient to represent the piecewise bi-linear Bingham constitutive relation with its associated discontinuity at zero shear rate by a continuous function (Papanastasiou, 1987).

$$\tau = \eta\dot{\gamma} + \tau_y\left(1 - e^{-m\dot{\gamma}}\right) \qquad (3.\ 3)$$

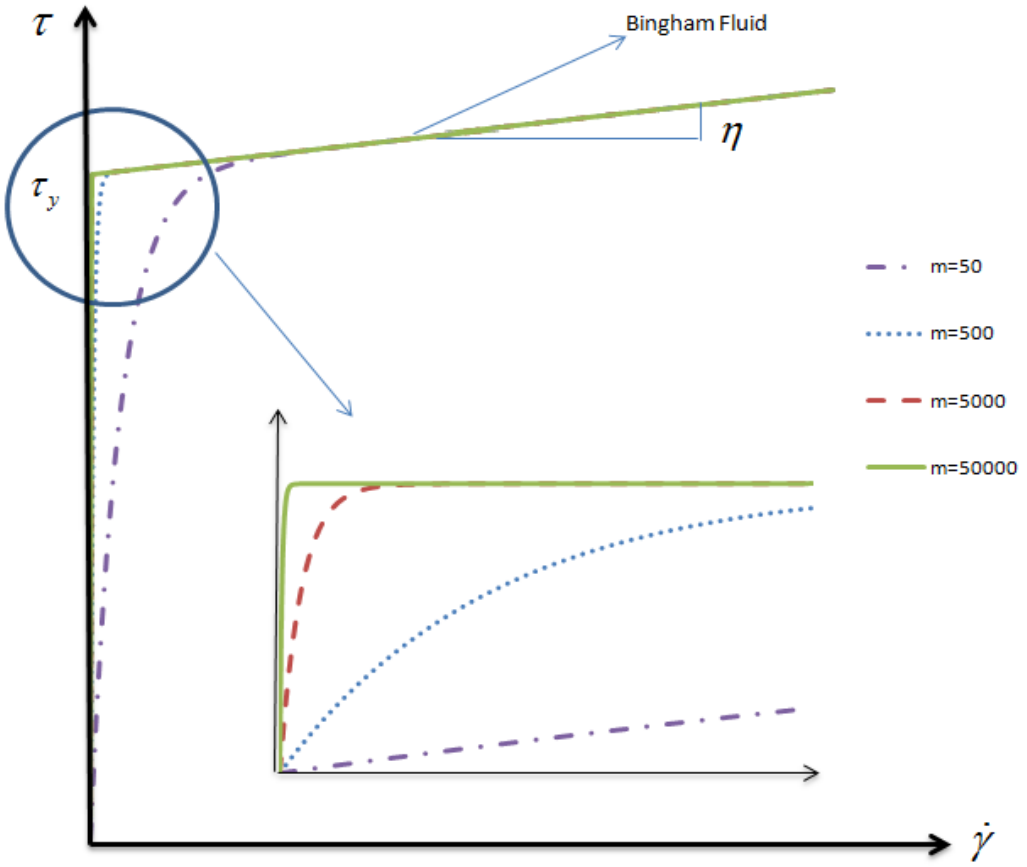


**Figure 3.1:A bi-linear Bingham fluid constitutive model replaced by the continuous function (3.3) (After: (Ghanbari, 2011)**

where *m* is a very large number. It can be seen from Figure 3.1 that the continuous function in Equation (3.3) approaches the bi-linear function for large *m*. On the scale of the figure, the discontinuity at $\tau_y$ cannot be distinguished for *m* =5000 and 50000.

The Herschel-Bulkley model is a generalization of the Bingham model in such a way that, upon deformation, the viscosity can be shear thinning or shear thickening. The constitutive equation is

$$\tau = \tau_y + \eta\dot{\gamma}^n \qquad \tau > \tau_y \qquad (3.\ 4)$$

$$\dot{\gamma} = 0 \qquad \tau \le \tau_y \qquad (3.\ 5)$$

For a shear thinning fluid, the index *n* may have any value between 0 and 1.0; the smaller the value of *n*, the greater is the degree of shear thinning. For a shear thickening fluid, the index *n* will be greater than unity.

### 3.1.2. Fluid classifications

Fluids have been classified in the literature as Newtonian or non-Newtonian depending on whether their response to shear rate is linear or non-linear, or as compressible or incompressible depending on their response to pressure. In this thesis, we shall be dealing with a non-Newtonian, incompressible fluid.

## 3.2. Simulation of SCC flow

The modelling of fresh concrete flow is an important issue for the construction industry. Concrete which has not been properly cast and compacted may be prone to defects such as honeycombs, air voids and aggregate segregation which are a major problem affecting the durability of concrete structures in service (Patzák and Bittnar, 2009; Dufour and Pijaudier-Cabot, 2005).

The computational modelling methods of concrete flow can be divided into two main groups: 1. Methods that treat concrete as a homogeneous medium, and 2. Methods that treat it as a heterogeneous medium. Choosing the right technique depends on the purpose of the simulation and whether the solid components of concrete are considered as separate particles or are embedded inside the mortar.

### 3.2.1. Simulation of concrete as a homogeneous medium

In this simulation concrete is regarded as a viscous fluid without particle inclusions. It is the easiest and fastest way to simulate fresh concrete. The drawback of this method is that the particle blocking and segregation cannot be predicted (Roussel, 2007). This approach has been taken by many researchers, e.g. Mori and Tanigawa (1992), Thrane

et al. (2004), Kitaoji et al. (1997), Kurokawa et al. (1997), Roussel and Coussot (2005), Roussel (2006), Patzák and Bittnar (2009), and Gao and Fourie (2015). They used either specialised mesh-based finite element approaches or the standard computational fluid dynamics (CFD) approach.

### 3.2.2. Simulation of concrete as a heterogeneous medium

Self-compacting concrete (SCC) in fresh state can exhibit a fluid-like behaviour or a granular medium-like behaviour depending on whether the volume fraction of coarse aggregates in the viscous suspension is small or large.

Gram (2009) used the Discrete Element Method (DEM) commercial software PFC$^{3D}$ to model the flow of SCC. Martys (2005) used the Dissipative Particle Dynamics method (DPD) which allowed for much larger time steps, as opposed to DEM.

Mori and Tanigawa (1992) used the so-called Visco-plastic suspension element method (VSEM) where concrete is divided between mono sized spherical coarse aggregates and mortar. Dufour and Pijaudier-Cabot (2005) used a finite element method with Lagrangian integration points (FEMLIP) to model the flow of concrete in L-Box.

Švec et al. (2012) have modelled the free surface flow of suspension of rigid particles in a non-Newtonian fluid using the Lattice Boltzmann method combined with Immersed Boundary Method and particle dynamics. This model is efficient and robust allowing simulations of tens of thousands of particles.

The Smooth Particle Hydrodynamics (SPH) will be used in the present research. Due to the fact that SCC undergoes large deformations during the flow and the fact that it contains particles of different sizes, SPH is an ideal computational method to represent with a good margin of accuracy its rheological behaviour. Unlike the mesh-based methods, SPH as a particle-based method does not require re-meshing. This method has

been tested and proved to be efficient and accurate in modelling SCC without fibres by Kulasegaram et al. (2011) and SCC with fibres by Kulasegaram and Karihaloo (2012), and Deeb et al. (2014a,b).

## 3.3. The governing equations of concrete flow

The flow of SCC can be described by the equations of fluid motion: the continuity, momentum and energy conservation equations which are based on the fundamental physical laws of conservation. However, when there is no change in the temperature during test and the heat flux in a continuum is absent, the energy can be assumed to be identically conserved. Also, as the viscosity and density are not affected by the temperature, the energy conservation equations can therefore be ignored.

### 3.3.1. Continuity equation (the mass conservation)

The continuity equation or the mass conservation equation in the Lagrangian form is

$$\frac{D\rho}{Dt} + \rho\nabla \cdot \mathbf{v} = 0 \tag{3. 6}$$

For an incompressible fluid, the density is constant, and therefore (3.6) becomes

$$\nabla \cdot \mathbf{v} = 0 \tag{3. 7}$$

Here $\rho$, $t$, and $\mathbf{v}$ the fluid particle density, time, and particle velocity respectively.

$D$ denotes the substantial or material derivative.

### 3.3.2. The momentum conservation equations

If gravity $\mathbf{g}$ is the only body force acting on the continuum the momentum conservation equations in the Lagrangian form can be written in the compact vectorial form as

$$\frac{D\mathbf{v}}{Dt} = -\frac{1}{\rho}\nabla P + \frac{1}{\rho}\nabla.\boldsymbol{\tau} + \mathbf{g} \tag{3. 8}$$

where $P$, $\mathbf{g}$ and $\boldsymbol{\tau}$ are pressure, gravitational acceleration, and shear stress, respectively.

## 3.4. Domain Discretization

In the numerical simulations, the continuum problem domain needs to be divided into a finite number of discrete components in order to solve the above governing equations. The discretization technique is different according to the numerical method used. Figure 3.2 illustrates the mesh-based and mesh-less discretizations of a geometrical domain.

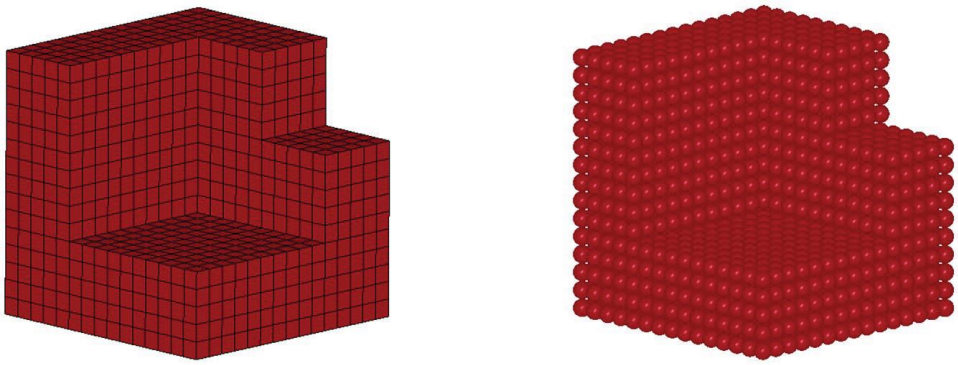

**Figure 3.2: Comparison between grid method (left) and particle method (right) for the same geometry (After: Vesenjak and Ren, 2007)**

### 3.4.1. Mesh-based method

In the grid or mesh-based method, the continuum domain is divided into small discrete domains connected to each other by nodes. Accuracy of the numerical approximation is closely related to the mesh topography (i.e. shape, size...etc.). Examples of mesh-based method are the finite element method (FEM), the finite difference method (FDM), and the finite volume method (FVM). Because the generation of the mesh for a grid method is a prerequisite, for complicated problems it can be more difficult than solving the problem itself since the results are based on the quality of the mesh (Vesenjak and Ren, 2007). Therefore, mesh-less methods become more attractive to treat problems where it is difficult to used grid based methods.

### 3.4.2. Mesh-less method

In particle (or mesh-less) methods a domain is represented by a set of nodal points or particles without using any mesh to connect those nodes. In these methods, large

deformations, moving interfaces, difficult boundary conditions and complex geometries are easy to handle, since the connectivity among nodes is generated as part of the computation. A number of mesh-free methods have been proposed for the analysis of fluid flow such as the smoothed particle hydrodynamics (SPH) (Kulasegaram and Karihaloo, 2012) (Deeb et al., 2014), Element Free Galerkin Method (EFGM) (Yang, 2013), Reproducing Kernel Particle Method (RKPM) (Xiong et al., 2005) and Cloud Method (Burke et al., 2010), etc. These methods share some common features, but are different in the means of function approximation and the implementation process (Liu and Liu, 2010).

#### 3.4.2.1. Eulerian and Lagrangian approaches

There are two fundamental approaches to describe the physical governing equations: Eulerian and Lagrangian.

- **The Eulerian approach** is a spatial description; it is used to track a certain fixed location in the flow field and follows the change in properties, as different materials pass through that location (Figure 3.3).

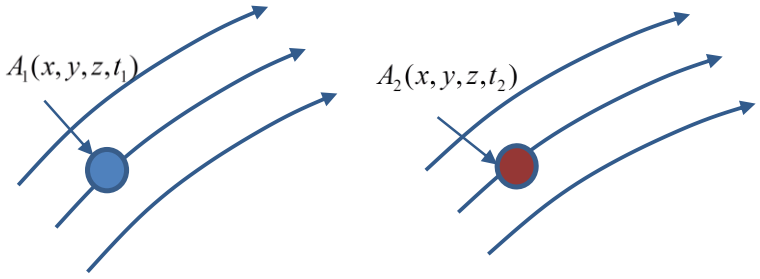


**Figure 3.3: Different fluid elements at different times at a fixed location in the fluid flow**

- The Lagrangian approach is used to track a material element of the fluid as it moves, and the changes in its properties, e.g. velocity are monitored (Figure 3.4).

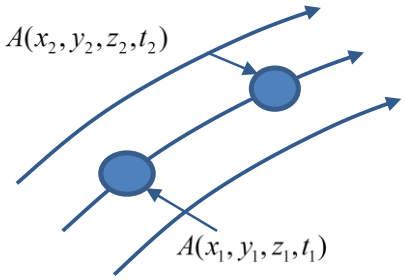


**Figure 3.4: Fluid particle motion from time $t_1$ to time $t_2$**

The Vortex, Finite Point set (FPM), gradient smoothing (GSM) and smooth particle hydrodynamics (SPH) are examples of Lagrangian methods.

The two derivatives, Lagrangian and Eulerian are related to each other, e.g. for velocity

$$\frac{D\mathbf{v}}{Dt} = \frac{\partial \mathbf{v}}{\partial t} + (\mathbf{v}.\nabla)\mathbf{v} \qquad (3.9)$$

where the term $\mathbf{v}.\nabla$ is the convective derivative, which defines the time rate of change as the fluid element moves from one location to another in the flow field.

## 3.5. Numerical approximation- Smoothed particle hydrodynamics (SPH)

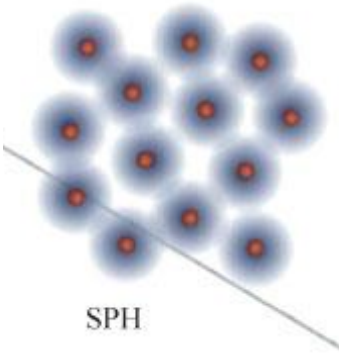


**Figure 3.5: SPH model (After: (Frédéric and Gilles, 2005)**

Lucy (1977), and Gingold and Monaghan (1977) independently proposed the Lagrangian particle-based numerical method SPH, to solve particular astrophysical problems. The SPH was first conceived for compressible flow problems in confined

flow simulations, until later Monaghan (1994) proposed and developed a modified SPH formulation to model free surface in viscid liquid flow. Other researchers have since solved various engineering problems including multi-phase problems (Monaghan and Kocharyan, 1995), quasi-incompressible flow (Monaghan, 1994; Morris et al., 1997), incompressible fluid flow (Shao and Lo, 2003; Solenthaler and Pajarola, 2009), flow through porous media (Zhu et al., 1999), viscous fluid flow (Takeda et al., 1994), shock simulations (Monaghan and Gingold, 1983), gravity currents (Monaghan, 1996), heat transfer (Chaniotis et al., 2002; Cleary et al., 2002), turbulent flows (Welton, 1998), interfacial flows, discontinuity and large deformability (Bui et al., 2008; Colagrossi and Landrini, 2003) and sloshing problems (Kelecy and Pletcher, 1997; Koshizuka et al., 1995). The interaction between fluids, free surfaces and many other applications can be also simulated using SPH (Amini et al., 2011).

Bonet and Kulasegaram (2000) applied SPH to simulate metal forming. Other notable modifications or corrections to the SPH method were made by Bonet and Kulasegaram (2000), and Dilts (1999, 2000). The Lagrangian nature of SPH allows the grid to be embedded in the material and thus reduces some of the material interface problems associated with Eulerian techniques.

### 3.5.1. SPH concept

SPH is an integral interpolation method to approximate values and derivatives of continuous field quantities by using discrete sample points (Gingold and Monaghan, 1977). The key characteristics of SPH as reported by Liu and Liu (2003) are: 1. **Domain discretisation**: the entire problem domain in the physical space is discretised into a finite number of macroscopic volumes of fluid. Each macroscopic fluid volume is represented by a particle in SPH. These particles possess individual material properties and move according to the governing conservation equations. 2. **Kernel**

**approximation**: Each particle, say particle '*a*' carries the field variables such as the mass $m_a$, density $\rho_a$, pressure $P_a$, velocity $v_a$, position $r_a$, temperature ($T_a$), internal energy ($\epsilon_a$), colour ($c_a$) which are represented by integral functions, the so-called kernel functions. 3. **Particle approximation**: The kernel is further approximated using particles, by replacing the integration in the integral representation of the field variable and its derivatives with summation over all the corresponding values at the neighbouring particles in a local domain called the support domain. 4. **Lagrangian:** The particle approximation is performed on all terms related to field variables to produce a set of ordinary differential equations (ODEs) in a discretized form with respect to time.

### 3.5.2. SPH support domain

The support for a particle '*a'* is the domain where all the information for all interior particles is used to determine the information at the point '*a'* (see Figure 3.6). This means that any physical property of a particle '*a'* can be obtained by summing the same property of particles that lie in the support domain Ω within a radius *ch* of the observed particle *'a'* and multiplying the sum by a smoothing function, where *c* is a scaling constant related to the smoothing function (usually equal to 2).

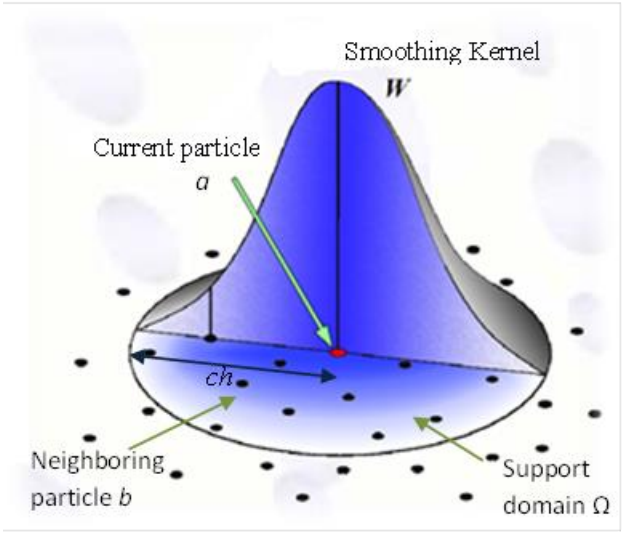


**Figure 3.6: Distribution of physical properties of a particle**

### 3.5.3. Kernel approximation

SPH provides a concept to approximate the spatial derivative using particles, which therefore makes computing the spatial derivatives in particle-based method as easy as in the grid-based methods. SPH is based on integral interpolation; for instance, a continuous quantity $f(\mathbf{x})$ over a space Ω can be written as the convolution of the quantity and Delta function

$$f(\mathbf{x}) = \int_{\Omega} f(\mathbf{x}') \, \delta(\mathbf{x} - \mathbf{x}') \mathrm{d}\mathbf{x}' \tag{3. 10}$$

where Ω is the volume of the domain, $\mathrm{d}\mathbf{x}'$ an elementary volume, and $\delta(\mathbf{x} - \mathbf{x}')$ is the Dirac Delta function i.e.

$$\delta(\mathbf{x} - \mathbf{x}') = \begin{cases} 1 & \mathbf{x} = \mathbf{x}' \\ 0 & \mathbf{x} \neq \mathbf{x}' \end{cases} \tag{3. 11}$$

The Dirac Delta function is approximated with the so-called smoothing kernel function *W* of limited support *h*

$$f(\mathbf{x}) \approx \int_{\Omega} f(\mathbf{x}') W(\mathbf{x} - \mathbf{x}', h) \, \mathrm{d}\mathbf{x}' \tag{3. 12}$$

*W* should be differentiable, normalised, and should converge to the Delta function.

The SPH approximation is highly dependent on the choice of the kernel function. The most common kernels are: Gaussian, cubic spline and quartic spline.

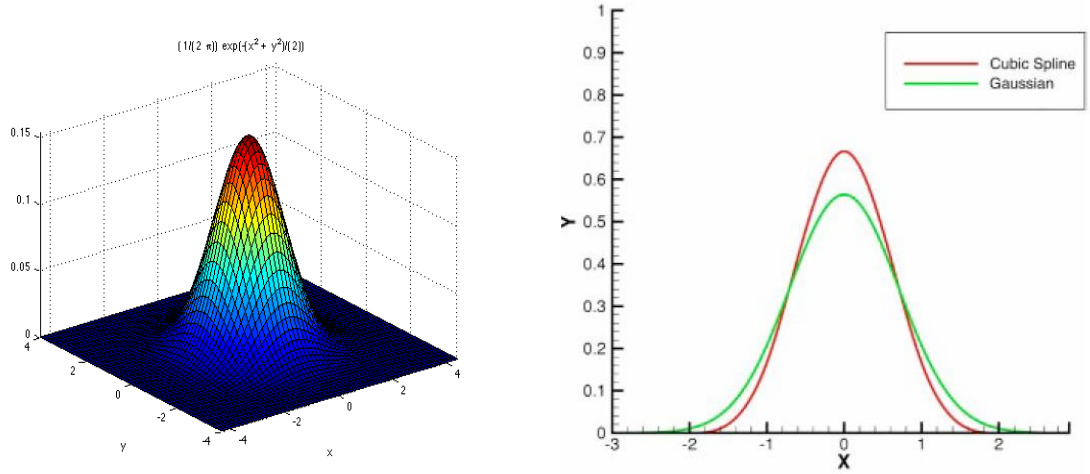


**Figure 3.7: Gaussian and cubic spline shape functions (After: Li and Liu, 2002)**

Figure 3.7 illustrates the Gaussian and the cubic spline functions; they look similar but the cubic spline has a more compact support as compared with the Gaussian function.

### 3.5.4. Particle interpolation

The entire domain of the problem is discretised into a limited number of particles *N* and then all the field variables are approximately calculated on these particles. First, the infinitesimal volume $d\mathbf{x}'$ at the location of particle '*b*' can be approximately replaced by the finite volume of the particle $V_b$ where $V_b = \frac{m_b}{\rho_b}$. The inclusion of density $\rho_b$ and mass $m_b$ makes SPH the ideal numerical solution to simulate dynamic fluid flow such as the flow of self-compacting concrete. The continuous integral in Equation (3.12) can be converted to a discretized form of summation over all the particles *N*.

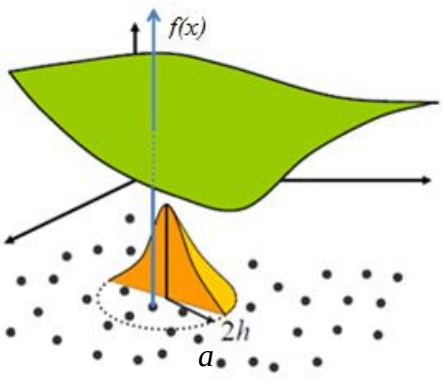


**Figure 3.8: Particle approximation of function *f*(x)**

Therefore, the continuous integral in Equation (3.12) can be expressed in the equivalent forms of discretized particle approximation (Figure 3.8)

$$f(\mathbf{x}) = \sum_{b=1}^{N} m_b \frac{f(\mathbf{x}_b)}{\rho_b} W(\mathbf{x} - \mathbf{x}_b, h) \tag{3. 13}$$

$$f(\mathbf{x}) = \sum_{b=1}^{N} V_b f(\mathbf{x}_b) W_b(\mathbf{x}) \tag{3. 14}$$

The differential of this function is given by

$$\nabla f(\mathbf{x}) = \sum_{b=1}^{N} V_b f(\mathbf{x}_b) \nabla W_b(\mathbf{x}) \tag{3. 15}$$

where the quantity $\nabla W_b(\mathbf{x})$ denotes the gradient of the kernel, which is taken as centred on the position of particle *a* (Figure 3.8). The application of Equation (3.14) to compute the approximate value for the density of a continuum leads to the classical SPH equation

$$\rho(\mathbf{x}) = \sum_{b=1}^{N} m_b W_b(\mathbf{x}) \tag{3. 16}$$

### 3.5.5. Corrected SPH integration

The basic SPH approximations as given by equation (3.14) and (3.15) do not accurately reproduce or approximate the function $f(\mathbf{x})$ and its derivative $\nabla f(\mathbf{x})$ because they do not conserve angular momentum. Therefore corrected SPH equations have been developed to address these issues (Bonet and Lok, 1999; Bonet and Kulasegaram, 2000). Using the corrected gradient of the corrected kernel, the SPH equations (3.14) and (3.15) can be rewritten as

$$f(\mathbf{x}) = \sum_{b=1}^{N} V_b f(\mathbf{x}_b) \tilde{W}_b(\mathbf{x}) \tag{3. 17}$$

$$\nabla f(\mathbf{x}) = \sum_{b=1}^{N} V_b f(\mathbf{x}_b) \tilde{\nabla} \tilde{W}_b(\mathbf{x}) \tag{3. 18}$$

where $\tilde{W}_b(\mathbf{x})$ indicates that the kernel function is corrected to satisfy the linear consistency conditions, and '*b*' is the neighbouring particle within the support domain.

### 3.5.6. Nearest neighbour search

One of the most computationally expensive parts of the simulation in SPH is to specify a particle's neighbours in the support domain. Many methods have been implemented to ensure an adequate way for neighbourhood search, e.g. Wróblewski et al. (2007), Monaghan and Lattanzio (1985), Liu and Liu (2003), and Bonet and Peraire (1991).

### 3.5.7. Treatment of boundary conditions

In SPH, boundary conditions should be imposed to ensure balancing the inner particle forces thus preventing those particles from penetrating the wall. A range of methods is available in literature to impose boundary conditions in SPH method, e.g. repulsive forces (Monaghan, 1994), mirror particles (Takeda et al., 1994; Cummins and Rudman, 1999) and dummy particles (Dalrymple and Knio, 2001; Shao and Lo, 2003; Lee et al., 2008; Amini et al., 2011). The dummy particle approach will be used in this thesis (see Chapter 5).

### 3.5.8. Incompressibility and weak compressibility in SPH approach

Enforcing incompressibility in SPH can be pursued using two different approaches - the weakly or quasi-compressible SPH will be referred to as WCSPH (Monaghan, 1994; Lee et al., 2008) and the truly incompressible SPH as ISPH (Kulasegaram et al., 2011). In this thesis the latter approach will be taken (Chapter 5).

## 3.6. Simulation of SCC flow with ISPH

For completeness of presentation, a brief description will be given of the incompressible SPH simulation method, as applied in this study to simulate the cone flow test.

A projection method based on the predictor-corrector time stepping scheme is used to track the Lagrangian non-Newtonian flow (Chorin, 1968; Cummins and Rudman, 1999; Koshizuka et al., 1998) and the incompressibility condition is satisfied exactly through a pressure Poisson equation.

### 3.6.1. Prediction step

The prediction step ignores incompressibility and only the viscous stress and gravity terms are considered in the momentum Equation (3.8) to obtain an intermediate particle velocity $\mathbf{v}_{n+1}^{*}$ and position by an explicit integration in time:

$$\mathbf{v}_{n+1}^{*} = \mathbf{v}_n + \left( \mathbf{g} + \frac{1}{\rho} \nabla . \boldsymbol{\tau} \right) \Delta t \tag{3. 19}$$

and

$$\mathbf{x}_{n+1}^{*} = \mathbf{x}_n + \mathbf{v}_{n+1}^{*} \Delta t \tag{3. 20}$$

### 3.6.2. Correction step

Then the correction step is applied to enforce the incompressibility condition prior to incrementing the time by considering the pressure term in Equation (3.8)

$$\frac{\mathbf{v}_{n+1} - \mathbf{v}_{n+1}^{*}}{\Delta t} = -\left( \frac{1}{\rho} \nabla P_{n+1} \right) \tag{3. 21}$$

where $\mathbf{v}_{n+1}$ is the corrected particle velocity at the time step $n$+1. Computing Equation (3.21) requires the pressure $P_{n+1}$. This is obtained by imposing the incompressibility

condition in the mass conservation Equation (3.6) (as the particle density remains constant during the flow)

$$\nabla.\mathbf{v}_{n+1} = 0 \tag{3. 22}$$

Equations (3.21) and (3.22) give

$$\nabla^2 P_{n+1} = \frac{\rho}{\Delta t}\nabla.\mathbf{v}^*_{n+1} \tag{3. 23}$$

where $\nabla^2$ is the Laplacian.

Once the pressure is obtained from the Poisson Equation (3.23), the particle velocity is updated by the computed pressure gradient Equation (3.21), followed by the instantaneous particle position:

$$\mathbf{v}_{n+1} = \mathbf{v}^*_{n+1} - \left(\frac{1}{\rho}\nabla P_{n+1}\right)\Delta t$$

$$\mathbf{x}_{n+1} = \mathbf{x}_n + \mathbf{v}_{n+1}\Delta t \tag{3. 24}$$

### 3.6.3. Time step

The time step $\Delta t$ is chosen based on the relevant stability conditions for the given problem. In the case of Bingham-type SCC fluid flow, the time step is primarily controlled by the effective plastic viscosity. Therefore, the time step size is generally decided by (Cummins and Rudman, 1999).

$$\Delta t = \min\left(\frac{\alpha_1 r_0}{\mathrm{v}_{\max}}, \frac{\alpha_2 r_0^2 \rho}{\mu}\right) \tag{3. 25}$$

where $r_0$ is the initial particle spacing, $\mathrm{v}_{\max}$ is the maximum particle velocity, $\alpha_1$ and $\alpha_2$ are the coefficients usually in order of 0.1. These coefficients depend on the choice of SPH kernel functions and the nature of the engineering application.

## 3.7. SPH discretisation of the governing equations

In the governing equations of SCC flow (Equations (3.6) and (3.8)), three terms need to be defined in the SPH formulation; these are the divergence of velocity field in the mass conservation equation (3.6), the gradients of pressure and viscous terms in the momentum conservation equation (3.8) and the Laplacian term $\nabla^2 P_{n+1}$ in the Poisson equation resulting from enforcing the incompressibility (3.23).

The divergence of the velocity field can be obtained by identifying $f(x)$ in the Equation (3.18) with the velocity term

$$(\nabla.\mathbf{v})_a = \sum_{b=1}^{N} V_b \mathbf{v}_b . \tilde{\nabla} \tilde{W}_b(\mathbf{x}) \tag{3. 26}$$

The gradient of pressure in the momentum equations can be obtained in the similar manner as above

$$(\nabla P)_a = \sum_{b=1}^{N} V_b P_b \tilde{\nabla} \tilde{W}_b(\mathbf{x}) \tag{3. 27}$$

The Laplacian in the pressure Poisson equation (3.23) can be formulated using the divergence and gradient operators of the SPH formulation to give

$$(\nabla^2 P)_a = \frac{\rho_a}{\Delta t} \sum_{b=1}^{N} V_b \mathbf{v}_b . \tilde{\nabla} \tilde{W}_b(\mathbf{x}) \tag{3. 28}$$

The viscous term, $\frac{1}{\rho}\nabla\boldsymbol{\tau}$ can be written in a similar manner as

$$\left(\frac{1}{\rho}\nabla\boldsymbol{\tau}\right)_a = \sum_{b=1}^{N} \frac{m_b}{\rho_b^2} \boldsymbol{\tau}_b \tilde{\nabla} \tilde{W}_b(\mathbf{x}) \tag{3. 29}$$

The above incompressible SPH computational strategy described in Sections 3.6 and 3.7 will be implemented to simulate the flow of SCC mixes in Chapters 5-7.

# Chapter 4

# Development of self-compacting concrete mixes with 20mm maximum size coarse aggregate

## 4.1. Introduction

The placement of SCC in congested or complex shape areas requires the use of a highly fluid mixture that can spread readily into place and fill the formwork and compact under its own weight with minimal /or no segregation (Khayat, 1998). These two conflicting objectives (fluidity and stability) are both attained by striking the right balance between the solids and liquids in the mix.

This Chapter will describe the steps taken to develop self-compacting concrete (SCC) mixes of a wide range of strengths and performance. The aim was to investigate how the proportions of solids and liquids, and the amount of super-plasticiser affect flow and passing ability of the SCC mixes, especially when they contain large coarse aggregates (20 mm maximum size).

The plastic viscosity of the SCC mixes so developed was next estimated by the micromechanical procedure described by Ghanbari and Karihaloo (2009). This plastic viscosity, together with the yield stress of the mix, is needed in the numerical simulation of SCC flow (Chapter 5-7).

The major part of the contents of this Chapter has been published in the journal "*Sustainable Cement-Based Materials*" (see publication 1 in the list in Chapter 1).

## 4.2. Experimental program flow-chart

The experimental program followed the steps outlined in Figure 4.1. The sequence of tests below for each trial mix starts with the most common slump flow test because it is easy to perform using a small volume of material. If the mix flows easily without segregation, the passing ability is then checked with the J-ring test. Finally the filling ability check is performed in the L-box.

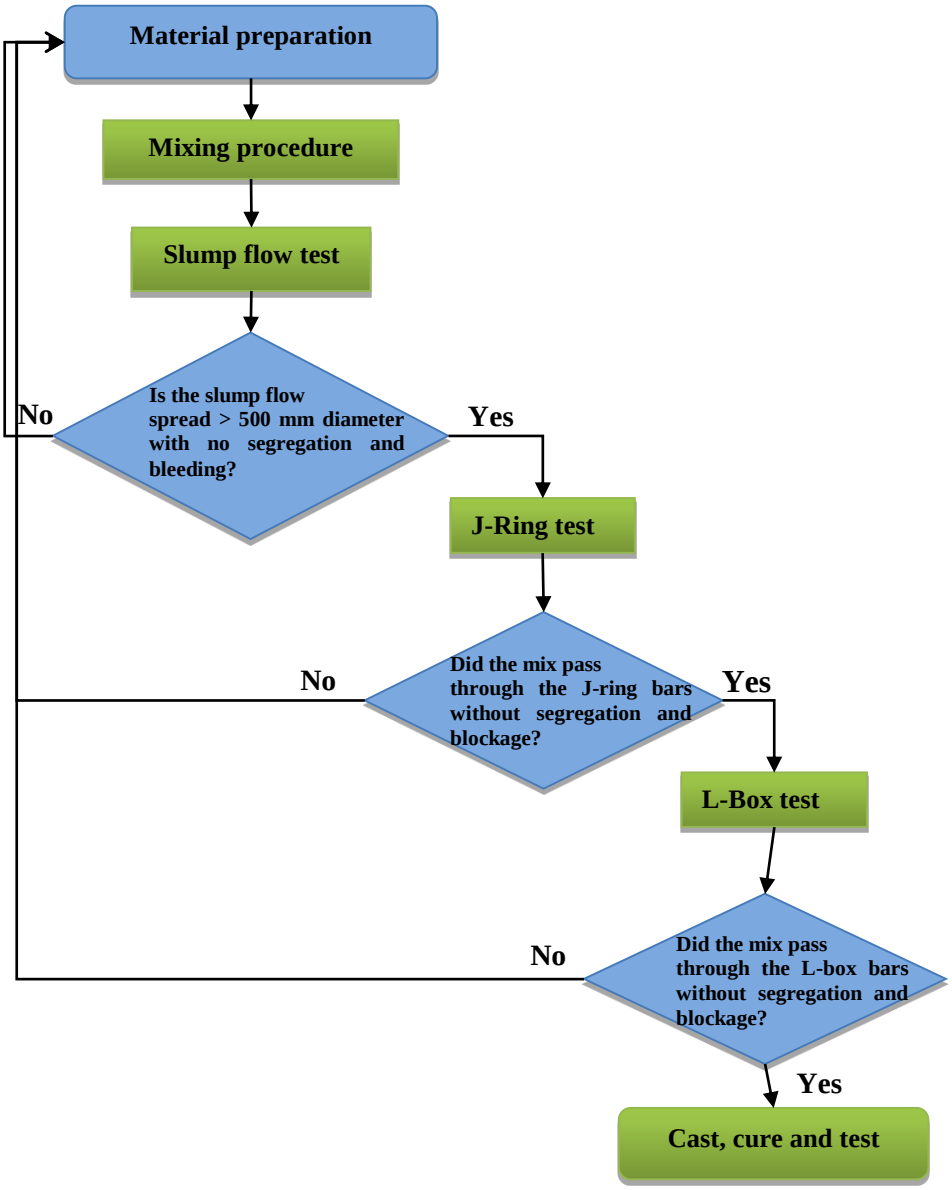


**Figure 4.1: Experimental program flow chart**

## 4.3. Development of SCC mixes with 20 mm maximum size aggregate

### 4.3.1. Self-compacting concrete

An extensive laboratory investigation was conducted to produce different grades of self-compacting concrete mixes with 28 day cube nominal compressive strengths of 30 MPa, 40 MPa, 50 MPa, 60 MPa, 70 MPa, and 80 MPa. These mixes had to be, on one hand as fluid as possible to ensure that they filled the formwork under their own weight, passed through closely spaced reinforcement cages without blockage and, on the other hand to be stable to prevent segregation of solids during the flow. This investigation followed the mix design procedure of Deeb and Karihaloo (2013) and the traditional trial and error approach, using the slump cone, J-ring and L-box tests on the trial mixes, until the mix that met the flow-ability and passing ability criteria and had no visible signs of segregation according to the Code (BS EN 206-9 2010) was found. The starting mix proportions were those of a vibrated mix of nominal strength 40MPa made in the same laboratory. The SCC mixes so developed were compared with the corresponding vibrated mixes, also made in the same laboratory. In addition, some of the mixes were found to match with the mixes according to the rational mix design procedure (and the corresponding) design charts very recently proposed by Abo Dhaheer et al. (2015a, b).

#### 4.3.1.1. Materials and mix preparation

The trial mixes were prepared in a small planetary mixer by mixing the coarsest constituent (coarse aggregate up to 20 mm) and the finest one (GGBS), followed by the next coarsest (sand) and next finest constituent (limestone filler), and so on. Before each addition, the constituents were mixed for 2 minutes. To fluidize the dry mix, two-thirds of the super-plasticiser (SP) was added to the water. One-half of this water-SP mixture was added to the dry constituents and mixed for two minutes. One-half of the remaining water-SP mixture was then added and mixed for another two minutes. This process was

continued until all water-SP mixture was added. The remaining one-third of the SP was added and mixed for two minutes just before transferring the SCC mix into the slump cone. The horizontal spread up to 500 mm diameter was timed ($t_{500}$), and the time when the flow stopped ($t_{stop}$) and the corresponding final spread diameter were recorded. If any segregation or bleeding was visible, the mix proportions were judiciously altered. This trial process was continued until the mix met the flow-ability criterion in BS EN 206-9 (2010).

The mix proportions of these mixes are shown in Table 4.1. The binder refers to cement plus GGBS (ground granulated blast furnace slag). The trial mixes with 28-day nominal cube strengths of 30, 40, 50, 60, 70 and 80 MPa (mixes 1, 2, 3, 4, 5, and 6 in Table 4.1) were proportioned guided by the corresponding 40 MPa vibrated concrete (VC) mix proportions produced in the same laboratory, as follows:

- Part of the cement was replaced by the lighter ground granulated blast furnace slag (GGBS) to increase the paste volume and lubricate the aggregate particles. For the same reason limestone filler (maximum particle size 2mm) was added to all SCC mixes;

- The water to binder ratio was reduced from 0.59 for 30 MPa mix to 0.4 for the 80 MPa, whereas the super-plasticiser to binder ratio was increased slightly from 0.0059 for 30 MPa to 0.010 for 80 MPa;

- The fine aggregate (particle size range 0.15-2 mm) content was slightly decreased (by 8.5% to 11%) in the SCC mixes in comparison with the starting vibrated mix;

- The coarse aggregate (crushed limestone without dust, particle size range 4-20mm) content was decreased by 18.5% in the 30 to 60 MPa mixes and by 20.5%

in the 70 and 80 MPa mixes in comparison with the vibrated mix, in order to reduce the inter-particle friction.

**Table 4.1: Mix constituents of the initial VC mix and SCC mixes 1-6 (kg/m$^3$)**

| Constituents | Initial VC Mix | Mix 1 | Mix 2 | Mix 3 | Mix 4 | Mix 5 | Mix 6 |
|---|---|---|---|---|---|---|---|
| **Cement (kg)** | 393 | 220 | 225 | 238.63 | 260 | 270 | 280 |
| **Ground granulated blast furnace slag (GGBS) (kg)** | 0 | 120 | 125 | 130 | 150 | 166 | 170 |
| **Limestone powder < 2mm (kg)** | 0 | 278 | 270 | 257 | 235 | 250 | 258 |
| **Sand (kg)< 2mm** | 786 | 720 | 720 | 715 | 715 | 700 | 700 |
| **Coarse aggregates (kg) (crushed limestone) <20 mm** | 982.5 | 801 | 801 | 801 | 801 | 780 | 780 |
| **Water (kg)** | 220.1 | 200 | 200 | 200 | 193 | 190 | 180 |
| **Water/binder** | 0.56 | 0.59 | 0.57 | 0.54 | 0.47 | 0.44 | 0.40 |
| **Super-plasticiser/binder** | 0 | 0.0059 | 0.0060 | 0.0060 | 0.0061 | 0.0069 | 0.0100 |
| **Super-plasticiser/water** | 0 | 0.010 | 0.010 | 0.011 | 0.013 | 0.016 | 0.025 |
| **Flow spread(mm)** | - | 700 | 700 | 715 | 735 | 720 | 730 |
| **Flow $t_{500}$ (s)** | - | 1.0 | 1.1 | 1.3 | 1.6 | 1.6 | 2.0 |
| **Flow time to stop $t_{stop}$(s)** | - | 15.7 | 16.4 | 17.2 | 20.3 | 17.9 | 20.4 |
| **J-Ring $t_{500j}$(s)** | - | 1.2 | 1.2 | 1.5 | 1.7 | 1.6 | 2.2 |
| **J-Ring Flow spread (mm)** | - | 685 | 680 | 700 | 715 | 695 | 710 |
| **L-box $t_{200}$ (s)** | - | 0.90 | 1.00 | 1.2 | 1.3 | 1.4 | 1.6 |
| **L-box $t_{400}$ (s)** | - | 1.55 | 1.60 | 1.80 | 1.80 | 1.95 | 2.1 |
| **L-box Level-off time (s)** | - | 12.0 | 12.6 | 13.5 | 16.3 | 17.7 | 20.5 |
| **Density of the mix (kg/m$^3$)** | | 2341.0 | 2343.1 | 2343.8 | 2356.5 | 2359.0 | 2372.5 |
| **Compressive strength range Average of 3 cubes (MPa)** | - | 33-35 | 42-46 | 52-54 | 62-65 | 70-73 | 83-84 |
| **Nominal compressive strength (MPa)** | 40 | 30 | 40 | 50 | 60 | 70 | 80 |

Table 4.2 gives the densities of the SCC ingredients.

**Table 4.2: The densities of the SCC ingredients (kg/m$^3$)**

| Cement | GGBS | Water | SP | Limestone | FA | CA |
|---|---|---|---|---|---|---|
| **2950** | 2400 | 1000 | 1070 | 2400 | 2650 | 2800 |

The time taken by the fresh SCC mix to reach a 500mm diameter spread in the slump cone flow ($t_{500}$) as well as the time to stop flowing ($t_{stop}$) were determined for each mix

from time sequencing a video recording of the test with an accuracy of a thousand of a second. Moreover from the same videos the rates of cone lifting also have been determined from the times taken to lift the cone to a height of 300mm (Table 4.3). The resistance to segregation was checked visually. Figures 4.2 to 4.4 show the horizontal spread of SCC Mixes 1 to 6, respectively. All these mixes fall into the low viscosity class 1 (VS1) with $t_{500} \leq 2$ s according to BS EN 206-9: 2010.

**Table 4.3: The cone lift rates for the mixes 1-6 determined from video recordings**

| Mix no. | 1 | 2 | 3 | 4 | 5 | 6 |
|---|---|---|---|---|---|---|
| **Cone lift rate CLR (m/s)** | 0.90 | 0.9 | 0.69 | 0.69 | 1.00 | 0.76 |

**Figure 4.2: Horizontal spread of SCC Mix 1 (left) and Mix 2 (right)**

**Figure 4.3: Horizontal spread of SCC Mix 3 (left) and Mix 4 (right)**

**Figure 4.4: Horizontal spread of SCC Mix 5 (left) and Mix 6 (right)**

It should be mentioned that in the development of the above mixes, we found no need to add a viscosity modifying admixture (VMA) to reduce bleeding or to increase the resistance to segregation.

#### 4.3.1.2. Passing ability test (J-Ring)

J-ring is a test used in conjunction with the slump cone to assess the passing ability of SCC through gaps in the obstacles, e.g. reinforcement. For this test, slump test

apparatus is used with an open steel ring with 10 steel rods (diameter = 16mm and height = 100mm), as shown in the Figure 4.5. The gap between the bars is 78mm$\pm$1.

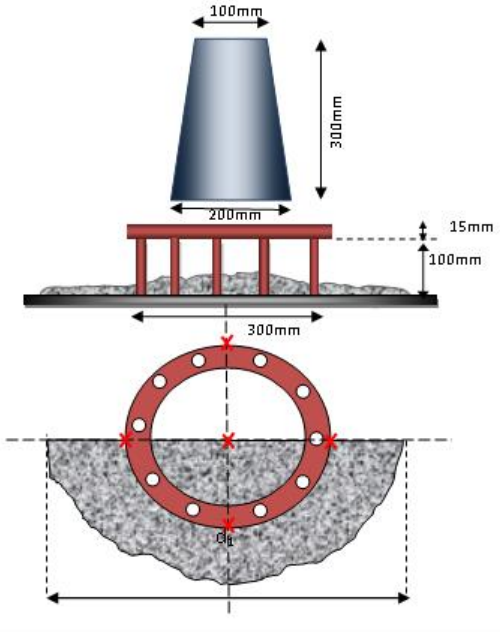


**Figure 4.5: J-ring test apparatus**

After filling the cone with concrete without using any vibration or rodding, the cone is lifted perpendicular to the steel base plate allowing the concrete to flow freely. The time needed for the flow to reach 500mm diameter is recorded as J-Ring $t_{500j}$, and the flow allowed to stop before recording the spread. All the above mixes that had satisfied the flow-ability criterion and had showed no signs of segregation were subjected to the passing ability test using the J-ring to ensure that they were able to pass through the narrow gaps that exist between the reinforcing bars in a real reinforced concrete structural element. For this purpose, a 300mm diameter J-ring apparatus with 10 steel rods (each of diameter 16mm) was used, as recommended by The European Federation of National Trade Associations (EFNARC, 2005).

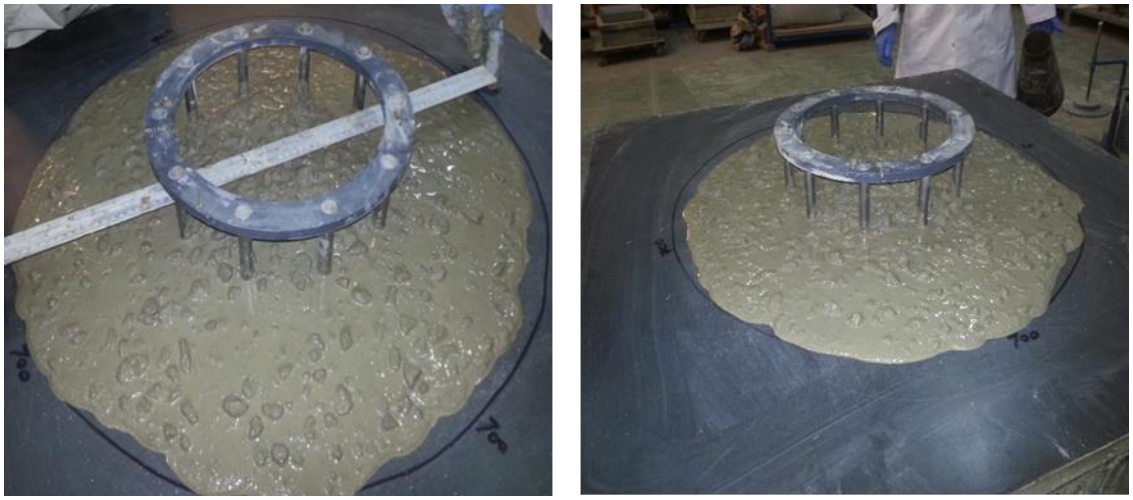

**Figure 4.6: Flow and passing ability of SCC Mix 1 (left) and Mix 2 (right)**

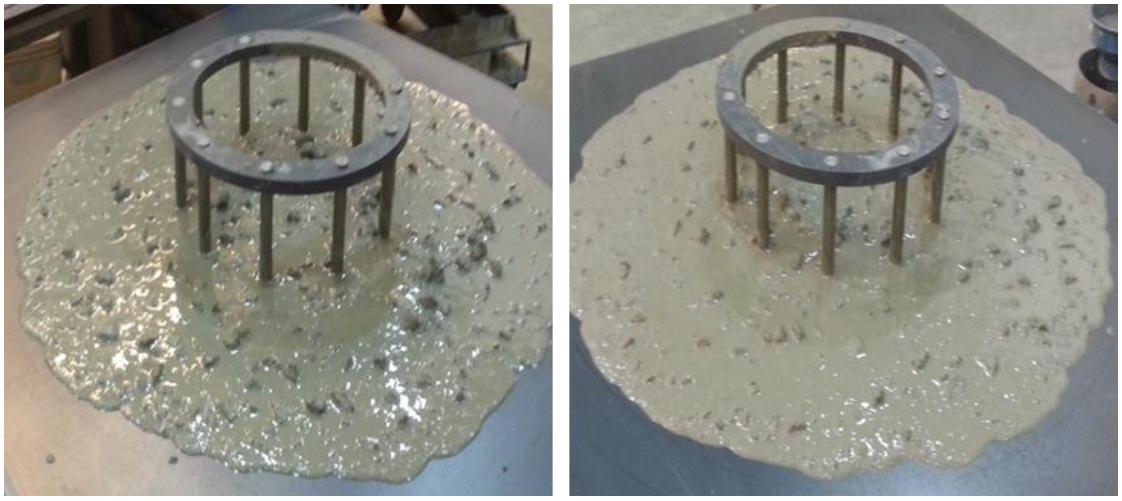

**Figure 4.7: Flow and passing ability of SCC Mix 3 (left) and Mix 4 (right)**

**Figure 4.8: Flow and passing ability of Mix 5 (left) and Mix 6 (right)**

All the SCC mixes reported in Table 4.1 met the passing ability criterion based on (BS EN 12350-12: 2010), (EFNARC, 2005) and (PCI, 2003) recommendations (Figures 4.6-4.8).

However, it is not unusual to find that mixes that pass the flow-ability test do not meet the passing ability criterion, especially when large aggregates are present in the SCC mix. Figure 4.9 shows large aggregates are nested around the steel rods in an earlier trial version of Mix 2 that had met the flow-ability criterion. In such instances, the paste content had to be increased.

**Figure 4.9: Large aggregates are nested around the steel rods in an earlier trial version of Mix 2 that had met the flow-ability criterion**

#### 4.3.1.3. L-box test

In order to test the ability of a SCC mix to fill the formwork containing reinforcement under its own weight, the L-box apparatus with adjustable steel rods (each of diameter 12mm) was used (BS EN12350-10: 2010; EFNARC, 2005; PCI, 2003). The vertical leg of the L-box is filled with the SCC mix. At the bottom of this leg is a gate with two or three rods in front of it. When the gate is lifted, the mix flows into the horizontal part of the L-box through the gaps between the rods. The times for the mix to reach 200 mm ($t_{200}$) and 400 mm ($t_{400}$) from the gate are recorded, as well as the time it takes the mix to level off in the horizontal leg of the L-box. Again, it is required that no large aggregate particles be blocked by the rods.

The clearance between the bars when using 2 bars and 3 bars is $59 \mp 1$mmand $41 \mp 1$ mm, respectively, as illustrated in Figure 4.10.

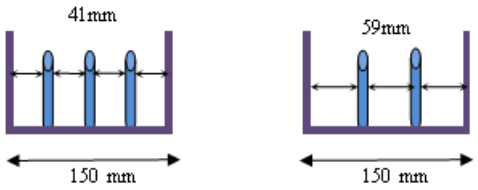


**Figure 4.10: Clearance when using 3 or 2 steel rod bars**

At least 14 litres (BS EN12350-10: 2010) of SCC concrete were prepared in a pan mixer and measurements were recorded.

**Figure 4.11: Flow and passing ability of SCC Mix 1 (left) and Mix 2 (right)**

**Figure 4.12: Flow and passing ability of SCC Mix 3 (left) and Mix 4 (right)**

**Figure 4.13: Flow and passing ability of SCC Mix 5 (left) and Mix 6 (right)**

Three steel rods were used for SCC mixes (Mix 1 to Mix 6), Figures 4.11 to 4.13.

All designed mixes that had passed the J-ring test also passed the L-box test without any further alteration.

## 4.4. Testing in hardened state

Cube specimens were cast from all SCC mixes that met the flow ability, passing ability and no segregation criteria and were cured in water. Some of the cubes from each mix were tested in compression at the age of 3 and 7 days in order to follow the trend in strength gain, Figure 4.14. As expected, the rate of strength gain increases with increasing compressive strength because of the increased amount of binder in the mix. The remaining cubes from each mix were further cured in water and then tested at the age of 28 days. The compressive strength range of each SCC mix is given in Table 4.1.

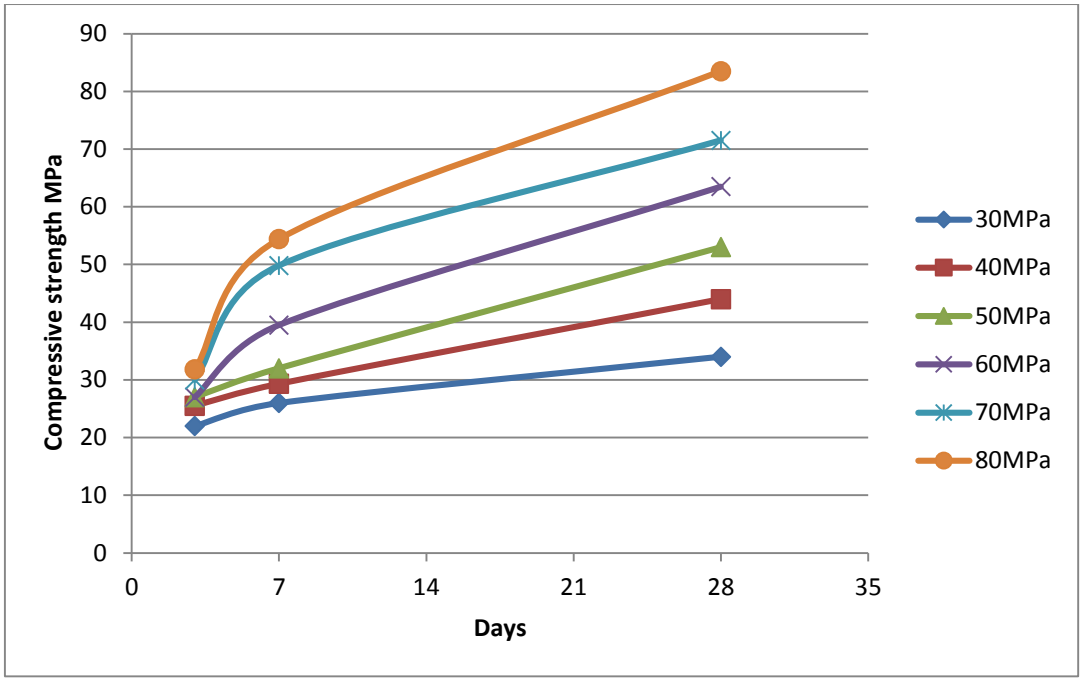


**Figure 4.14: Gain of mean cube compressive strength with age**

## 4.5. Comparison between self-compacting and vibrated concrete mixes

The paste to solids ratios by volume in the above self-compacting concrete mixes are compared in Table 4.4 with their counterpart vibrated concrete mixes, Taylor (1997), ranging in the 28-day compressive strength from 30 to 80 MPa which had also been developed in the same laboratory at Cardiff University over many years.

**Table 4.4: Comparison of paste to solids ratio by volume between SCC and VC mixes of equal compressive strength**

| Compressive strength (MPa) | 30 | 40 | 60 | 80 |
|---|---|---|---|---|
| **Paste(SCC)** | 0.442 | 0.442 | 0.444 | 0.457 |
| **Solids(SCC)** | 0.558 | 0.558 | 0.556 | 0.543 |
| **Water/Binder (SCC)** | 0.59 | 0.57 | 0.47 | 0.40 |
| **Paste/Solids(SCC)** | 0.792 | 0.792 | 0.798 | 0.841 |
| **Paste(VC)** | 0.353 | 0.337 | 0.316 | 0.309 |
| **Solids(VC)** | 0.647 | 0.663 | 0.684 | 0.691 |
| **Water/Binder (VC)** | 0.56 | 0.50 | 0.44 | 0.39 |
| **Paste/Solids(VC)** | 0.545 | 0.509 | 0.462 | 0.447 |

Table 4.4 confirms that, for the same compressive strength and almost the same water to binder ratio, the paste to solids ratio in a SCC mix is much higher than in the counterpart vibrated concrete mix.

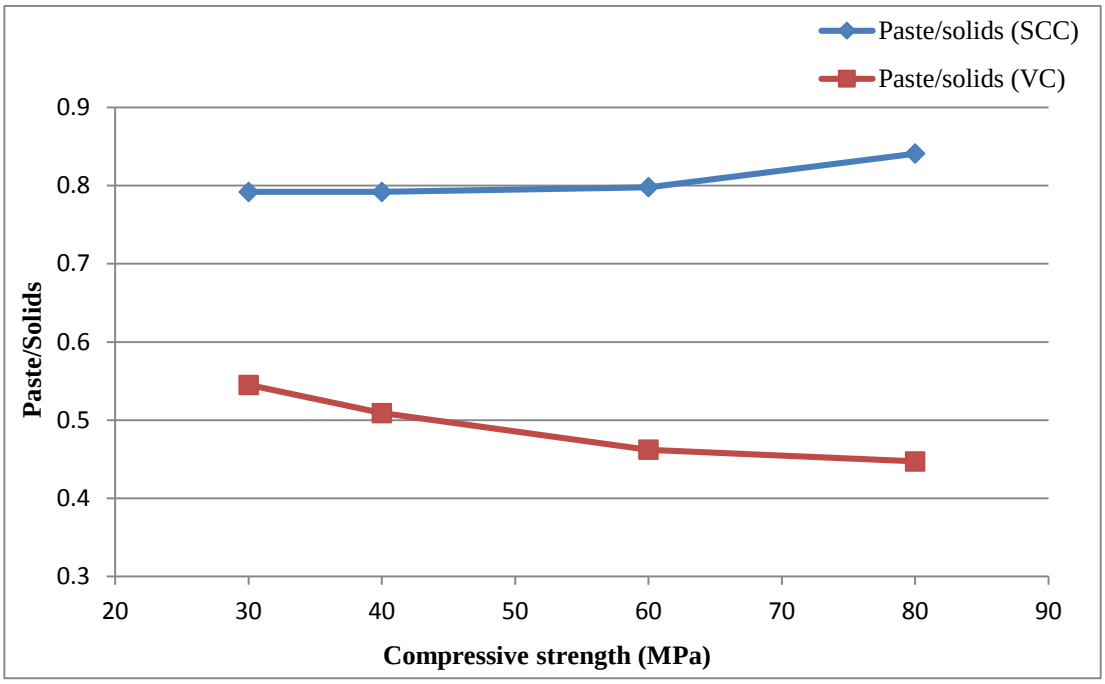


**Figure 4.15: Paste to solids ratio by volume in SCC and vibrated concrete (VC) mixes (Taylor,1997)**

It should be noted that the compressive strength of concrete can be increased mainly by decreasing the water to binder ratio which can be achieved by either increasing the binder content or decreasing the water content. These changes have an opposite effect on the volume of paste; an increase in the binder content increases this volume, whereas a decrease in the water content reduces it. This explains the different trends for SCC and VC mixes observed in Figure 4.15.

## 4.6. Estimation of the plastic viscosity

The rheology of SCC is best described by the Bingham constitutive model. This model contains two material properties, namely the yield stress $\tau_y$ and the plastic viscosity $\eta$. The yield stress of SCC mixes is very low (around 200 Pa) in comparison with normal

concretes (thousands of Pascal) and remains nearly constant over a wide range of plastic viscosities (Dransfield, 2003).

The viscosity of a homogeneous viscous fluid such as the cement paste can be measured accurately which cannot be said about heterogeneous viscous fluids such as SCC. Ghanbari and Karihaloo (2009) have developed a micromechanical procedure for accurately estimating the plastic viscosity of SCC from the known plastic viscosity of cement paste and the volume fraction of the solid constituents. This procedure has been shown to predict the plastic viscosity of SCC mixes that agree very well with measured values (Ghanbari and Karihaloo, 2009). Deeb, et al. (2014a, b) used the same procedure to estimate the plastic viscosity of the SCC mixes with steel fibres.

There is contradictory evidence available in the literature on the effect of GGBS replacement on the viscosity of cement paste, depending on the type of viscometer used (Nehdi and Rahman, 2004: Table 1 page 1998). Some results show a slight decrease in the viscosity, while others show the opposite trend. Therefore we assume

$\eta_c \approx \eta_b$

where

$\eta_c$ = viscosity of cement paste alone

$\eta_b$= viscosity of cement paste containing GGBS

The plastic viscosities of the cement pastes used in the SCC mixes (Tables 4.1) developed above, which is mainly influenced by water to cement and super-plasticiser to water ratios, (Sun et al., 2006) was estimated to be between 0.145 Pa s and 0.315 Pa s. The effect of air voids (volume fraction = 2%) on the viscosity of cement paste is calculated using Eq. 4.1 (see below for explanation)

$$\eta_{b+airvoids}=\eta_b(1+\phi_{air\ voids}) \quad (4.1)$$

**Table 4.5: Estimated plastic viscosity of cement paste (cement + GGBS + water + SP + air voids)**

| Mix No. | w/b | $\eta_b$ | $\eta_{b+\text{ air voids}}$ |
|---|---|---|---|
| **1** | 0.59 | 0.145 | 0.148 |
| **2** | 0.57 | 0.170 | 0.173 |
| **3** | 0.54 | 0.195 | 0.199 |
| **4** | 0.47 | 0.270 | 0.275 |
| **5** | 0.44 | 0.290 | 0.296 |
| **6** | 0.40 | 0.315 | 0.321 |

In the procedure proposed by Ghanbari and Karihaloo (2009), a viscous concrete mix is regarded as a succession of two-phase suspensions. At each stage, the suspension consists of a liquid phase in which is suspended a discrete solid phase. Figure 4.16 shows the hierarchy of these two-phase liquid-solid suspensions used in the estimation of the plastic viscosity of all mixes developed above based on the viscosity of the binder paste used in them.

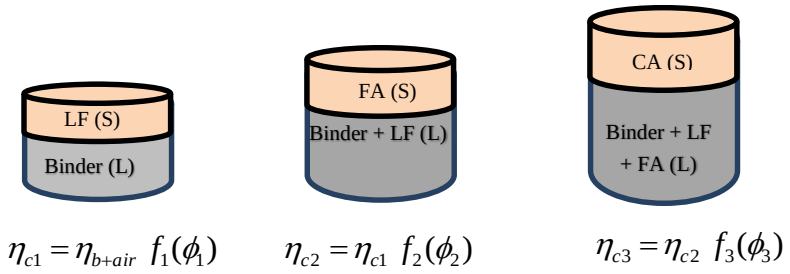


**Figure 4.16: Hierarchy of two-phase liquid-solid suspensions constituting an SCC mix showing the liquid (L) and solid (S) phases in each suspension.**

In Figure 4.16

LF= Limestone filler

FA= Fine aggregate

CA= Coarse aggregate

The plastic viscosity of the *i*-th liquid-solid suspension can be estimated from the plastic viscosity of the preceding phase as follows:

$$\eta_{Ci} = \eta_{Ci-1} f_i(\phi_i) \quad (4.2)$$

with $\eta_{C0} = \eta_b$ being the known plastic viscosity of the binder paste. For instance, limestone filler (LF) materials form the solid phase in the viscous binder paste (with air voids) in the first liquid-solid suspension. The plastic viscosity of this suspension is calculated from the known plastic viscosity of the binder paste (with air voids) (Table 4.5). This process is repeated until all the solid ingredients of SCC have been accounted for.

The function $f_i(\phi_i)$ depends only on the volume fraction of solid phase $\phi_i$

$$\phi_i = \frac{v_i}{v_i + v_0} \quad (4.3)$$

where

$v_i$: volume of solid phase $i$; $v_0$: volume of the continuous matrix liquid phase in which the solid phase $i$ is suspended;

If the volume fraction is less than 10%, the function $f_i(\phi_i)$ can be expressed by the Einstein equation in the following form

$$f_i(\phi_i) = 1 + [\eta]\phi_i \quad (4.4)$$

where $[\eta]$ is a numerical factor. It equals 2.5 for rigid spheres and 1.0 for spherical voids arranged in a random hexagonal form and when the distance between them is large compared to the mean particle or void diameter. It was subsequently shown that the numerical factor 2.5 is accurate even for ellipsoidal particles with aspect ratio less than 3. The expression for spherical voids was used above in Eq. 4.1.

However, when the volume fraction of solid phase exceeds 10% but is less than the maximum possible volume fraction $\phi_m$, then $f_i(\phi_i)$ depends not only on the volume fraction of the solid phase but also on how they are dispersed in the fluid and on their shape. $\phi_m$ represents the situation in which the particles have the minimum possible separation, i.e. the void fraction (porosity) is the least and the viscosity is infinite. The value is 0.74 for hexagonal closed packing, 0.637 for random hexagonal packing, and 0.524 for cubic packing.

This dependence is captured by the formula proposed by Krieger and Dougherty (1959) given below:

$$f_i(\phi_i) = (1 - \frac{\phi_i}{\phi_m})^{-[\eta]\phi_m} \tag{4. 5}$$

The numerical factors $[\eta]$ and $\phi_m$ depend upon the shear rate; the former tends to decrease with increasing shear rate (i.e. shear thinning), whereas the latter shows the opposite trend. However $[\eta]$ and $\phi_m$ change in such a way that an increase in the one leads to a decrease in the other, but the product of the two changes remains practically the same and equal on average to 1.9 for rigid spheres. The numerical factor changes because the packing changes from loose to dense as the volume fraction of solid phase increases.

## 4.7. Application to designed SCC mixes

In this section the plastic viscosity of mix compositions (Table 4.1) is determined using the above micro-mechanical procedure proposed by Ghanbari and Karihaloo (2009). As mentioned above, this plastic viscosity together with yield stress is necessary to simulate the flow of SCC mixes.

The calculation of the plastic viscosity will be demonstrated on the example of Mix 3. The plastic viscosities of all SCC mixes developed above have been calculated in the same manner.

**Step 1:** Estimating the plastic viscosity of the liquid phase (binder paste (CP))

The plastic viscosity of the binder paste (cement + GGBS+ super-plasticiser +water + air) is estimated (Table 4.5) to be:

$$\eta_{cp}(\phi_{cp}) = 0.199 \text{ Pa s} \quad (4.6)$$

**Step 2:** The first solid phase limestone filler (LF) is added to the liquid binder phase, as shown in Figure 4.17

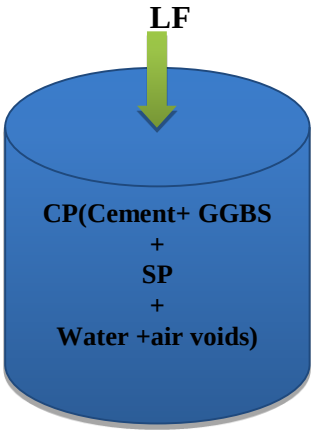


**Figure 4.17: The first solid phase (LF) is added to the liquid phase (Paste)**

The volume fraction of the solid phase is determined using Equation (4.7)

$$\phi_{LF} = \frac{v_{LF}}{v_{LF} + v_{CP}} \quad (4.7)$$

Here, $v_{LF}$ is the volume of the solid phase (LF), $v_{CP}$ is the volume of the continuous liquid phase in which the solid phase is suspended.

After calculating the volume of each ingredient in the mix (Table 4.1) using the densities from Table 4.2 the volume of paste is $v_{CP} = 0.35\,\mathrm{m}^3$

The volume fraction of LF is (See Tables 4.1 and 4.2)

$$\phi_{LF} = \frac{0.105}{0.105 + 0.35}$$

$$\phi_{LF} = 0.2307 > 10\% \qquad (4.\ 8)$$

Using Equation (4.5) for cubic packing with [η] $\phi_m$ = 1.9 and $\phi_m$= 0.524, gives

$$f_{LF}(\phi_{LF}) = (1 - \frac{0.2307}{0.524})^{-1.9} = 3.01 \qquad (4.\ 9)$$

Based on Equation (4.2) the plastic viscosity of the mix so far is:

$$\eta_{LF+CP}(\phi_{LF+CP}) = 3.01 \text{ x } 0.199 = 0.599 \text{ Pa s} \qquad (4.\ 10)$$

**Step 3:** Next add the fine aggregates (FA) to the liquid phase from the previous step (Figure 4.18)

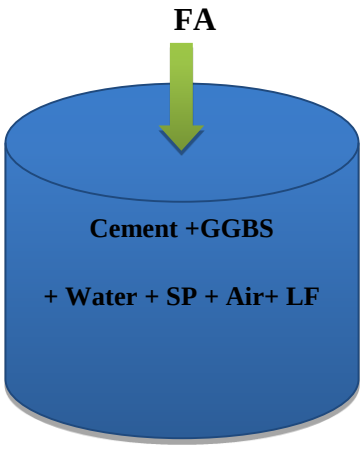


**Figure 4.18: Adding the second solid phase (fine aggregates)**

The volume fraction of FA is

$$\phi_{FA} = 0.3676 > 10\% \quad (4.11)$$

Using Equation (4.4) for random hexagonal packing with $[\eta]\phi_m$ = 1.9 and $\phi_m$= 0.637, gives

$$f_{FA}(\phi_{FA}) = (1 - \frac{0.3676}{0.637})^{-1.9} = 5.13 \quad (4.12)$$

Based on Equation (4.2) the plastic viscosity of the mix so far is:

$$\eta_{FA+LF+CP}(\phi_{FA+LF+CP}) = 5.13\text{x}0.599 = 3.07 \text{Pa s} \quad (4.13)$$

**Step 5:** Final step is adding the coarse aggregates (CA) to the liquid phase from the previous step (Figure 4.19)

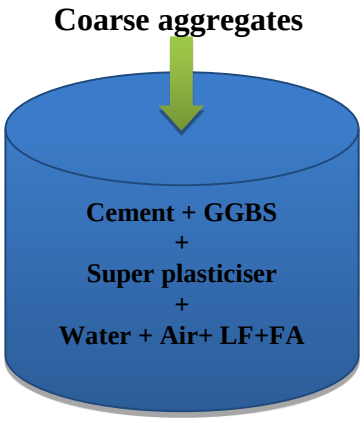


**Figure 4.19: Adding the next solid phase (coarse aggregates)**

The volume fraction of CA is:

$$\phi_{CA} = 0.2804 > 10\% \quad (4.14)$$

Using Equation (4.4) for hexagonal closed packing with $[\eta]\phi_m$ = 1.9 and $\phi_m$= 0.74, gives

$$f_{CA}(\phi_{CA}) = (1 - \frac{0.2804}{0.74})^{-1.9} = 2.47 \quad (4.15)$$

Based on Equation (4.2) the eventual plastic viscosity of the SCC mix 3 is:

$$\eta_{CA+FA+LF+CP}(\phi_{CA+FA+LF+CP}) = 2.47\text{x}3.07 = 7.6 \text{ Pa s} \quad (4.16)$$

**Table 4.6: Estimated plastic viscosity of SCC mixes**

| Mix | Plastic viscosity, Pa s |
|---|---|
| **Mix 1** | 6.57 |
| **Mix 2** | 7.31 |
| **Mix 3** | 7.60 |
| **Mix 4** | 9.31 |
| **Mix 5** | 9.36 |
| **Mix 6** | 10.62 |

The plastic viscosities of the SCC mixes reported above (see Table 4.1) estimated using the procedure just described are given in Table 4.6. Judging by the excellent predictive capability of this procedure (Ghanbari and Karihaloo, 2009), it is reasonable to assume that the plastic viscosities given in Table 4.6 are very accurate. The use of three packing types from the loose cubic in Step 2 to dense hexagonal close in Step 3 is justified by the fact that the mix packing increases progressively as more solid material is added.

## 4.8. Comparison of the SCC mixes with the rational mix design

As mentioned above, the SCC mixes of Table 4.1 were proportioned using the rigorous method proposed by Deeb and Karihaloo (2013) based on the desired plastic viscosity of the mix and the traditional trial and error. The desired viscosity depends on the application and can be chosen following the EFNARC guidelines (2005). The rational mix proportioning method of Deeb and Karihaloo (2013) exploits the expression for the plastic viscosity (Eq. 4.2) of an SCC mix developed by Ghanbari and Karihaloo (2009). As described above, this expression shows how the known plastic viscosity of the paste is increased by the addition of solid phase particles, i.e. filler, fine and coarse aggregates. The contribution of each of the solid phases to the overall increase depends on its volume fraction and shape of its particles. As a result, the final expression for the plastic viscosity of an SCC mix is the product of the known plastic viscosity of the paste and contributions of each of the solid phases. Whilst this method for proportioning SCC

mixes is rigorous and based on sound physical principles, it produces a bewildering array of mixes that reach the target plastic viscosity but does not give any practical guidelines on how to choose the most appropriate mix. That is why it had to be combined with the traditional trial and error based on a vibrated concrete mix. Moreover, the method was developed on the basis of reference mixes of a range of known cube compressive strength, but the latter was not explicitly imposed as a design criterion.

Very recently Abo Dhaheer et al. (2015 a, b) have overcome the above shortcomings of this method for proportioning SCC mixes and provided practical guidelines in the form of design charts for choosing the mix proportions that achieve the target plastic viscosity in the range 3 to 15 Pa s and the target cube compressive strength in the range 30 to 80 MPa. It is therefore appropriate to check whether or not the SCC mixes of Table 4.1 fall within the design charts provided by Abo Dhaheer et al. (2015a). In the design charts (typical charts for cube compressive strengths ranging from 30 to 80 MPa are shown in Figures 4.20-4.25) the vertical axis gives the ratio of the mass of a solid phase to the desired plastic viscosity. As seen from Figures 4.20-4.25, the charts give four curves, each with mean and scatter. The bottom most curve gives the mass of binder (i.e. cementitious material, cm), the second curve from bottom gives the combined mass of binder and LP (i.e. limestone powder), the third curve from bottom gives the combined mass of binder, LP and FA, and finally the top curve gives the combined mass of binder, LP, FA and CA. Thus knowing the desired plastic viscosity it is possible to calculate the masses of binder, LP, FA, and CA in a stepwise manner beginning with the bottom curve on the chart corresponding to the desired cube compressive strength.

It is important to distinguish LF used in SCC mixes of Table 4.1 from LP used in design charts. The LP refers only to the fine fraction (≤125 $\mu m$) of LF; the coarser fraction of LF (125 $\mu m$ -2 $mm$) is regarded as a part of FA in the charts. In the LF used in mixes 1-6 of Table 4.1 it has been found by particle size analysis that the fractions of fine and coarse LP are in the ratio 0.4 to 0.6. This will be used below. It is however clear that this distinction makes no change to the mix plastic viscosity. Also, Abo Dhaheer et al. (2015b) have shown that it has very little, if any, effect on the cube compressive strength of the mix.

Let us check if the mixes 1-6, Table 4.1 (cube compressive strength from 30 to 80 MPa, plastic viscosity from 6.57 to 10.62 Pa s) could have been proportioned using the corresponding design charts of Abo Dhaheer et al. (2015a) reproduced in Figures 4.20-4.25.

**Table 4.7: Comparison of the mixes 1- 6 (Table 4.1) with the rational mix design**

| | **cm (cement + GGBS)** | **cm + 0.4 LF = cm + LP** | **cm + LP 0.6 LF + FA** | **cm + LP +0.6 LF + FA + CA** | **Compressive strength, MPa** | **w/b** | **$\eta_{mix}$, Pa s** |
|---|---|---|---|---|---|---|---|
| **Mix 1 (kg)** | 340 | 451.2 | 1338 | 2139 | 30 | 0.59 | 6.57 |
| **(Column / $\eta_{mix}$)** | 51.7 | 68.7 | 203.6 | 325.6 | | | |
| **Mix 2 (kg)** | 350 | 458 | 1340 | 2141 | 40 | 0.57 | 7.3 |
| **(Column / $\eta_{mix}$)** | 48 | 63 | 183 | 293 | | | |
| **Mix 3 (kg)** | 368.6 | 471.4 | 1340.6 | 2141.6 | 50 | 0.54 | 7.6 |
| **(Column / $\eta_{mix}$)** | 48 | 62 | 176 | 282 | | | |
| **Mix 4 (kg)** | 410 | 504 | 1360 | 2161 | 60 | 0.47 | 9.31 |
| **(Column / $\eta_{mix}$)** | 44 | 54 | 146 | 232 | | | |
| **Mix 5 (kg)** | 436 | 536 | 1386 | 2166 | 70 | 0.44 | 9.34 |
| **(Column / $\eta_{mix}$)** | 47 | 57 | 148 | 232 | | | |
| **Mix 6 (kg)** | 450 | 553.2 | 1408 | 2188 | 80 | 0.40 | 10.62 |
| **(Column / $\eta_{mix}$)** | 42 | 52 | 133 | 206 | | | |

The entries above for mixes 1-6 of Table 4.1 are plotted on Figures 4.20-4.25; the vertical line corresponds to the plastic viscosity of a given mix (last column in Table 4.6), whereas the four horizontal lines correspond to entries in row (Column / $\eta_{mix}$ ) of this mix.

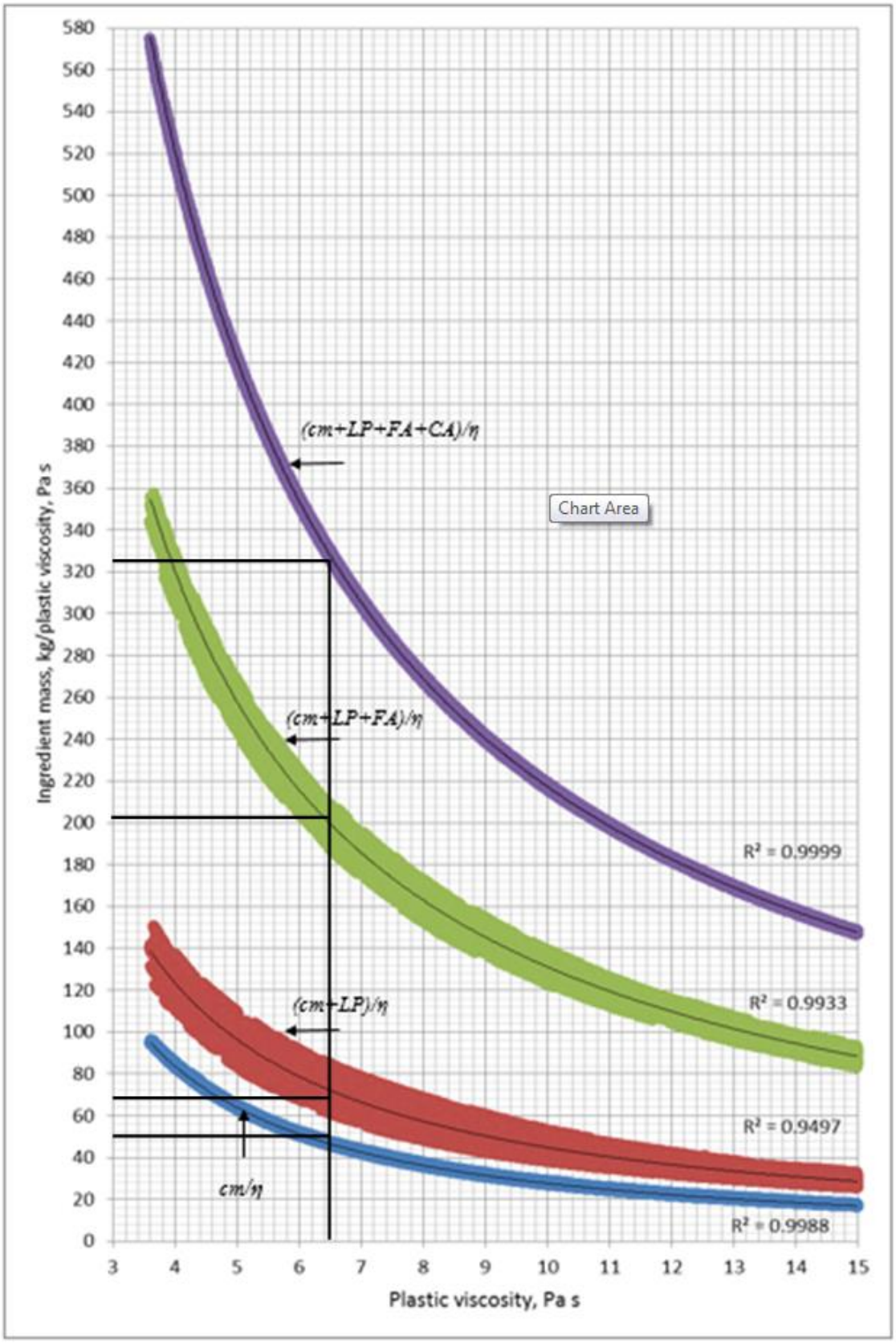


**Figure 4.20: Ingredient mass (kg) normalised by mix plastic viscosity vs plastic viscosity for 30 MPa mix (After: Abo Dhaheer et al., 2015a)**

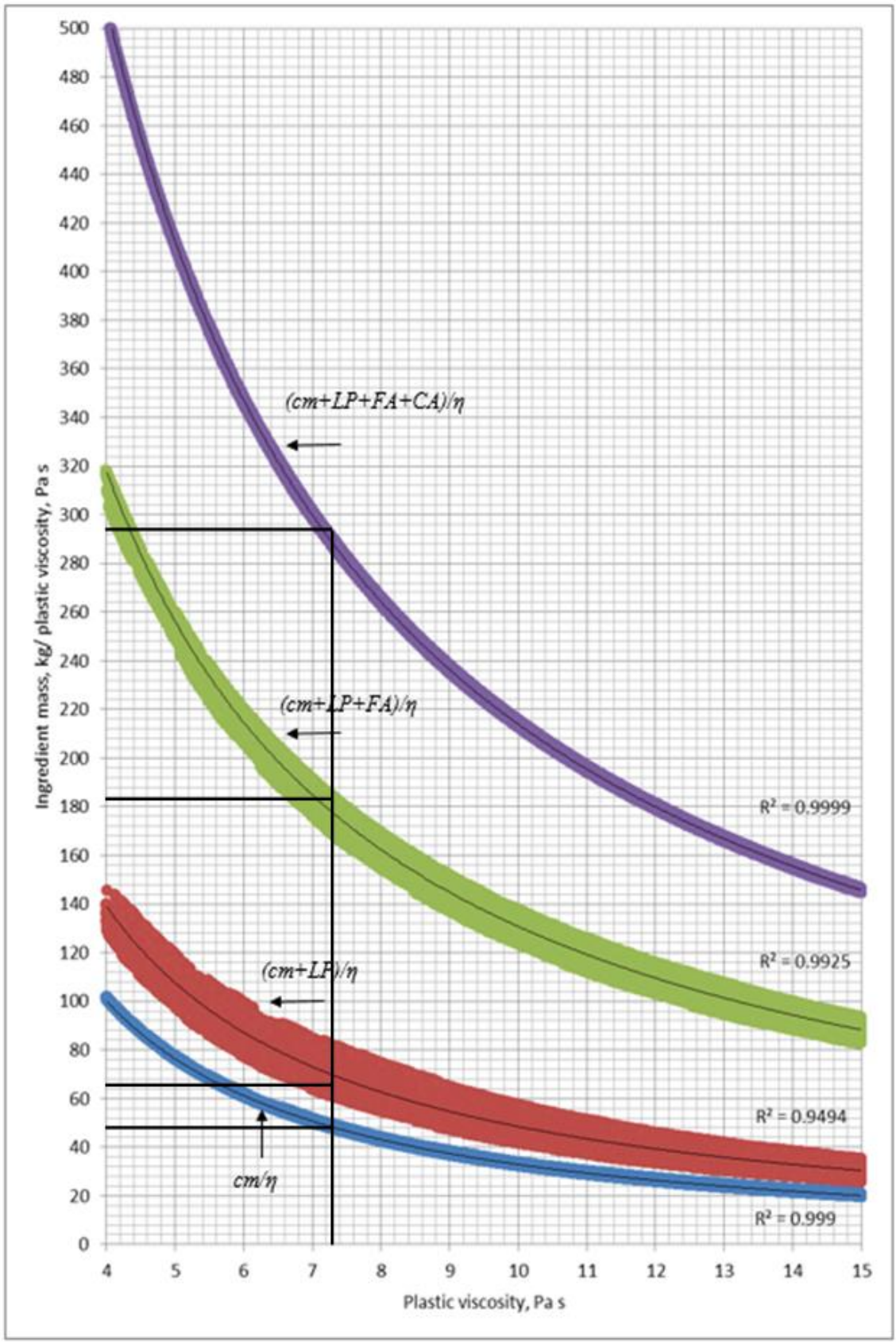


**Figure 4.21: Ingredient mass (kg) normalised by mix plastic viscosity vs plastic viscosity for 40 MPa mix (After: Abo Dhaheer et al., 2015a)**

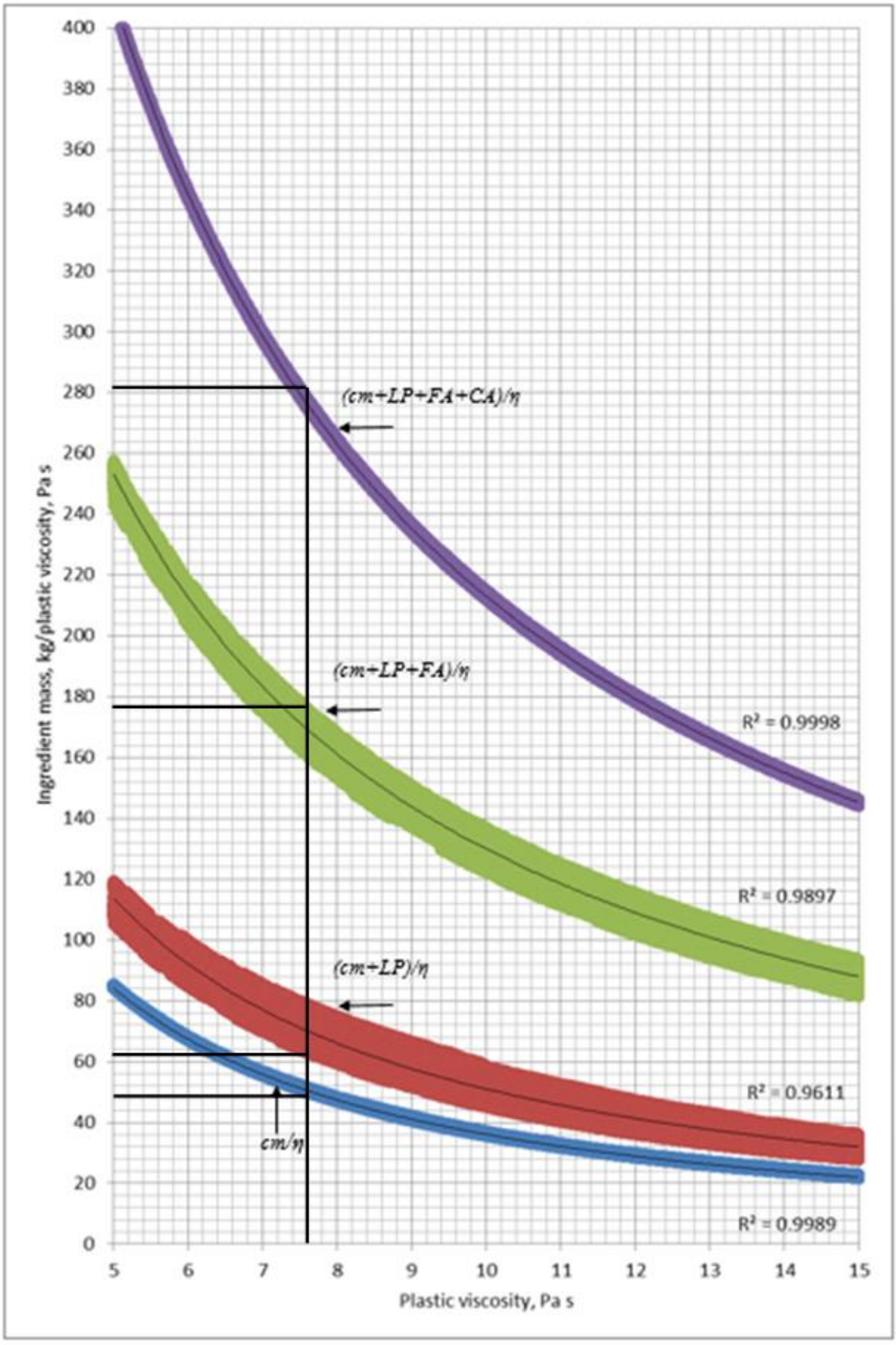


**Figure 4.22: Ingredient mass (kg) normalised by mix plastic viscosity vs plastic viscosity for 50 MPa mix (After :Abo Dhaheer et al. 2015a)**

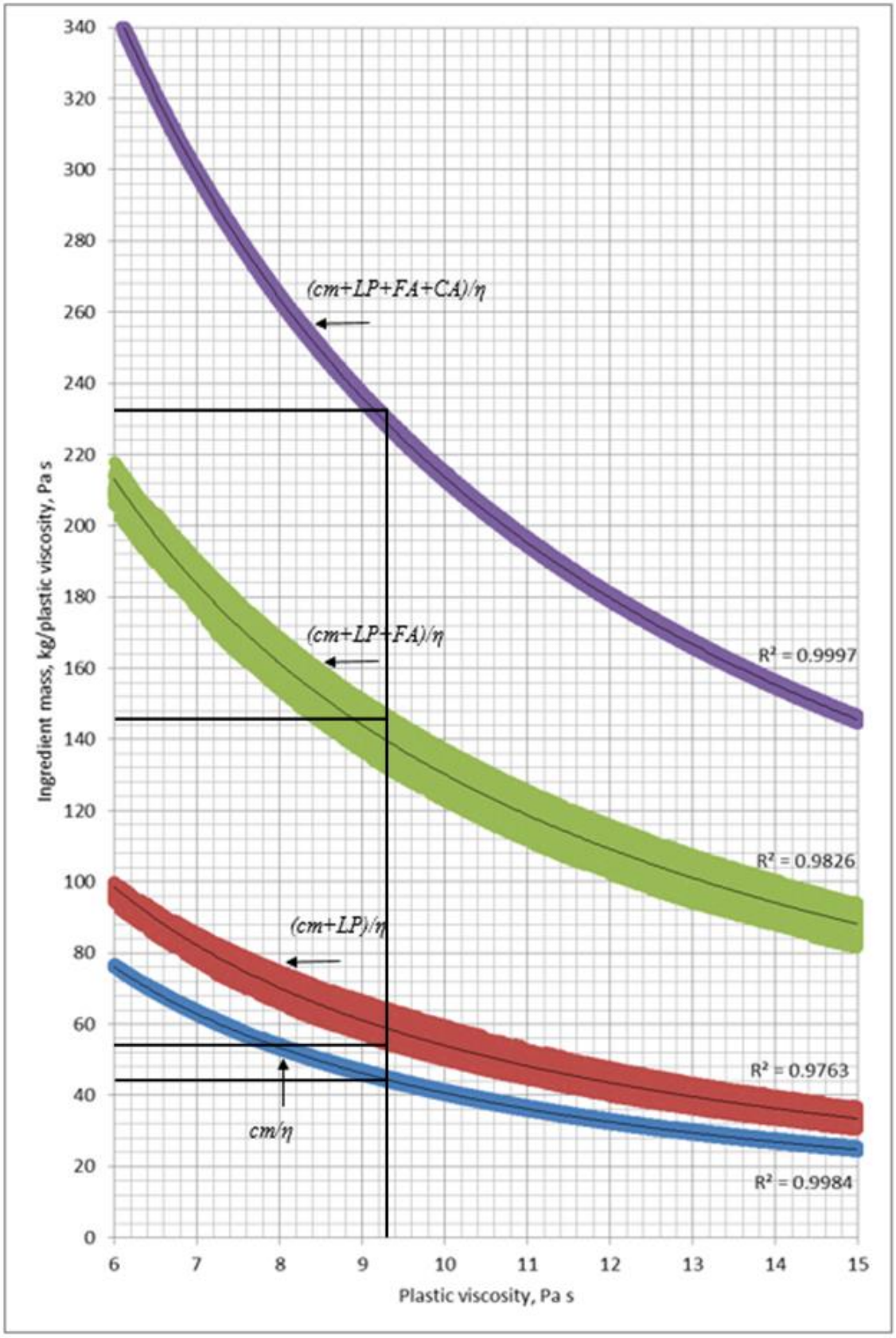


**Figure 4.23: Ingredient mass (kg) normalised by mix plastic viscosity vs plastic viscosity for 60 MPa mix (After :Abo Dhaheer et al. 2015a)**

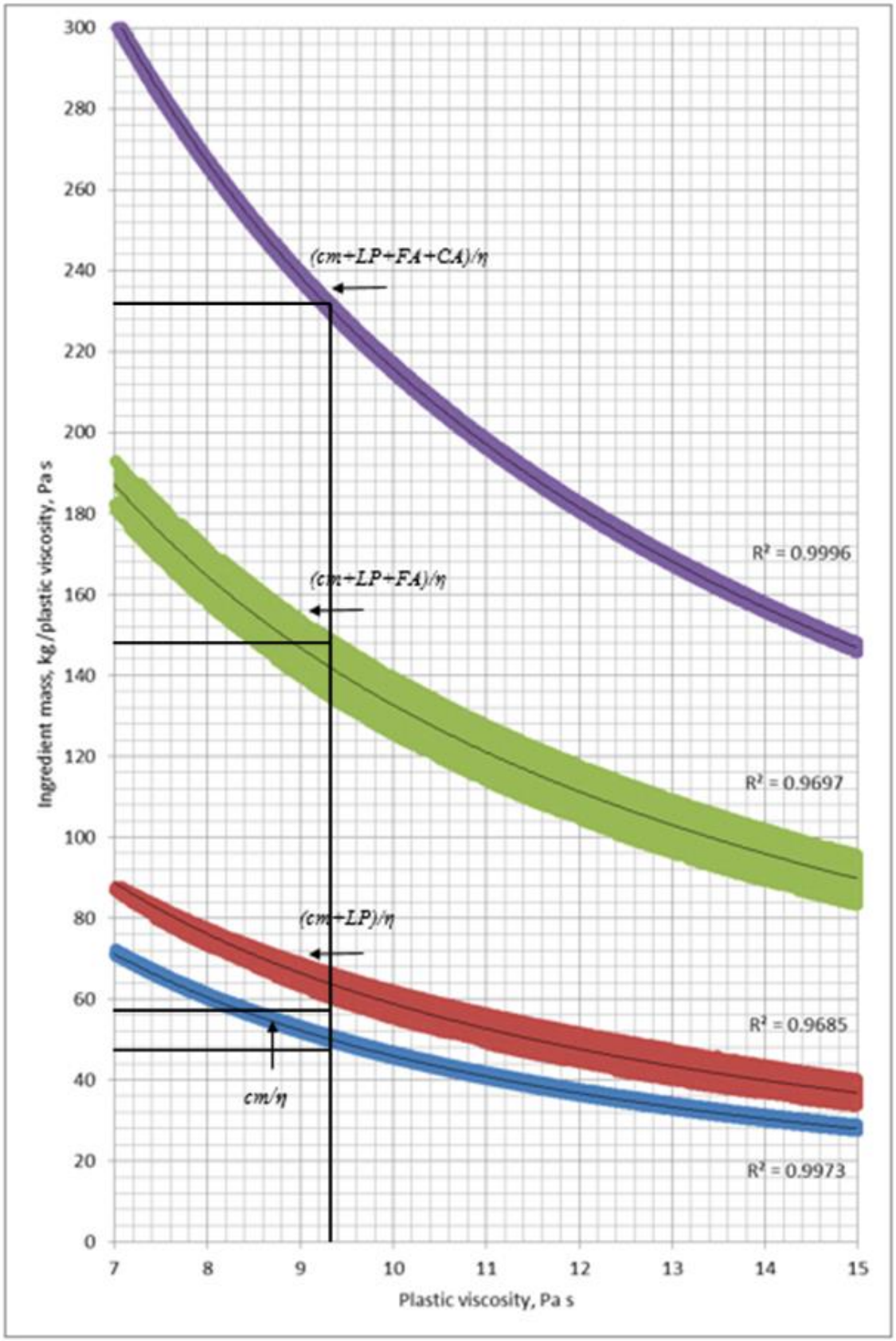


**Figure 4.24: Ingredient mass (kg) normalised by mix plastic viscosity vs plastic viscosity for 70 MPa mix (After :Abo Dhaheer et al. 2015a)**

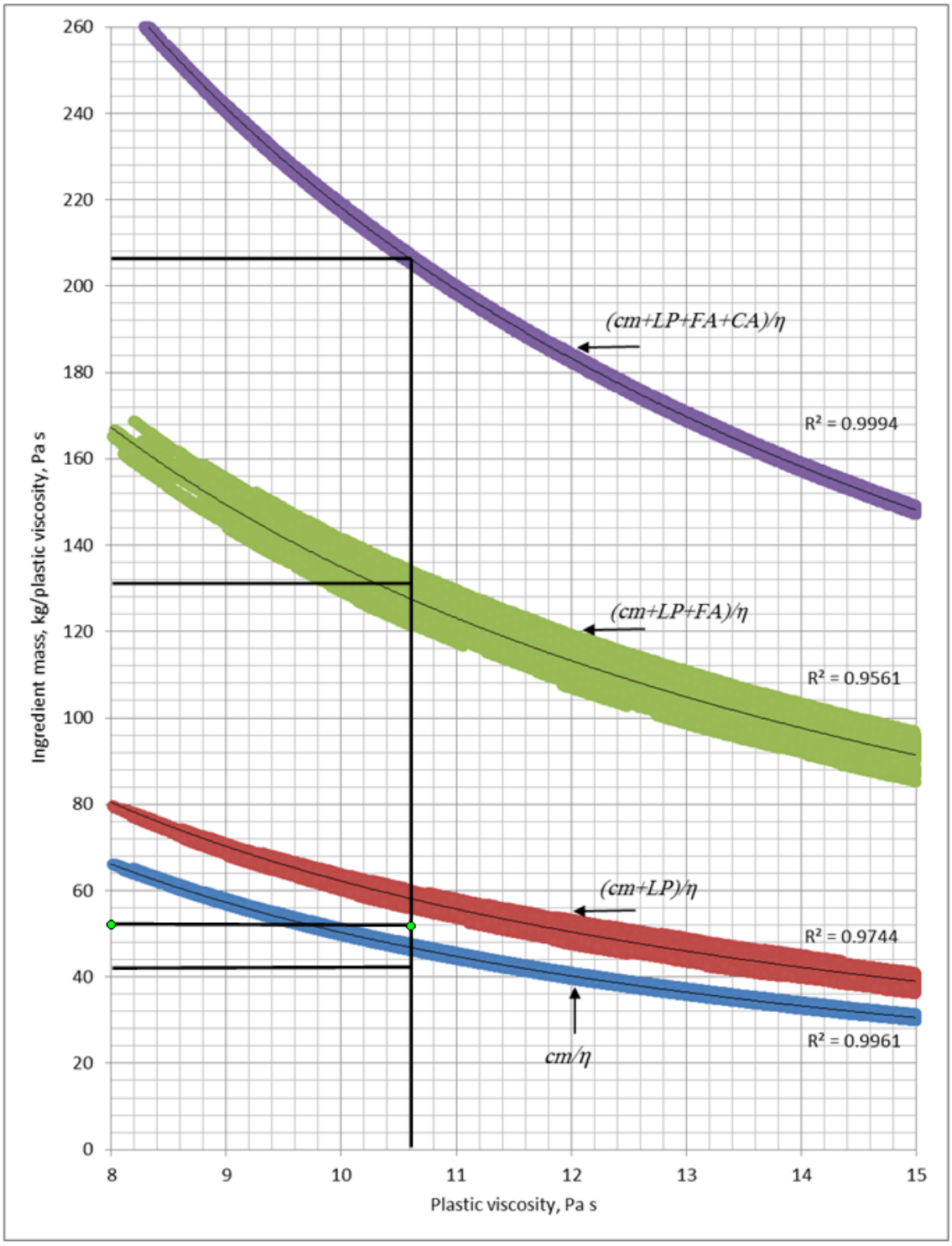


**Figure 4.25: Ingredient mass (kg) normalised by mix plastic viscosity vs plastic viscosity for 80 MPa mix (After :Abo Dhaheer et al. 2015a)**

From Figures 4.20-4.23 above it can be noted that the mix proportions of SCC mixes 1-4 of Table 4.1 with cube compressive strengths 30, 40, 50 and 60 MPa fall within the ranges obtained by the rational method for proportioning SCC mixes proposed by Abo Dhaheer et al. (2015a). However, the mix proportions of cm and LP of SCC mixes 5-6 of Table 4.1 with cube compressive strengths of 70 and 80 MPa (Figures 4.24-4.25) fall slightly outside the ranges obtained by the rational method. This is no doubt a result of the fact that the above design charts followed the typical ranges of the various constituents suggested by EFNARC (2005). The EFNARC guidelines however recognize that "these proportions are in no way restrictive and many SCC mixes will fall outside the range for one or more constituents" (EFNARC, 2005).

## 4.9. Critical remarks

Self-compacting concrete is a two phase (solid and liquid) particle suspension and is very fluid. The challenge then is to maintain the flow-ability of the suspension and to avoid the segregation of the phases. The development of self-compacting concrete mixes is a complex and sensitive process, requiring a balance to be struck between flow-ability and non-segregation of constituent materials. These aims can be achieved by increasing the paste volume fraction and decreasing the large aggregate volume fraction. Our extensive investigations lead us to the following major conclusions.

Self-compacting normal strength concrete mixes with maximum size of aggregate 20 mm designed to satisfy the flow-ability and stability (i.e. resistance to segregation) criteria using the slump cone flow test may not meet the passing ability criterion. It is additionally necessary to check that the mixes meet the passing ability criterion using the J-ring and L-box tests. These mixes often need to be more flow-able than required by the slump flow test, in order to satisfy the passing ability test.

The viscosity of SCC mixes so produced can be accurately estimated using a micromechanical procedure based on the known plastic viscosity of the cement paste and the mix proportions. The plastic viscosity of the homogeneous paste can be measured accurately using the traditional viscometers (Heirman et al., 2008). The measurement of the plastic viscosity of heterogeneous SCC, using the rheometers often gives inaccurate results with a large scatter (Ghanbari and Karihaloo, 2009).

The mix proportions of the SCC mixes developed in this Chapter are shown to fall within the ranges obtained using the recently proposed rational method for proportioning (Abo Dhaheer et al., 2015a).

An appropriate computational strategy using the SPH method will implemented in the next Chapter to back calculate the yield stress of self-compacting concrete mixes from slump flow test.

# Chapter 5

# Estimation of yield stress of self-compacting concrete from the numerical simulation of slump flow test

## 5.1. Introduction

Simulation of the flow of SCC is a significantly useful and inexpensive way to understand the behaviour of SCC in the fresh state. It can be used as a tool to accurately estimate some of the constitutive properties of SCC mix. It has been described in Chapter 3 that the SCC mix behaves like a non-Newtonian fluid best described by a Bingham model. This model contains two crucial material parameters, the yield stress $\tau_y$ and the plastic viscosity $\eta$.

This Chapter will focus on the numerical simulation of the normal strength (30 to 80 MPa) SCC mixes developed in the previous Chapter (Table 4.1) using the three dimensional incompressible SPH methodology (Chapter 3). The entire cone flow test was simulated from the moment the cone was lifted until the SCC mix stopped to flow. The SPH numerical simulation was employed here to back calculate the yield stress $\tau_y$ of the mix from the measured $t_{500}$ time and the final spread diameter, knowing the plastic viscosity of the mix (Table 4.6) as discussed in Chapter 4.

## 5.2. Initial configuration and boundary conditions

When solving the mass and momentum conservation equations (3.6) and (3.8), appropriate initial and boundary conditions have to be applied.

Three types of boundary conditions need to be considered in the simulation of slump cone test:

i. Zero pressure condition (i.e. atmospheric pressure) on the free surface;

ii. Dirichlet (or first-type) boundary condition has to be imposed on the normal component of the velocity field at the walls and the bottom plates; this component must vanish.

iii. Neumann (or second-type) boundary condition has to be imposed on the pressure gradient; this zero pressure gradient is used only for solving the pressure Poisson equation (3.23)

The rate of cone lift will be assumed to be 1 m/s (compare with the actual cone lift rates given in Table 4.2). This sets the initial condition at t = 0. The part of the mix which is not in contact with the cone surface during the lifting of the cone is a free surface with pressure $p = 0$, but the part in contact is subjected to sliding frictional resistance (Figure 5.1 (d)). For realistic simulations, the friction between the SCC mix and the contacting surfaces should be considered. After several trials on mix 1, an appropriate dynamic coefficient of friction (DCOF) for numerical simulations was chosen to be 0.54 Ns/m for all mixes. This value of the coefficient was determined by comparing the numerical simulations and experimental test results for a given $t_{500}$ of mix 1 (Table 5.1).

**Table 5.1: simulation trials on mix 1 to determine the dynamic coefficient of friction between SCC and rigid boundaries**

| Mix No. | Trial coefficient of friction | Plastic viscosity (Pa s) | Yield stress (Pa) | $t_{500}$ experimental (s) | $t_{500}$ simulated (s) |
|---|---|---|---|---|---|
| **Mix1 (30MPa)** | 0.52 | 6.57 | 175 | 1.0 | 0.9 |
| | 0.53 | | | | 0.9 |
| | 0.54 | | | | 1.0 |
| | 0.55 | | | | 1.1 |

The effect of the frictional boundary condition depends on the relative tangential velocity between the contacting surface and the fluid flow and ensures that slip with friction boundary condition is enforced along the tangential direction of the contacting surfaces.

In SPH, a number of techniques have been developed in the past to enforce various boundary conditions. Some of these techniques have been mentioned in Chapter 3. In this research, the technique based on arrays of dummy rigid particles (Koshizuka et al.,

1998) was used to implement the cone wall and base plate boundary conditions, as illustrated in Figure 5.1.

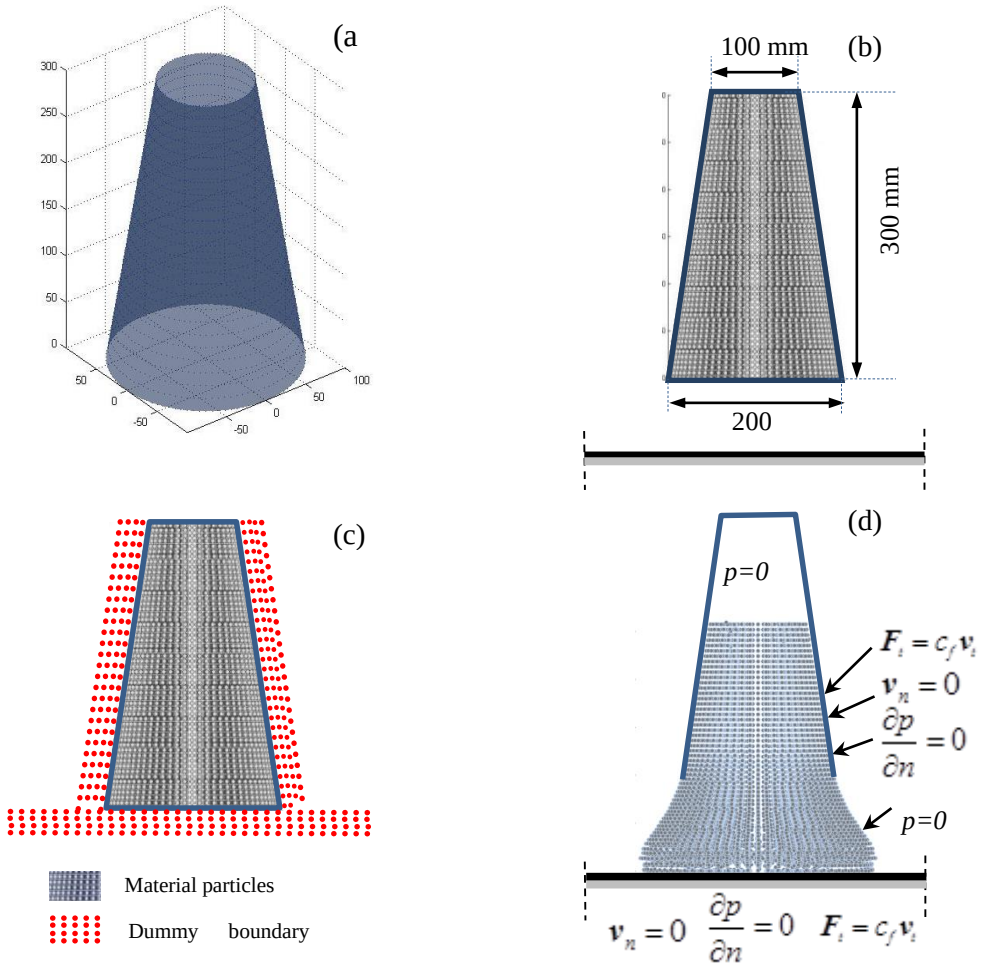


**Figure 5.1: (a) Three dimensional view, (b) Two dimensional section, (c) Dummy particles for enforcing boundary conditions, (d) Slump cone test boundary conditions (p – pressure, $v_n$ – normal velocity, $v_t$ – tangential velocity, and $c_f$ – the dynamic coefficient of friction). Pressure vanishes on a free surface. Note that the condition that the normal pressure gradient vanishes on rigid surfaces is only needed in the solution of the pressure Poisson Equation (3.23).**

Four arrays of rigid dummy particles placed outside the wall particles of the cone were used to implement the wall boundary conditions. The thickness of the array containing the dummy particles depends on the kernel smoothing length *h*. If the smoothing length $h=2r_o$, where $r_o$ is the initial particle spacing, four arrays of dummy particles at a spacing $r_o$ between the lines were used.

The boundary conditions along the slump wall are same as on the bottom plate. However, as the cone is lifted, the condition $p = 0$ is imposed on the newly formed free (exposed) surfaces of the flowing SCC mix. Figure 5.1d shows the slump cone test initial configurations and enforced boundary conditions.

## 5.3. Treatment of aggregates in SPH modelling of slump cone test

The number of particles used to represent the volume of the test cone contents sets a lower limit on the volume element that can be distinguished from the homogeneous mass, i.e. the resolution of the modelling technique. In the simulations below, a total of 23,581 particles have been used to represent the volume of mix in the cone ($5.498 \times 10^6$ $mm^3$) giving a resolution of 233.15 $mm^3$ per particle if all particles have the same density as the viscous homogeneous continuum. The resolution will be somewhat different if the particles have different densities (see Table 5.3). Thus, in all the mixes the large aggregates that can be distinguished from the homogeneous mass must have a volume exceeding this minimum. It is for this reason that only the aggregates of size 8 mm and above could be treated as discrete identities.

Sieve analysis was first performed to determine the grading curve of aggregate particle sizes within a given test sample. According to the sieve analysis of the SCC mixes 1–6 (Table 4.1), Table 5.2 presents the volume fractions of coarse aggregates in the size ranges ($g \geq 20$, $16 \leq g < 20$, $12 \leq g < 16$ and $8 \leq g < 12$ mm).

**Table 5.2: volume fractions of coarse aggregates for each range ($g \geq 20$, $16 \leq g < 20$, $12 \leq g < 16$ and $8 \leq g < 12$ mm) for all mixes**

| Mix No. | $g \geq 20$ | $16 \leq g < 20$ | $12 \leq g < 16$ | $8 \leq g < 12$ | $< 8$ |
|---|---|---|---|---|---|
| **Mix (1 – 4)** | 2.93% | 8.67% | 5.39% | 8.38% | 74.63% |
| **Mix (5 and 6)** | 2.86% | 8.45% | 5.26% | 8.18% | 75.25% |

For the purpose of modelling, each aggregate size range was replaced by a single aggregate size that best represented the range as illustrated in Figure 5.2. This required, at times, the size range to be further subdivided and the sieve analysis to be repeated. The representative aggregate size in each size range is given in Table 5.3.

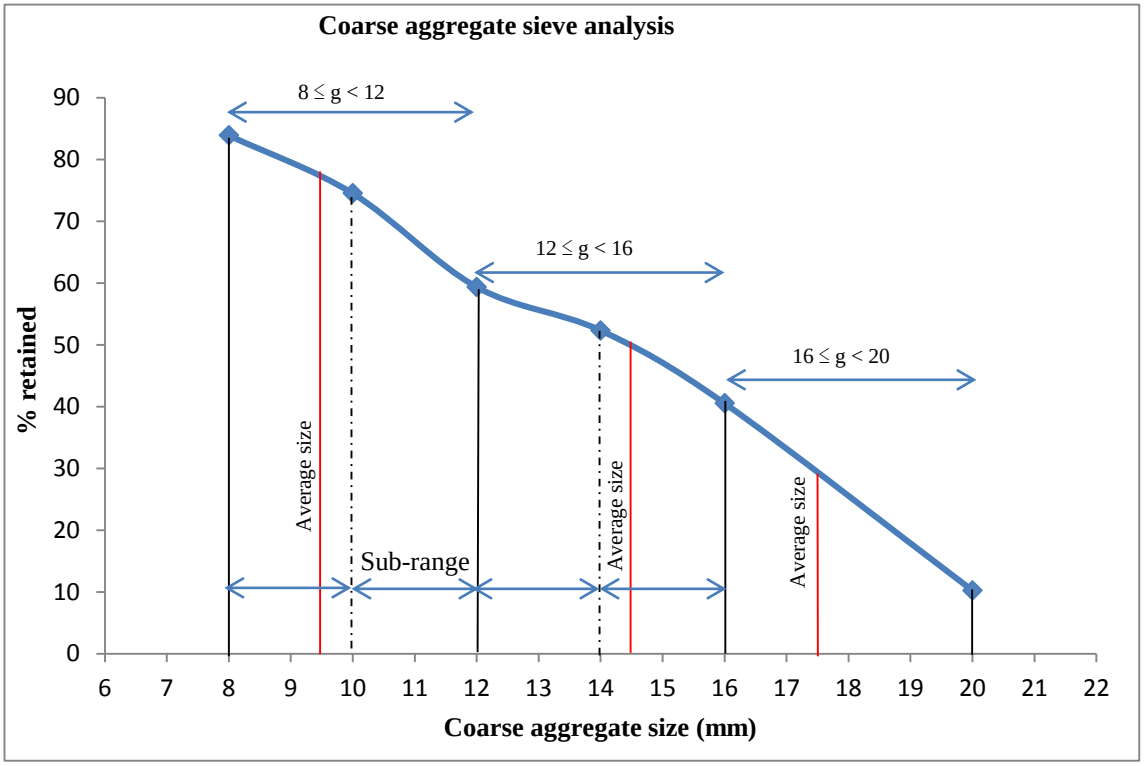


**Figure 5.2: The coarse aggregate sieve analysis with size ranges (g ≥ 20, 16 ≤ g < 20, 12 ≤ g < 16 and 8 ≤ g < 12 mm) and the average size for each range.**

It should be mentioned that the average sizes of particles in the size ranges $8 \leq g < 12$ and $12 \leq g < 16$ were skewed towards the lower and upper limits, respectively as shown by additional sieve analysis in the sub-ranges $12 \leq g < 14$ and $14 \leq g < 16$ (Figure 5.2). This is reflected in the average particle sizes in these two ranges in Table 5.3.

The assigned volume ($V_a$) for each particle size which appears in the discrete form of SPH equations is equal to the ratio of its actual mass to the density of the continuum. An example is presented below on how to calculate the assigned volume of the discrete

particles in mix 1. We first calculate the density of the mortar (i.e. cement + GGBS + Limestone powder + FA + water + SP + CA particles < 8 mm in size) whose volume fraction is 0.7463 (Table 5.2). It can be calculated as follows using the rule of mixtures. The density of SCC mix1 = sum of the volume fractions of CA > 8 mm x density of CA + volume fraction of mortar x density of mortar, i.e. 2341 = (0.0293 + 0.0867 +0.0539 + 0.0838) x 2800 + 0.7463 x density of mortar. This gives the density of mortar (particles < 8 mm) to be 2185 kg/$m^3$.

The number of particles of each size used in the simulation $N_p$ is calculated as follows:

$N_p$= volume fraction x volume of cone/volume of one particle

$N_p$ ($g \geq 20$) = 0.0293 x 5498000 / 4189.2 = 38

$N_p$ ($16 \leq g < 20$) = 0.0867 x 5498000 / 2806.44 = 170

$N_p$ ($12 \leq g < 16$) =0.0539 x 5498000 / 1596.41 = 186

$N_p$ ($8 \leq g < 12$) = 0.0838 x 548000 / 448.96 = 1027

$N_p$ (<8) = 23581- (38+170+186+1027) = 22160

Next the assigned volume $V_a$ ($mm^3$) for each size is = actual average volume x actual density/ density of continuum:

$V_a$ ($g \geq 20$) = 4189.2 x 2800 / 2341= 5010.6

$V_a$ ($16 \leq g < 20$) = 2806.44 x 2800 / 2341= 3356.7

$V_a$ ($12 \leq g < 16$) = 1596.41 x 2800 / 2341= 1909.4

$V_a$ ($8 \leq g < 12$) = 448.96 x 2800 / 2341= 537.0

$V_a$ (< 8) = 185.15 x 2185 / 2341= 172.8

**Table 5.3: Volume fractions of aggregates larger than or equal to 8 mm in mix 1, $N_p$ and $V_a$ is the number and assigned volume of the particles representing them in the 3D simulation of slump cone test.**

| SCC Mix 1 | Particle range (mm) | Representative particle diameter (mm) | Density (kg/m$^3$) | Volume fraction (%) | 3D slump cone test | |
|---|---|---|---|---|---|---|
| | | | | | $N_p$ | $V_a$ / particle (mm$^3$) |
| | **g ≥ 20** | 20 | 2800 | 2.93 | 38 | 5010.6 |
| **Aggregates g ≥8 mm** | **16 ≤ g <20** | 17.5 | 2800 | 8.67 | 170 | 3356.7 |
| | **12 ≤ g < 16** | 14.5 | 2800 | 5.39 | 186 | 1909.4 |
| | **8 ≤ g < 12** | 9.5 | 2800 | 8.38 | 1027 | 537.0 |
| **Particles <8 mm** | **g < 8** | 8 mm | 2185 | 74.63 | 22160 | 172.8 |
| **Total** | | - | 2341 | 100 | 23581 | |

## 5.4. Estimation of mix yield stress

It should be mentioned that in previous studies (Kulasegaram et al., 2011; Kulasegaram and Karihaloo, 2012; Deeb et al., 2014, a, b) the yield stress $\tau_y$ was assumed to be equal to 200 Pa irrespective of the mix characteristic compressive strength. Here we estimate it in an inverse manner which requires a trial-and-error approach; for a given mix and plastic viscosity (Table 4.6), an arbitrary initial trial yield stress is assumed (200 Pa) and the mix flow is simulated. If the computed $t_{500}$ time and the final spread diameter differ by more than one per cent from the measured values in the test, then the simulation is repeated with a new trial yield stress. This process is repeated until the computed and measured times are nearly the same. It should be mentioned that in all trial simulations the dynamic coefficient of friction was not altered and the plastic viscosity of the mix was equal to that given in (Table 4.6).

The simulations were carried out on HPZ820 workstation (clock 3.3 Hz, Intel Xeon CPU E5-26430). The time taken to simulate the flow for 15 s was approximately 7 days. However, as this workstation allows four programs to be run simultaneously, four trial flows up to 15 s were simulated in approximately 10 days.

The numerical results of this trial and- error procedure for the six mixes are shown in Figures 5.3-5.8, and the estimated yield stresses of the six mixes are given in Table 5.4. Figures 5.3-5.8 illustrate the numerical mix spread diameter for each yield stress trial with respect to flow time from the moment the flow started until the mix stopped to flow. These figures are sectioned into two parts to illustrate the flow characteristics at the most crucial times of the flow i.e. $t_{500}$ and $t_{stop}$. From Figures 5.3-5.8, it is clear that for a given mix, the yield stress has a noticeable influence on $t_{500}$. However, it can be noted from Table 5.4, the estimated yield stress varies only marginally with SCC compressive strength, thus confirming the observations made in (Ghanbari and Karihaloo, 2009) and the use of a nominal value (200 Pa) in several previous studies(Kulasegaram et al., 2011; Kulasegaram and Karihaloo, 2012; Deeb et al., 2014, a,b).

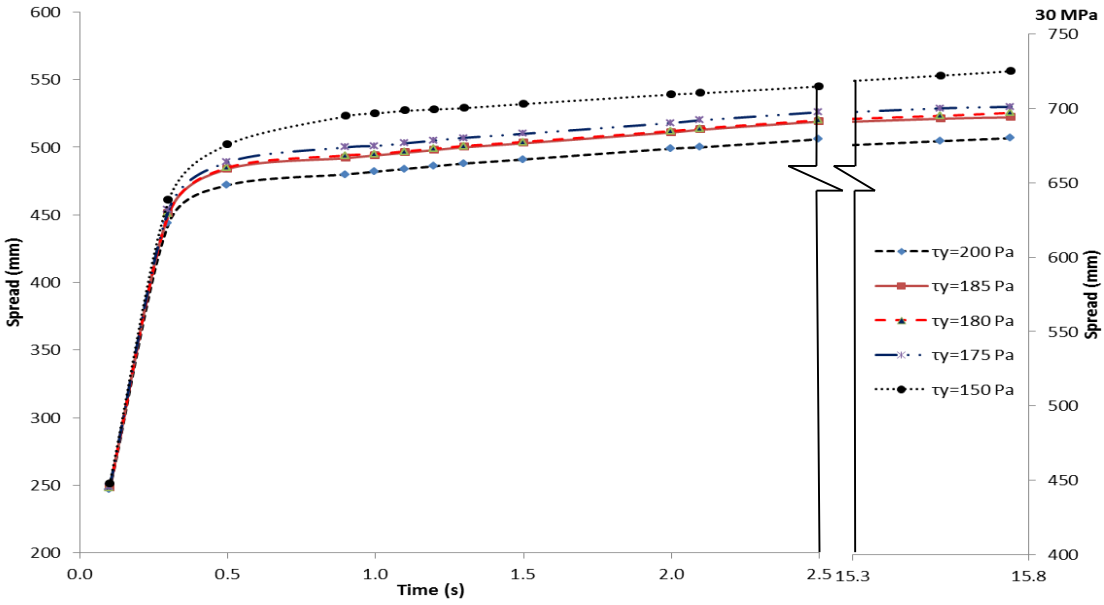


**Figure 5.3: Effect of changing $\tau_y$ on the $t_{stop}$ and the final spread of mix 1.**

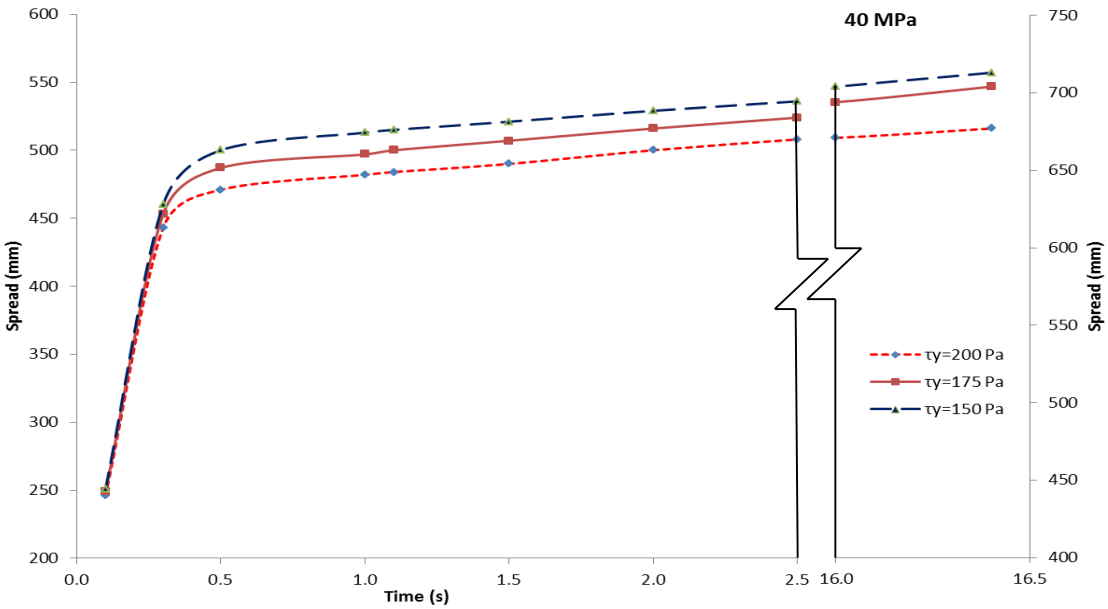


**Figure 5.4: Effect of changing $\tau_y$ on the $t_{stop}$ and the final spread of mix 2.**

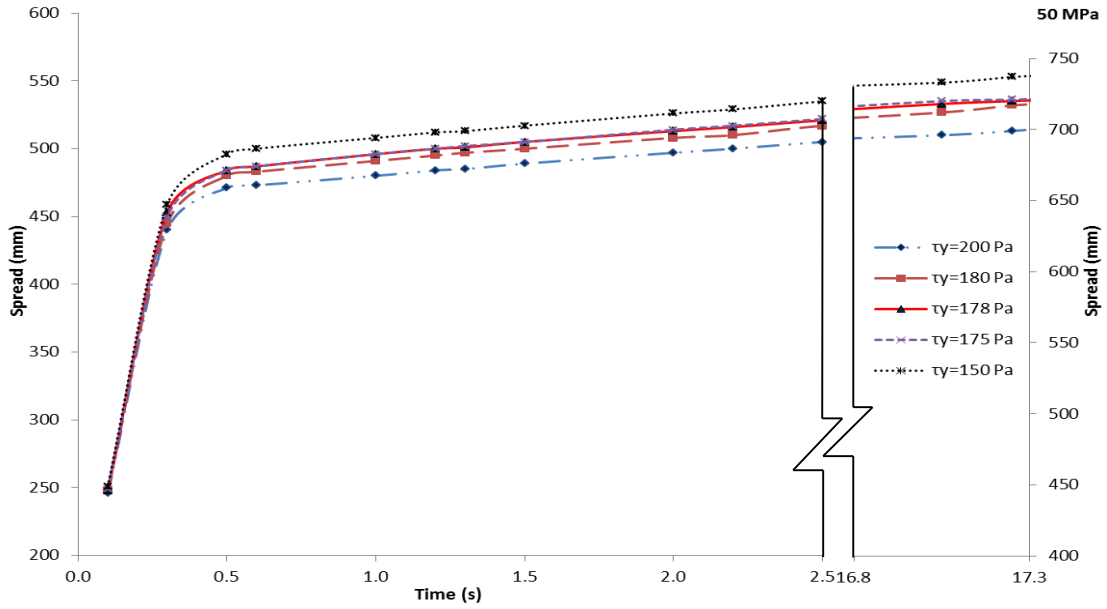


**Figure 5.5: Effect of changing $\tau_y$ on the $t_{stop}$ and the final spread of mix 3.**

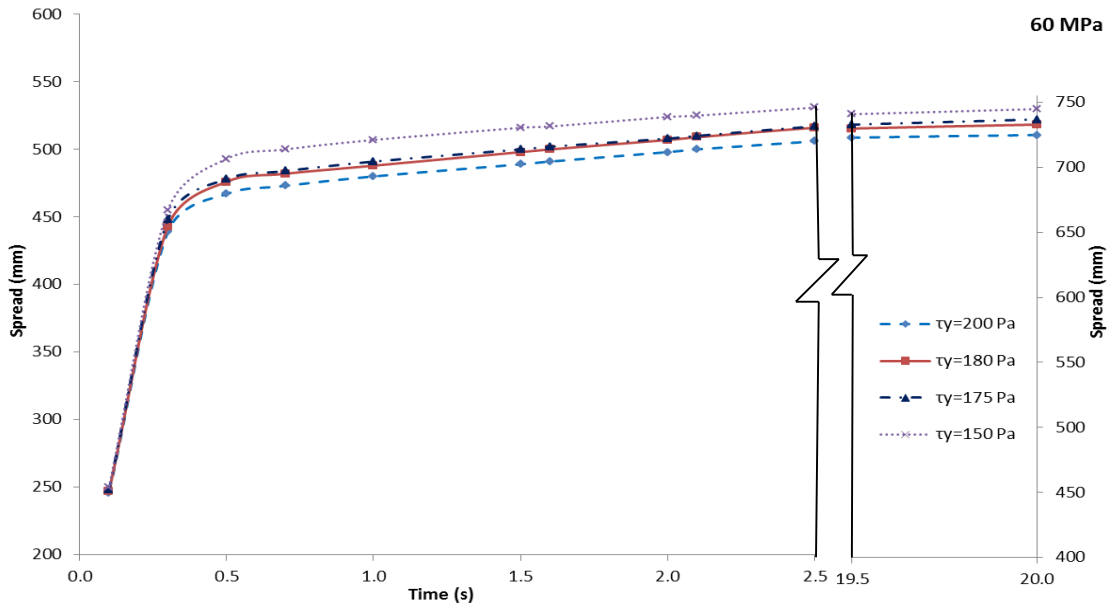


**Figure 5.6: Effect of changing $\tau_y$ on the $t_{stop}$ and the final spread of mix 4.**

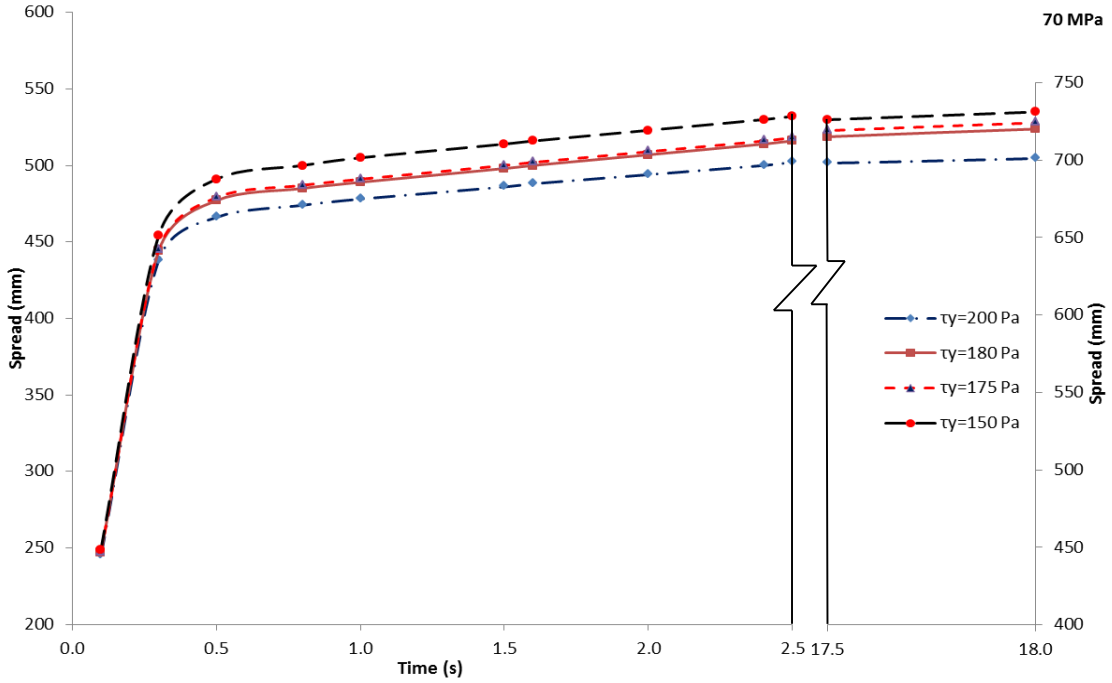


**Figure 5.7: Effect of changing $\tau_y$ on the $t_{stop}$ and the final spread of mix 5.**

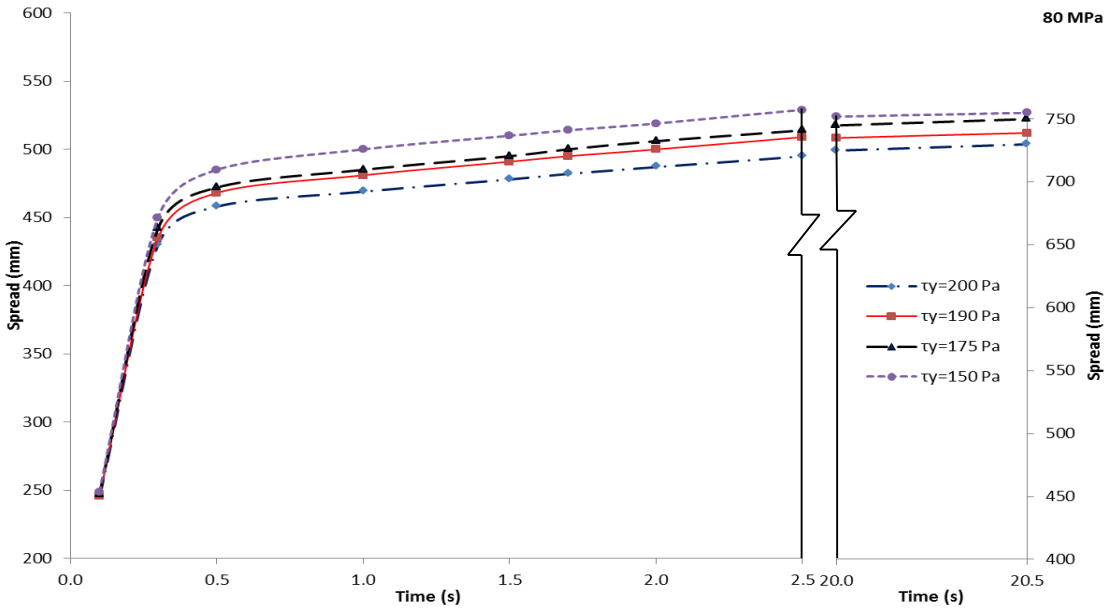


**Figure 5.8: Effect of changing $\tau_y$ on the $t_{stop}$ and the final spread of mix 6.**

**Table 5.4: Numerically estimated yield stress of mixes 1–6.**

| Mix No. | Spread/mm | | $t_{500}$ /s | | Viscosity | $\tau_y$ (estimated) |
|---|---|---|---|---|---|---|
| | Test | Numerical | Test | Numerical | (Pa s) | Pa |
| **1 (30MPa)** | 700 | 700 | 1.0 | 1.0 | 6.57 | 175 |
| **2 (40MPa)** | 700 | 704 | 1.1 | 1.1 | 7.31 | 175 |
| **3 (50MPa)** | 715 | 720 | 1.3 | 1.3 | 7.60 | 178 |
| **4 (60MPa)** | 735 | 733 | 1.6 | 1.6 | 9.31 | 180 |
| **5 (70MPa)** | 720 | 720 | 1.6 | 1.6 | 9.36 | 180 |
| **6 (80MPa)** | 730 | 739 | 2.0 | 2.0 | 10.62 | 190 |

## 5.5. Conclusions

All the self-compacting concrete mixes developed in the Chapter 4 have been simulated using a three dimensional corrected Lagrangian incompressible SPH method in the slump cone test from the moment the cone was lifted until the mix stopped to flow. The plastic viscosities of the mixes have been calculated using the micromechanical model described in Chapter 4.

As demonstrated in this Chapter, the yield stress of an SCC mix can be predicted in an inverse manner using the SPH simulation methodology by comparing the measured and

simulated $t_{500}$, and the final spread diameter. The yield stress of SCC mixes varies only slightly with an increase in the characteristic compressive strength of the mix. The plastic viscosity on the other hand shows a marked increase with the increase in the characteristic compressive strength of the mix.

The SPH simulation methodology provides a useful tool for predicting the yield stress of SCC mixes accurately. As argued in Chapter 2, the measurement of $\tau_y$ by rheometers is inconsistent and fraught with inaccuracies.

# Chapter 6

# Assessment of the distribution of large aggregates during the flow of self-compacting concrete mixes

## 6.1. Introduction

An essential requirement of a SCC mix is that heavier aggregate particles do not segregate from the paste but stay homogeneously distributed during the flow. If not, a non-homogenous distribution during transport or placement can have an adverse effect on the properties of hardened concrete.

In this Chapter two mixes (30 and 50 MPa) from the 6 mixes developed and reported in Chapter 4 have been chosen to investigate the distribution of coarse aggregates during the numerical simulations as well as slump flow tests. The aim of the simulations is to compare the distribution of coarse aggregate particles larger than or equal to 8 mm in the cone spread after it stopped to flow as revealed by the numerical simulations with the distribution of the aggregate particles of the corresponding sizes in the cut sections of the cured cone spread obtained during the laboratory slump flow tests.

## 6.2. Colour coding of coarse aggregates in the slump flow mixes

Tracking the coarse aggregate particles during the flow of SCC is very challenging. A novel idea was implemented in this study to track the movement of large coarse aggregates ($g \geq 8$ mm) at least after the flow had stopped. In two mixes (1 and 3) the large coarse aggregate particles in the size ranges $8 \leq g < 12$, $12 \leq g < 16$, $16 \leq g < 20$ and $g \geq 20$ mm of the test SCC mixes (Table 4.1) were colour coded with non-toxic non-water soluble paints, so that the outlines of the aggregate particles could be clearly distinguished in the cut sections of the hardened cone spread and can be easily compared with the numerical simulations.

Figure 6.1 show the coloured aggregates that were used in the test mixes 1 and 3. The slump cone spread produced using coloured aggregates was allowed to dry for 24 hours after the flow had stopped. The hardened slump "pancake" was then carefully scraped

from the steel base plate and placed in a water tank for a further 7 days, after which it was cut along two diagonal perpendicular sections with a diamond saw (Figures 6.2 and 6.3). The number of aggregates in the different size ranges (according to their different coloured outlines) was counted. Table 6.1 lists the number of different size aggregates counted along the two diagonal sections of the cone spreads in the two test mixes. From the cut sections, it was evident that the coarse aggregates were evenly distributed; the larger particles were suspended in the paste and had not gravitated to the bottom.

**Figure 6.1: Colour-coded coarse aggregates; $g \geq 20$ mm (white, top), $16 \leq g < 20$ mm (green, bottom right), $12 \leq g < 16$ mm (red, bottom centre), and $8 \leq g < 12$ mm (yellow, bottom left)**


**Figure 6.2: (a) Cut-hardened slump cone spread (mix 1) (b) Coloured coarse aggregate outlines in section (mix 1).**


**Figure 6.3: (a) Cut-hardened slump cone spread (mix 3) (b) Coloured coarse aggregate outlines in section (mix 3).**

**Table 6.1: Number of coarse aggregate particles in the size ranges $8 \leq g < 12$, $12 \leq g < 16$,$16 \leq g < 20$ and $g \geq 20$ mm in the two diametrical sections of hardened cone spread of mixes 1 and 3.**

| | | $g \geq 20$ mm | $16 \leq g < 20$ mm | $12 \leq g < 16$ mm | $8 \leq g < 12$ mm |
|---|---|---|---|---|---|
| Mix 1 | **Section 1** | 6 | 13 | 12 | 22 |
| | **Section 2** | 4 | 12 | 12 | 32 |
| Mix 3 | **Section 1** | 3 | 14 | 11 | 28 |
| | **Section 2** | 5 | 12 | 14 | 25 |

## 6.3. Modelling of coarse aggregates in SPH simulation

### 6.3.1. Modelling of slump cone test

As it was mentioned in the Chapter 5, a total of 23,581 particles have been used to represent the volume of mix in the cone ($5.498 \times 10^6$ $mm^3$) giving a resolution of 233.15 $mm^3$ per particle or particle diameter 7.6 mm if all particles have the same density as the viscous homogeneous continuum. The resolution will be somewhat different if the particles have different densities (see Table 5.1). Thus, in all the mixes the large aggregates that can be distinguished from the homogeneous mass must have a volume exceeding this minimum. It is for this reason that only the aggregates of size 8 mm and above could be treated as discrete identities during the numerical simulation.

In order to be able to monitor the velocity vectors and positions of aggregates of different representative sizes, as well as those of the fluid particles representing the paste, the particles were represented by distinct colours as shown in Figure 6.4. Further, the following steps were taken during the numerical simulations.

- All particles representing the mix were generated randomly;
- Particles representing the mortar as well as the large aggregates form a homogeneous mass and have the same continuum properties except for their assigned volumes;
- The masses of the SPH particles representing the various aggregate particles in the SCC mix were calculated based on their respective volume fractions in the mix;
- Particles representing the large aggregates according to their assigned volumes were tagged (and colour coded as shown below) throughout the simulation in order to monitor their velocity vectors and positions.

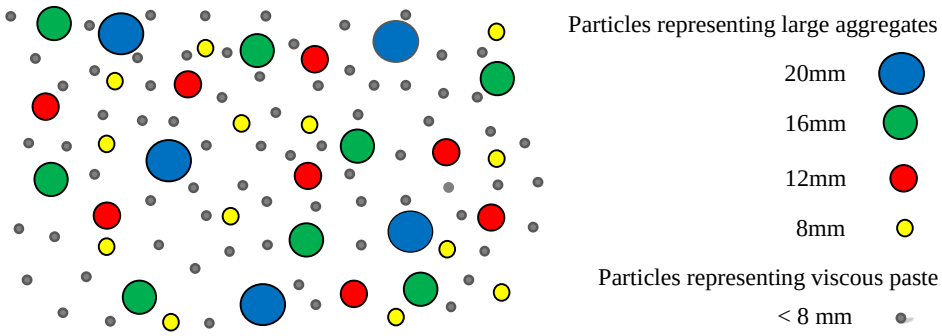


**Figure 6.4: Schematic sketch of particle representation when simulating large aggregate distribution**

## 6.4. Simulation results

The 3D numerical simulations of the slump cone test highlight the distribution of the large aggregates (larger than or equal to 8 mm) in the mix. Figures 6.5, 6.6 and 6.7 illustrate the 3D simulation of the SCC mix 1. The results of numerical simulation performed on mix 3 are illustrated in Figures 6.8, 6.9 and 6.10. It was observed that the larger aggregates indeed stayed homogeneously distributed in the mix exactly as in the slump cone test in the laboratory at all times during the flow. The surface of the spreads when the flow stopped after 15.7 s for mix 1 (Figure 6.7) and 17.2 s in the case of mix 3 (Figure 6.10) looks smooth as a ‘pancake’ identical to that observed in the laboratory test on these mixes.

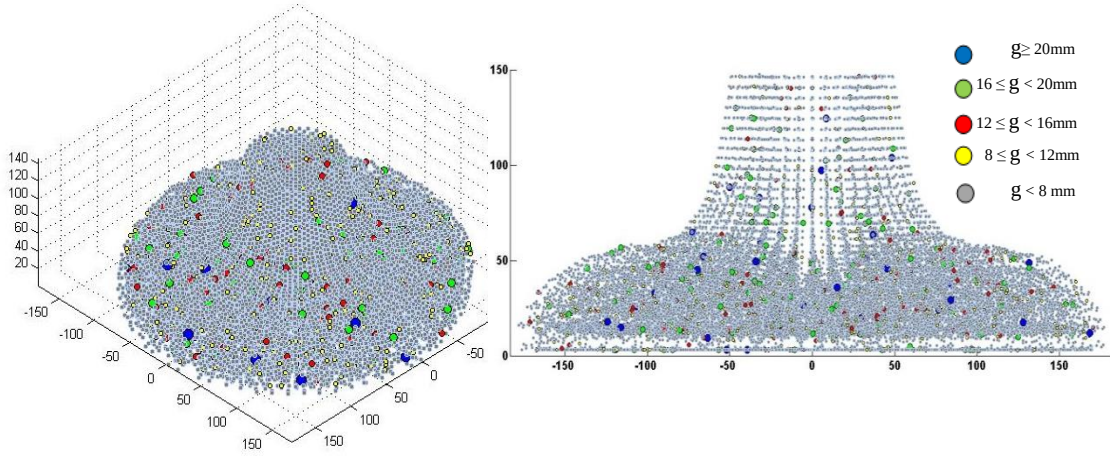


**Figure 6.5: Flow of SCC mix 1 after 0.2 s in 3D and 2D section showing the large aggregates**

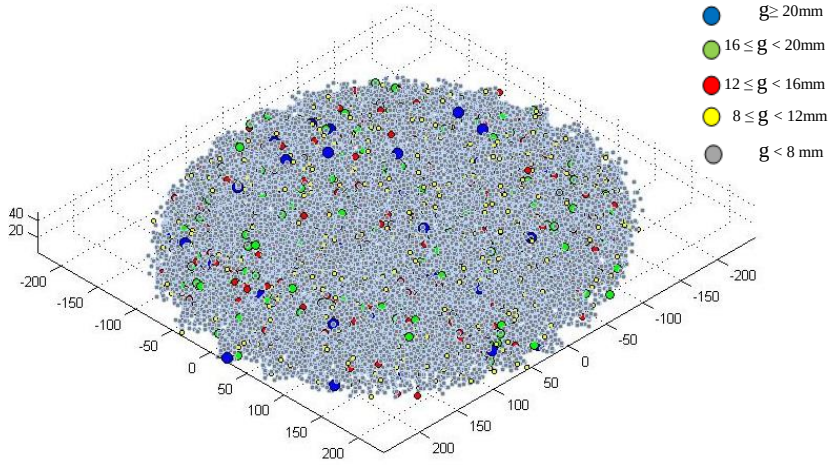


**Figure 6.6: Flow pattern of SCC mix 1 after 1.0s ($t_{500}$) showing the large aggregates**

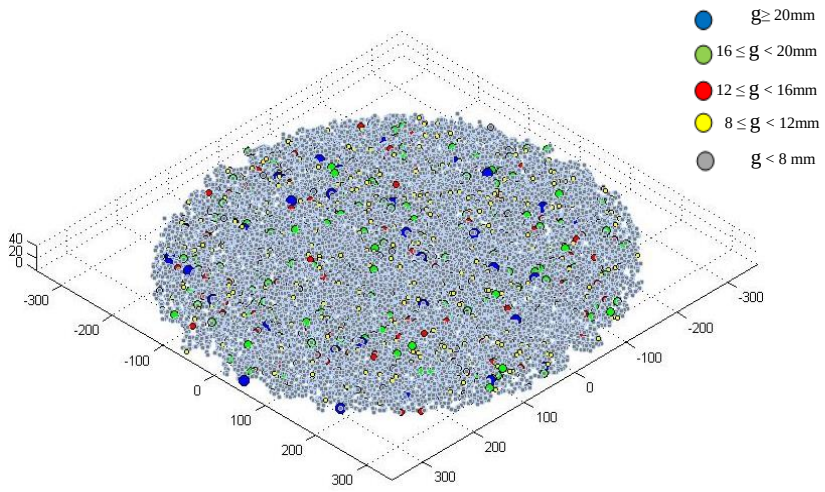


**Figure 6.7: Flow spread of SCC mix 1 after 15.7s ($t_{stop}$) showing the large aggregates**

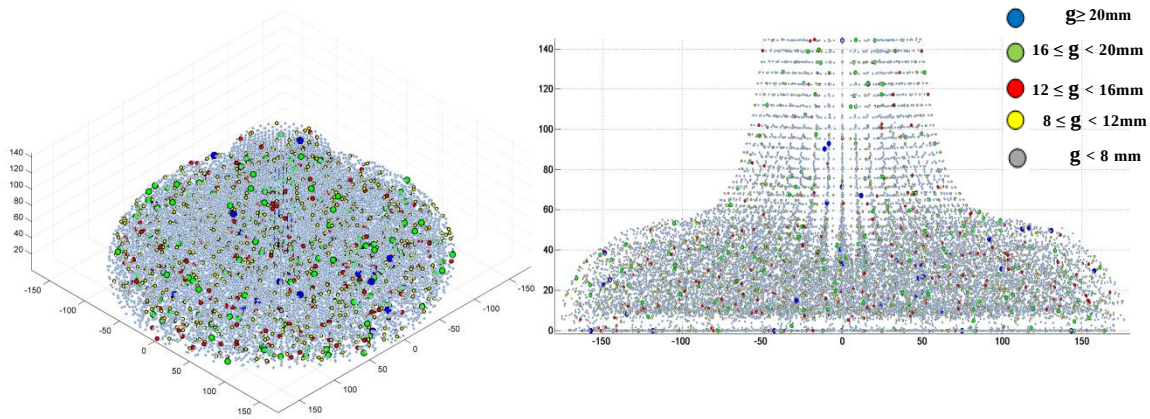


**Figure 6.8: Flow of SCC mix 3 after 0.2 s in 3D and 2D section showing the large aggregates**

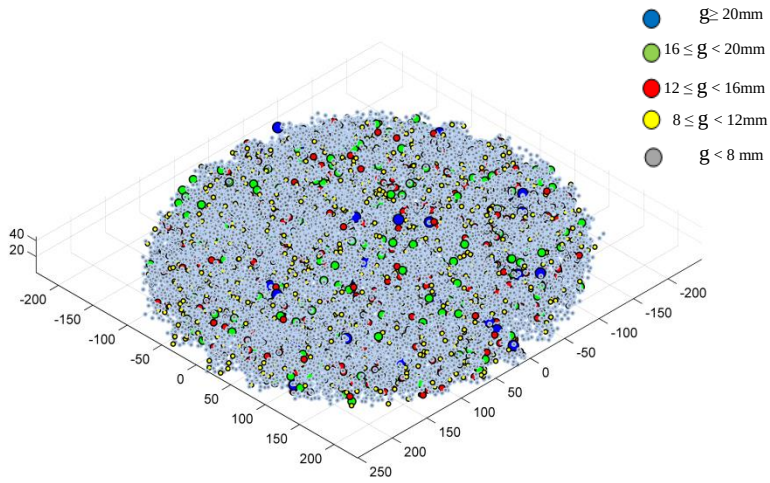


**Figure 6.9: Flow pattern of SCC mix 3 after 1.1s ($t_{500}$) showing the large aggregates**

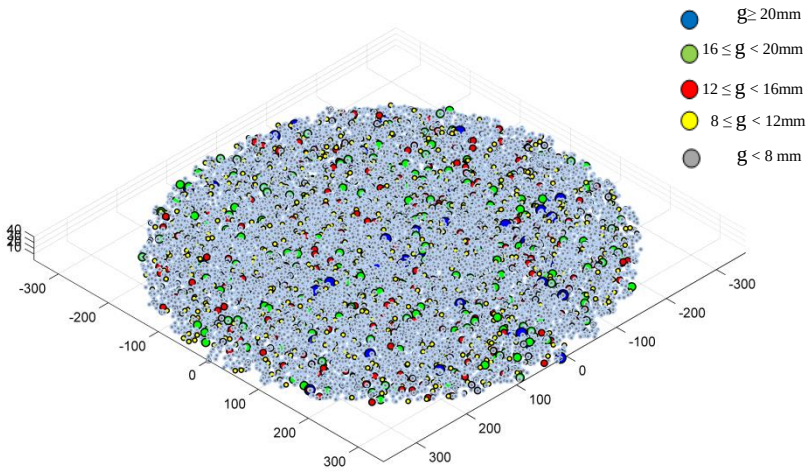


**Figure 6.10: Flow spread of SCC mix 3 after 17.2s ($t_{stop}$) showing the large aggregates**

The simulated slump flow spread was also cut by diametrical perpendicular planes A and B (Figure 6.11), after it had stopped to flow ($t_{stop}$= 15.7 s for mix 1 and 17.2 s for mix 3). These sections are shown in Figures 6.12 and 6.13 for mixes 1 and 3, respectively. The number of larger aggregates in the cut sections was counted and are listed in Table 6.2.

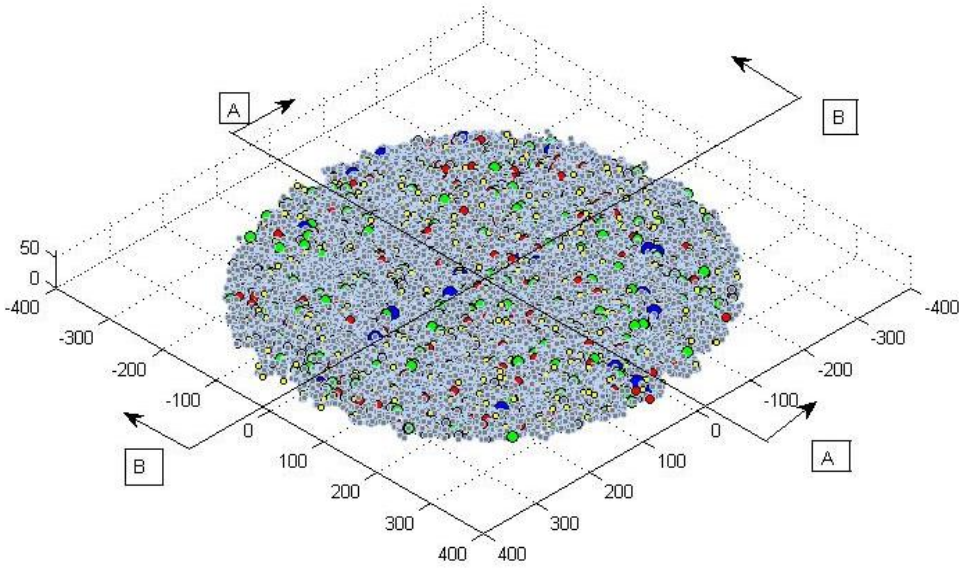


**Figure 6.8: Flow spread after 15.7 s mix 1 (mix 3 after 17.2 s) and the cut sections A and B**

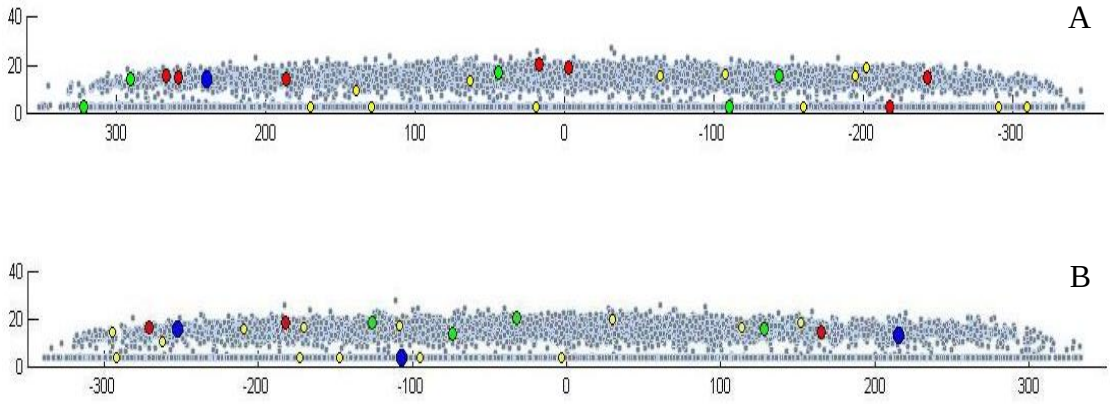


**Figure 6.9: Diametrical cross-sections (A and B) of slump flow spread of mix 1 after 15.7 s**

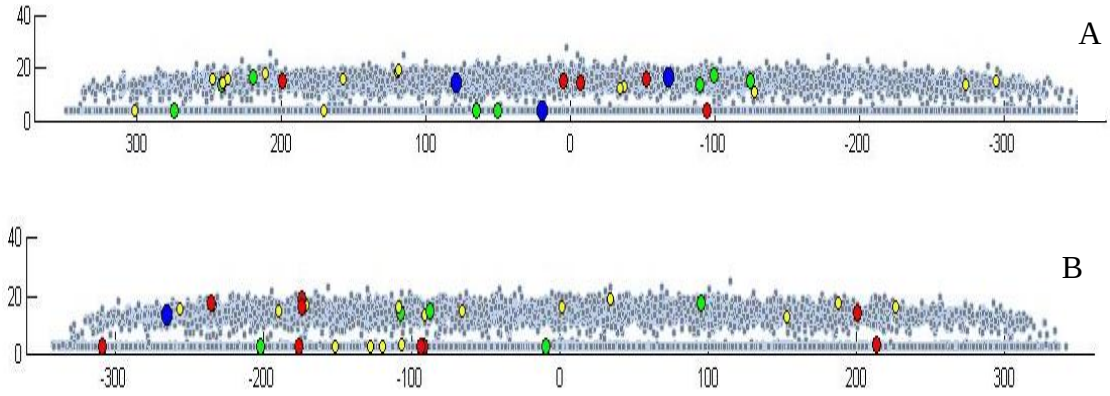


**Figure 6.10: Diametrical cross-sections (A and B) of slump flow spread of mix 3 after 17.2 s**

**Table 6.2: Number of coarse aggregate particles in cut sections of mixes 1 and 3**

| Nominal aggregate size | | g ≥ 20 mm | 16 ≤ g < 20 mm | 12 ≤ g <16 mm | 8 ≤ g < 12 mm |
|---|---|---|---|---|---|
| Mix 1 | **Section A** | 1 | 5 | 7 | 12 |
| | **Section B** | 3 | 4 | 3 | 13 |
| Mix 3 | **Section A** | 3 | 8 | 5 | 13 |
| | **Section B** | 1 | 5 | 8 | 15 |

The average number of large aggregate particles in the cut sections counted in the experimental cone spread and in the simulated cone spread are compared in Table 6.3.

**Table 6.3: Average number of coarse aggregates along two perpendicular sections of mixes 1 and 3**

| **Mix** | **Size range (mm)** | **Average number in experiment** | **Average number in simulation** | **Ratio of average number in experiment to average number of 20 mm** | **Ratio of average number in simulation to average number of 20 mm** |
|---|---|---|---|---|---|
| **Mix 1** | g ≥ 20 | 5.0 | 2.0 | 1 | 1 |
| | 16 ≤ g < 20 | 12.5 | 4.5 | 2.50 | 2.25 |
| | 12 ≤ g <16 | 12.0 | 5.0 | 2.40 | 2.50 |
| | 8 ≤ g < 12 | 27.0 | 12.5 | 5.40 | 6.25 |
| | | | | | |
| **Mix 3** | g ≥ 20 | 4.0 | 2.0 | 1 | 1 |
| | 16 ≤ g < 20 | 13.0 | 6.5 | 3.33 | 3.25 |
| | 12 ≤ g <16 | 12.5 | 6.5 | 3.12 | 3.25 |
| | 8 ≤ g < 12 | 26.5 | 14.0 | 6.62 | 7.00 |

As the volume fractions of the aggregates of different size ranges (but not their actual numbers) are the same in the test mixes and simulations, their numbers in the cut sections of the test cone spread and the simulated spread must necessarily be correlated. This correlation may, for instance, be revealed by considering the ratio of the average number of aggregates of a certain size range to the number of aggregates of the largest size. This has been done for the test and simulated cone spread in columns 5 and 6 of Table 6.3 from which it is seen that the relative numbers of aggregates of different size ranges are indeed nearly the same.

## 6.5. Conclusions

The simulation of SCC mixes using the SPH methodology is capable of accurately predicting the distribution of large coarse aggregates in the simulated cone spread. This distribution is indeed very similar to that revealed in the cut sections of the hardened test cone spread. These large coarse aggregates had been painted with non-toxic non-water soluble paints prior to being used in the test mix. The colour coding of the coarse aggregates as described above has proved very effective in identifying various sizes of coarse aggregates in the cut section of the cone spread. Further, the experiments and numerical simulations also revealed that the coarse aggregates were evenly distributed and suspended by the paste without being gravitated to the bottom of the flow. This confirmed the fact that the two test mixes were indeed self-compacting mixes behaving as a homogeneous mass despite the presence of heavy aggregates.

# Chapter 7

# Effect of cone lift rate on the flow behaviour of self-compacting concrete

## 7.1. Introduction

Workability was defined as a way of describing the performance of concrete in the plastic state, and for a self-compacting concrete (SCC) it is often characterised by the following properties: flow ability, filling ability, passing ability and stability (segregation resistance) (PCI, 2003).

The flow ability of SCC is characterised by its fluidity and cohesion, and is often assessed using the slump flow test. This is an inexpensive test; it is a modified version of the standard slump test (ASTM, C143/C143M), and has been advocated as a more useful test for SCC (Domone, 1998). The slump flow test is used to assess the horizontal flow of SCC and self-compacting fibre-reinforced concrete (SCFRC), mainly when there are no obstacles.

## 7.2. The slump cone test guidelines

The guidelines for slump testing of conventional vibrated concrete recommend that the cone be lifted vertically, slowly and carefully, to ensure a correct result, with the lifting operation taking approximately 2-5 s (BS EN 12350-2) and 5 ± 2 s (ASTM, C143/C143 M). Wilson and Stowe (1971), however, reported that for a normal vibrated concrete a slight but significant difference was observed in slump due to a change in cone lift rate.

In general, for SCC there is no precise recommendation for how fast the cone must be lifted. Thus, in ASTM C1611M1-14 (2014) it is recommended that the cone be raised in 3 ± 1 s to a height of 230 ± 75mm (cone lift rate < 0.1 m/s).

In BS EN 12350-8 (2010) it is recommended that the cone be lifted in 1–3 s in one movement, implying that the flow characteristics (e.g. $t_{500}$ and flow spread) are insensitive to a three-fold change in the cone lift rate. Thus identical mixes (i.e. mixes with identical plastic viscosity and spread) tested according to these standards would

exhibit very different $t_{500}$ leading to the erroneous conclusion that they have different yield stresses. In fact, a careful examination of published data on SCC mixes that have been tested for flow-ability according to ASTM C1611M1-14 (2014) shows that their $t_{500}$ is consistently and significantly longer than that of similar mixes (i.e. mixes having nearly the same plastic viscosity and spread) tested according to BS EN 12350-8 (2010). Several examples are given in Table 7.1.

**Table 7.1: comparison between nearly similar mixes tested for flow-ability according to BS EN 12350-8 (2010) and ASTM C1611M1-14 (2014)**

| Parameter | Mix 1 | Mix [1] | Mix 2 | Mix [2] | Mix 5 | Mix [3] |
|---|---|---|---|---|---|---|
| | Table 4.1 | | Table 4.1 | | Table 4.1 | |
| **Plastic viscosity $\eta$ (Pa s)** | 6.57 | 6.17 | 7.31 | 7 | 9.36 | 9.35 |
| **Spread (mm)** | 700 | 700 | 700 | 650 | 720 | 710 |
| **$t_{500}$ (s)** | 1.0 | 6 | 1.1 | 2.5 | 1.6 | 3 |

**1** ASTM; Jadiri and Rand (2010), **2** ASTM; Youjun et al. (2007), **3** ASTM; Gesoğlu et al. (2009)

No systematic investigation on the effect of cone lift rate on the SCC flow characteristics has been reported in the literature, although it has been recognised (Emborg et al., 2003) that the details of some influencing factors are still missing. The present study aims to fill in this blank with the help of computational modelling and laboratory testing.

## 7.3. SCC mixes and numerical simulation of the slump flow test

In the numerical simulations (Chapter 5 and 6) a fixed cone lift rate of 1 m/s was used as one of the control variables.

The major aim of the this Chapter is to investigate the effect of the cone lift rate on the SCC flow and to verify whether the use of cone lift rate of 1 m/s in Chapter 5 was prudent.

All mixes developed in Chapter 4 have been re-simulated from the moment the cone was lifted until the mix stopped flowing using the SPH computational approach. The numerical simulations were conducted with various cone lift rates ranging between 0.1 and 1.0 m/s to investigate the effect of cone lift rate on the predicted $t_{500}$. The actual cone lift rates for the test mixes 1-6 were given in Table 4.3.

## 7.4. Investigation of the effect of cone lift rate (CLR) on the slump flow characteristics

Full 3D computer simulations of the SCC slump flow test of all the mixes were carried out using the SPH technique described in Chapter 3. Figures 7.1 and 7.2 give examples of the numerically observed flow behaviour of mix 1 when two different cone lift rates were used. In the figures the coloured particles show coarse aggregates in the size (g in mm) ranges; $g \geq 20$ (blue), $16 \leq g < 20$ (green), $12 \leq g < 16$ (red), and $8 \leq g < 12$ (yellow).

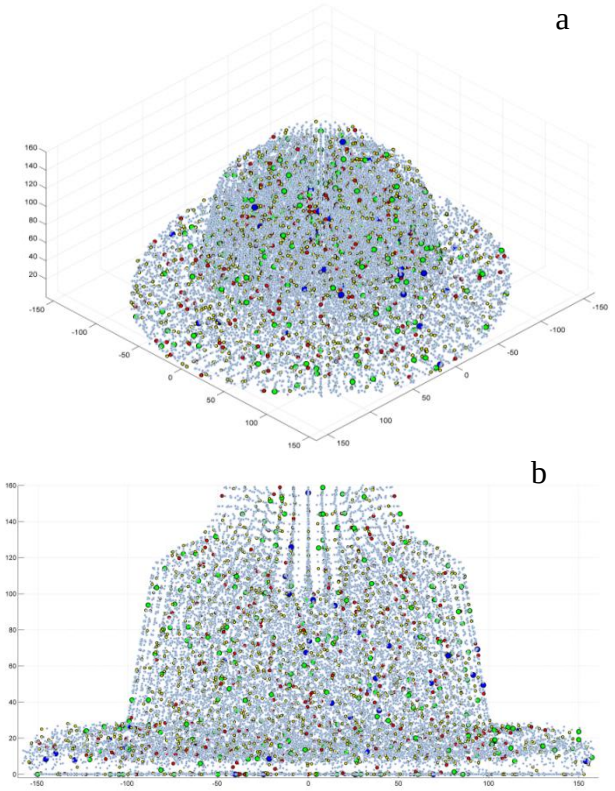


**Figure 7.1: Slump flow bell-shaped pattern of SCC mix 1 after 0.2 s in a 3D configuration (a) and 2D section (b) at a cone lift rate of 0.15 m/s**

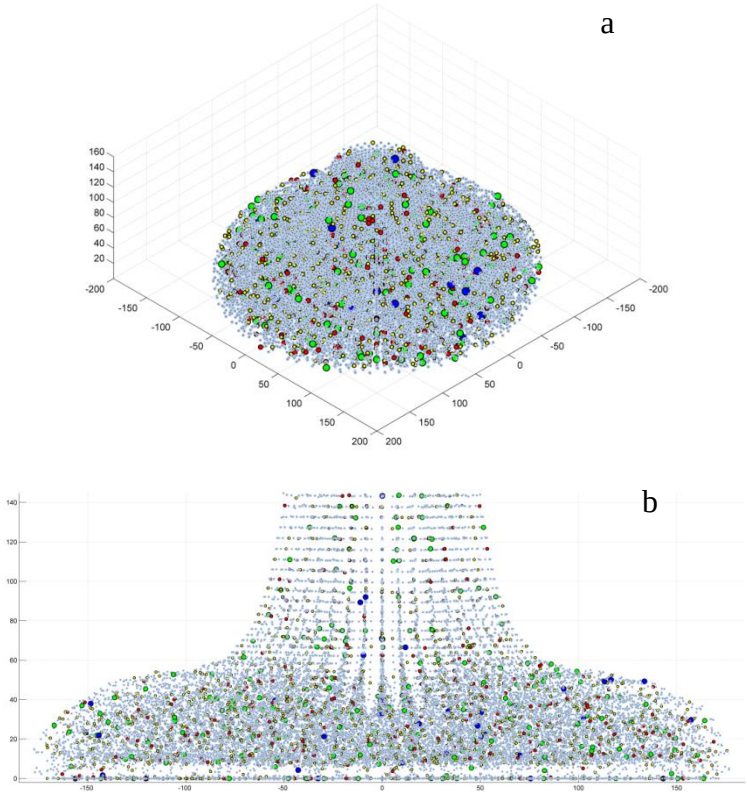


**Figure 7.2: Slump flow pattern of SCC mix 1 after 0.2 s in a 3D configuration (a) and 2D section (b) at a cone lift rate of 1 m/s. Note the absence of the bell shape**

It can be seen from Figure 7.1 that the flow test with a slow cone lift rate of 0.15 m/s produces a bell-like flow pattern after 0.2 s due to the fact that the top part of the content of the cone is still in contact with its surface. The bell-like pattern is absent after 0.2 s when a cone lift rate of 1 m/s was used (Figure 7.2) because at this fast rate the entire content of the cone has been released from the cone during this time. This flow behaviour is consistent with observations made during the laboratory trials (mix 1) at a cone lift rate of 0.9 m/s (Figure 7.3).

**Figure 7.3: Bell-like flow pattern absent at a CLR 0.9 m/s in mix 1.**

For other mixes, the cone lift rate during the laboratory trials varied between 0.69 and 1.0 m/s (Table 4.3).

Figure 7.4 illustrates the relationship between the cone lift rate and $t_{500}$ predicted by the numerical simulations for the six test mixes. It can be seen that $t_{500}$ decreases considerably as the cone lift rate is increased from 0.1 to 0.5–0.7 m/s, depending on the mix compressive strength. However, the influence of cone lift rate on $t_{500}$ becomes less pronounced when the cone lift rate is between 0.5–0.7 and 1.0 m/s for all mixes having a nominal cube compressive strength between 30 and 80MPa.

However, as expected, the cone lift rate has an insignificant influence on $t_{stop}$ (i.e. the spread) as exemplified by the 30MPa mix in Figure 7.5.

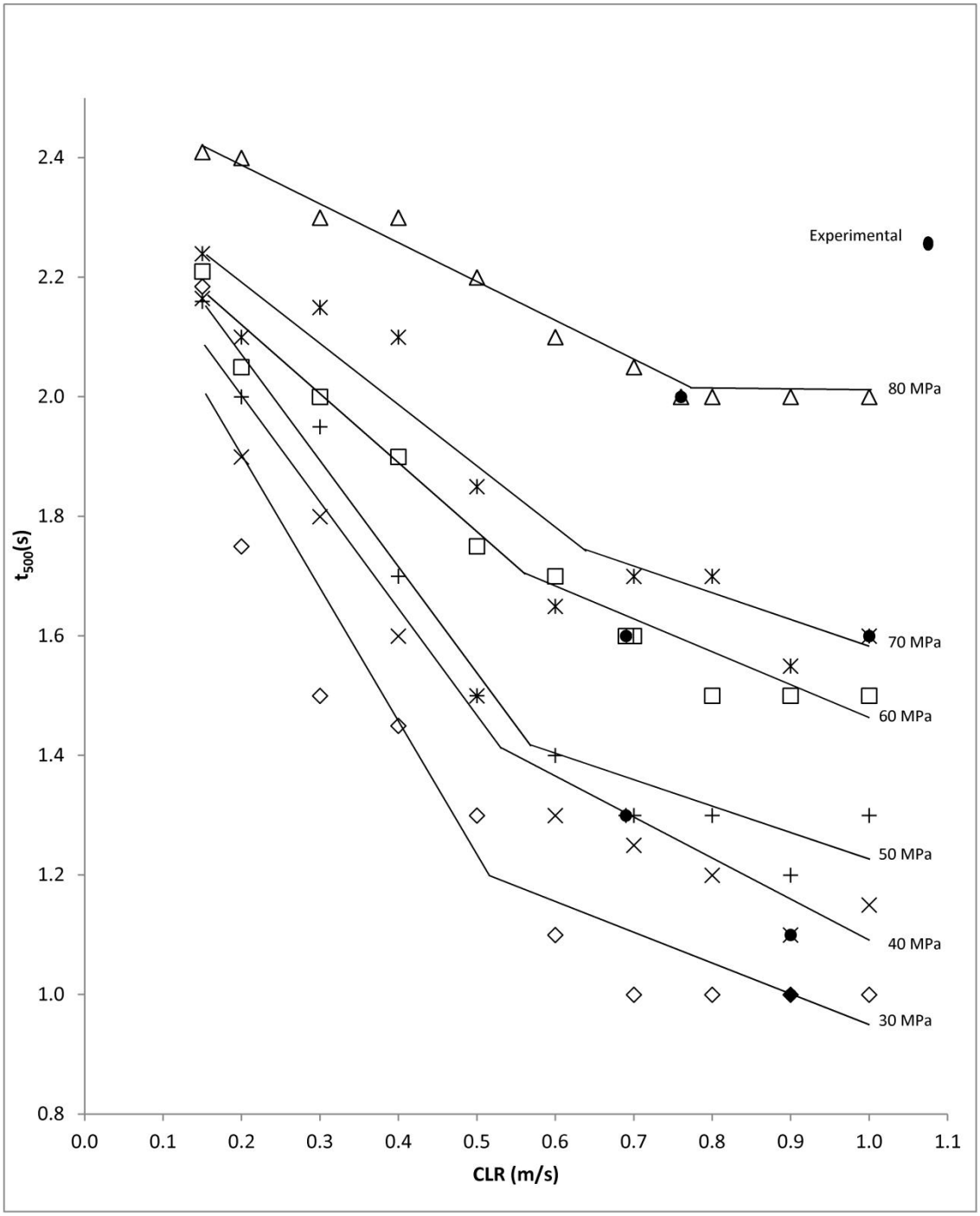


**Figure 7.4: Variation in $t_{500}$ with cone lift rate for mixes having a cube compressive strength in the range 30–80 MPa**

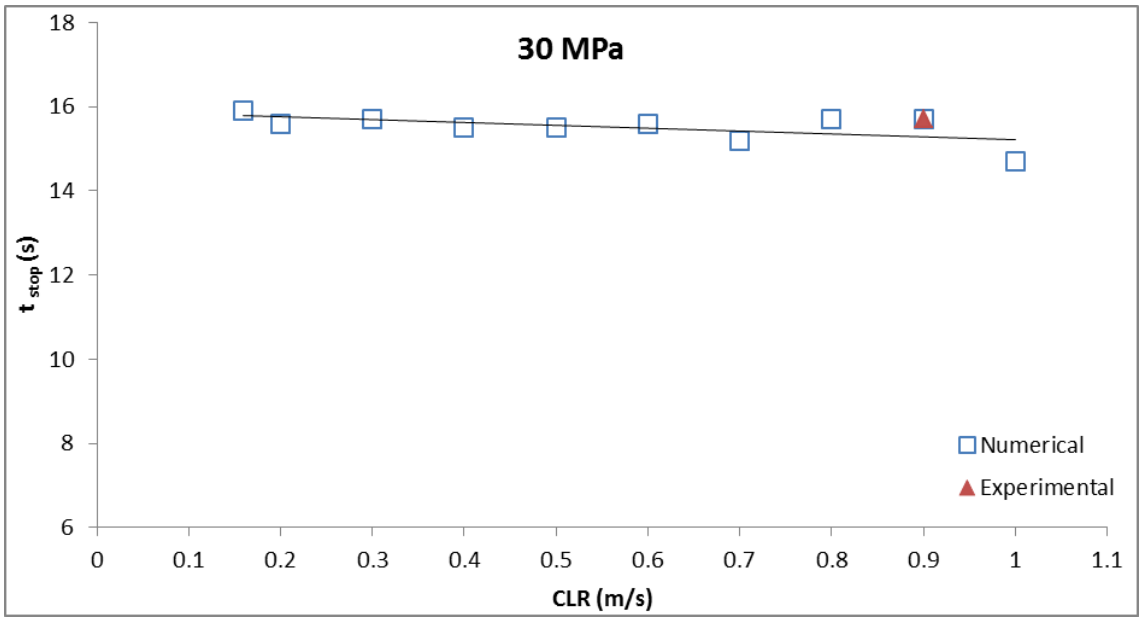


**Figure 7.5: Variation in $t_{stop}$ with cone lift rate for mix 1**

## 7.5. Conclusions

From the numerical simulations, which are consistent with laboratory observations, the following conclusions can be drawn.

- The cone lift rate has a significant effect on the measured $t_{500}$. The latter decreases as the cone lift rate is increased from 0.1 to 1 m/s. The effect on the spread (i.e. $t_{stop}$) is, however, insignificant.
- For SCC mixes having a cube compressive strength between 30 and 80MPa the reduction in $t_{500}$ with the cone lift rate is not monotonic but exhibits a bilinear response with a distinct discontinuity at approximately 0.5–0.7 m/s, depending on the mix grade. In the range of cone lift rate between 0.1 and 0.5–0.7 m/s, which covers the range recommended in BS EN 12350:2010 (BSI, 2010), $t_{500}$ reduces at a fast rate. The rate of reduction slows considerably when the cone lift rate is increased beyond 0.5–0.7 m/s.

- Judging by the trend, if the mixes were tested at the cone lift rate (<0.1 m/s) recommended in ASTM C1611M1-14 (ASTM, 2014), the $t_{500}$ of all mixes would be longer than that corresponding to the cone lift rate of 0.1 m/s in Figure 7.4.
- It is recommended that, in practice, the cone be lifted in one movement to a height of 300 mm in 0.5 s or less in order to minimise the influence of the cone lift rate on $t_{500}$.
- It is hoped that the results of the present investigation will help to bring much needed precision to the rather loose current recommendations given in the relevant American and British standards.

# Chapter 8

# Conclusions and Recommendations for Future Research

## 8.1. Conclusions

The main conclusions on the basis of the research work embodied in Chapters 4 to 7, inclusive, are summarised below:

- The development of self-compacting concrete mixes is a complex and sensitive process, requiring a balance to be struck between flow-ability and non-segregation of constituent materials. These aims can be achieved by increasing the paste volume fraction and decreasing the large aggregate volume fraction. Self-compacting normal strength concrete mixes with maximum size of aggregate 20 mm designed to satisfy the flow-ability and stability (i.e. resistance to segregation) criteria using the slump cone flow test may not meet the passing ability criterion. It is additionally necessary to check that the mixes meet the passing ability criterion using the J-ring and L-box tests (Chapter 4).
- The yield stress of an SCC mix can be predicted in an inverse manner using the SPH simulation methodology and matching the measured and simulated $t_{500}$, $t_{stop}$ and the final spread. The yield stress of SCC mixes varies only slightly with an increase in the characteristic compressive strength of the mix. The plastic viscosity on the other hand shows a marked increase (Chapter 5).
- The SPH simulation methodology provides a useful tool for predicting the yield stress of SCC mixes accurately. This is particularly relevant to the characterisation of an SCC mix because the measurement of $\tau_y$ by rheometers is inconsistent and fraught with inaccuracies (Chapter 5).
- The simulation of SCC mixes using the SPH methodology is capable of accurately predicting the distribution of large coarse aggregates in the simulated cone spread. This distribution is indeed very similar to that revealed in the cut

sections of the hardened test cone spread. These large coarse aggregates had been painted with non-toxic non-water soluble paints prior to being used in the test mix (Chapter 6). The SPH methodology is therefore most suitable for assessing the segregation resistance of SCC mixes.

- The cone lift rate has a significant effect on the measured $t_{500}$. The latter decreases as the cone lift rate increased from 0.1 to 1.0 m/s. The effect on the spread (i.e. $t_{stop}$) is, however, insignificant (Chapter 7).
- For SCC mixes having a cube compressive strength between 30 and 80MPa the reduction in $t_{500}$ with the cone lift rate is not monotonic but exhibits a bilinear response with a distinct discontinuity at approximately 0.5–0.7 m/s, depending on the mix grade. In the range of cone lift rate between 0.1 and 0.5–0.7 m/s, which covers the range recommended in BS EN 12350:2010 (BSI, 2010), $t_{500}$ reduces at a fast rate. The rate of reduction slows considerably when the cone lift rate is increased beyond 0.5–0.7 m/s (Chapter 7).
- It is recommended that, in practice, the cone be lifted in one movement to a height of 300 mm in 0.5 s or less in order to minimise the influence of the cone lift rate on $t_{500}$. It is hoped that the results of the present investigation will help to bring much needed precision to the rather loose current recommendations given in the relevant American and British standards (Chapter 7).

## 8.2. Recommendations for future research

- It would be advisable to measure the plastic viscosity of the paste with a viscometer rather than estimating it from published data.
- It would be interesting to study self-compacting concrete (SCC) mixes whose plastic viscosity is well above the upper limit of approximately 11 Pa s. This may require the mixes to have a more viscous paste achieved, for example by adding a viscosity modifying agent (VMA). Such mixes are likely to be used for casting on ground rather than for pumping to higher floors.
- It would be interesting to investigate if the large scatter in the published data on $t_{500}$ is due to effect of the cone lift rate revealed in this thesis. There is reason to believe that this is so because the data from North America where the ASTM standard is used always shows that the $t_{500}$ is much longer, up to twice, than for a similar mix tested in Europe according to the EN standard.
- There is an obvious need to accelerate the simulation process using the SPH, if it is to be used for simulating the flow of SCC into practical size formworks and in the presence of dense reinforcement.

# References

Abo Dhaheer, M.S. Al-Rubaya, M.M. Alyhya, W.S., Karihaloo, B.L., Kulasegaram, S., (2015). Proportioning of self-compacting concrete mixes based on target plastic viscosity and compressive strength: experimental validation. Journal of Sustainable Cement-Based Materials, pp. 1–16. doi: 10.1080/21650373.2015.1036952.

Abo Dhaheer, M.S. Al-Rubaya, M.M. Alyhya, W.S., Karihaloo, B.L., Kulasegaram, S., (2015). Proportioning of self–compacting concrete mixes based on target plastic viscosity and compressive strength: mix design procedure. Journal of Sustainable Cement-Based Materials , pp. 1–18. doi: full/10.1080/21650373.2015.1039625.

Aïtcin, P. C., Bentur, A., Mindess, S., (2008). Binders for durable and sustainable concrete. Modern Concrete Technology 16, Taylor & Francis, pp. 500.

Amini, Y., Emdad,H., Farid, M., (2011). A new model to solve fluid-hypo-elastic solid interaction using the smoothed particle hydrodynamics (SPH) method. European Journal of Mechanics-B/Fluids 30(2), pp. 184–194.

ASTM:C143/C143M-12 (2012). Standard Test Method for Slump of Hydraulic-Cement Concrete. ASTM International, pp. 12–15.

ASTM:C1611/C1611M-14 (2014). Standard Test Method for Slump Flow of Self-Consolidating Concrete. Annual Book of ASTM Standards, pp. 1–6.

ASTM:C1621/1621M-14 (2014). Standard Test Method for Passing Ability of Self-Consolidating Concrete by J-Ring. Annual Book of ASTM Standards , pp. 1–5.

Badry, F., Kulasegaram, S., Karihaloo, B. L., (2014). Estimation of the yield stress and distribution of large aggregates from slump flow test of self-compacting concrete mixes using smooth particle hydrodynamics simulation. Journal of Sustainable Cement-Based Materials, pp. 1-18. doi:10.1080/21650373.2014.979266

Banfill, P. B. G., (2006). Rheology of fresh cement and concrete. The British Society of Rheology, School of the Built Environment, Heriot-Watt University, Edinburgh. pp. 61-130.

Banfill, P. B. G., Beaupré, D., Chapdelaine, F., de Larrard, F., Domone, P. L., Nachbaur, L., Sedran, T., Wallevik, J. E., Wallevik, O., (2001). Comparison of concrete rheometers: International tests at LCPC, Ferraris, C. F. and Brower, L. E. (eds), NISTIR 6819, National institute of standards and technology, Nantes, France.

Bartos, P. J. M., Marrs, D. L., (1999). Development and testing of self-compacting grout for the production of SIFCON. In: PRO 6: 3rd International RILEM Workshop on High Performance Fiber Reinforced Cement Composites (HPFRCC 3), Reinhardt, H. W. and, Naaman, A. E. (eds), Germany, pp. 171-180.

Billberg, P., (1999). Self-compacting concrete for civil engineering structures: The Swedish experience, Report no 2:99. Swedish Cement and Concrete Research Institute, Stockholm.

Blask, O., Honert, D., (2003). The electrostatic potential of highly filled cement suspensions containing various superplasticizers. In: Seventh CANMET/ACI International Conference on Superplasticizers and Other Chemical Admixtures in Concrete, Germany, Berlin, pp.87-102.

Bonen, D., Shah, S.,P., (2004). The effects of formulation on the properties of self-consolidating concrete. In: International RILEM Symposium on Concrete Science and Engineering, A Tribute to Arnon Bentur, RILEM Publications SARL, North America, Evanston, IL. pp. 43–56.

Bonet, J., Kulasegaram, S., (2000). Correction and stabilization of smooth particle hydrodynamics methods with applications in metal forming simulations. International Journal for Numerical Methods in Engineering, 47(July 1998), pp. 1189–1214.

Bonet, J., Lok, T. S. L., (1999). Variational and momentum preservation aspects of Smooth Particle Hydrodynamic formulations. Computer Methods in Applied Mechanics and Engineering 180(1-2), pp. 97–115.

Bonet, J., Peraire, J. (1991). An alternating digital tree (ADT) algorithm for 3D geometric searching and intersection problems. International Journal for Numerical Methods in Engineering 31(1), pp. 1–17.

Boukendakdji, O., Kadri, E. H., Kenai, S., (2012). Effects of granulated blast furnace slag and superplasticizer type on the fresh properties and compressive strength of self-compacting concrete. Cement and Concrete Composites 34(4), pp. 583–590.

Bouzoubaa, N., Lachemi, M., (2001). Self Compacting Concrete Incorporating High-Volumes of Class F Fly Ash : Preliminary Results. Cement and Concrete Research 31(3), pp. 413–420.

Brouwers, H. J. H., Radix, H. J., (2005). Self-compacting concrete: Theoretical and experimental study. Cement and Concrete Research 35(11), pp. 2116–2136.

BS EN 12350-8, (2010). Testing fresh concrete, Part 8: Self-compacting concrete, Slump-flow test, British Standards Publication.

BS EN 12350-10, (2010). Testing fresh concrete, Part 10: Self-compacting concrete, L-box test, British Standards Publication.

BS EN12350-12, (2010). Testing fresh concrete, Part 12: Self-compacting concrete, J-ring test, British Standards Publication.

BS EN 206-9, (2010). Concrete, Part 9: Additional rules for self- compacting concrete (SCC). British Standards publication.

Bui, H.H., Fukagawa, R., Sako, K., Ohno, S., (2008). Lagrangian meshfree particles method (SPH) for large deformation and failure flows of geomaterial using elastic--plastic soil constitutive model. International Journal for Numerical and Analytical Methods in Geomechanics 32(12), pp. 1537–1570.

Burke, D.R., Tabrizi, S. M., Smy, T. J., (2010). Simulation of inhomogeneous models using the finite cloud method. Simulation inhomogener Modelle unter Benutzung der Finite-Wolken-Methode. Materialwissenschaft und Werkstofftechnik 41(5), pp. 336–340.

Carlsward, J., Emborg, M., Utsi, S., Oberg, P., (2003). Effect of constituents on the workability and rheology of self-compacting concrete, The 3rd International RILEM Symposium on Self-Compacting Concrete, Iceland, pp. 143–153.

Castro, A. L. D., Liborio, J. B. L. (2006). Initial rheological description of high performance concretes. Materials Research 9(4), pp. 405–410.

Cattaneo, S., Mola, F., (2012). Assessing the quality control of self-consolidating concrete properties. Journal of Construction Engineering and Management 138(2), pp. 197–205.

Chan, K. D., Ong, K. C. G, Tan, C. T., (2010). Passing ability of SCC- Improved method based on the J-ring. In 35th Conference on our world in concrete and structures (OWICs), Singapore, Singapore Concrete Institute. Available at:
http://cipremier.com/100035002

Chaniotis, A. K., Poulikakos, D., Koumoutasakos, P., (2002). Remeshed smoothed particle hydrodynamics for the simulation of viscous and heat conducting flows. Journal of Computational Physics 182(1), pp. 67–90.

Chorin, A. J., (1968). Numerical solutions of the Navier-Stokes equations. Mathematics of computation 22(104), pp. 745–762.

Cleary, P., Ha, J., Alguine, V., Nguyen, T., (2002). Flow modelling in casting processes. Applied Mathematical Modelling, 26(2), pp. 171–190.

Colagrossi, A., Landrini, M., (2003). Numerical simulation of interfacial flows by smoothed particle hydrodynamics. Journal of Computational Physics 191(2), pp. 448-475.

Collepardi, M. (2005). Chemical Admixtures Today. Proceedings of Second International Symposium on Concrete Technology for Sustainable Development with Emphasis on Infrastructure, Hyderabad, India, pp. 527-541.

Cummins, S. J., Rudman, M., (1999). An SPH Projection Method. Journal of Computational Physics, 152(2), pp. 584–607.

Dalrymple, R., Knio, O. (2001). SPH Modelling of Water Waves, Coastal Dynamics,1, pp. 779-787.

Deeb, R., Ghanbari, A., Karihaloo, B. L., (2012). Development of self-compacting high and ultra-high performance concretes with and without steel fibres. Cement and Concrete Composites, 34(2), pp. 185–190.

Deeb, R., Karihaloo, B.L., (2013). Mix proportioning of self-compacting normal and high-strength concretes. Magazine of Concrete Research 65(9), pp. 546–556.

Deeb, R., Karihaloo, B. L., Kulasegaram, S., (2014). Reorientation of short steel fibres during the flow of self-compacting concrete mix and determination of the fibre orientation factor, Cement and Concrete Research, 56, pp. 112–120.

Deeb, R., Kulasegaram, S., Karihaloo, B. L., (2014a). 3D modelling of the flow of self-compacting concrete with or without steel fibres. Part I: slump flow test. Computational Particle Mechanics 1(4), pp. 373–389.

Deeb, R., Kulasegaram, S., Karihaloo, B. L., (2014b). 3D modelling of the flow of self-compacting concrete with or without steel fibres. Part II: L-box test and the assessment of fibre reorientation during the flow, Computational Particle Mechanics, 1 (4), pp. 391-408.

Dilts, G. A., (1999). Moving-least-squares-particle hydrodynamics-I: consistency and stability. International Journal for Numerical Methods in Engineering 44(8), pp. 1115-1155.

Dilts, G. A., (2000). Moving least-squares particle hydrodynamics II: conservation and boundaries. International Journal for Numerical Methods in Engineering 48(10), pp. 1503–1524.

Dinakar, P., Sethy, K. P., Sahoo, U. C., (2013). Design of self-compacting concrete with ground granulated blast furnace slag. Materials and Design 43, pp. 161–169.

Domone, P., (1998). The slump flow test for high-workability concrete. 28(2), pp. 177–182.

Domone, P., Illston, J., (2010). Construction materials: Their nature and behaviour - 4th edition. Taylor and Francis Publication, ISBN. 041546515X, pp.590.

Domone, P. L., (2003). Fresh Concrete. In: Advanced Concrete Technology: Concrete properties. Newman, J. and Choo, B., (eds). Oxford: Elsevier Ltd, pp. 20-30.

Domone, P.L., (2006). Self-compacting concrete: An analysis of 11 years of case studies. Cement and Concrete Composites 28(2), pp. 197–208.

Domone, P. L. J., Yongmo, X., Banfill, P. F. G., (1999). Developments of the two-point workability test for high-performance concrete. Magazine of Concrete Research 51(3), pp. 171–179.

Domone, P.L., Thurairatnam, H., (1988). The effect of water/cement ratio, plasticizers and temperature on the rheology of cement grouts. Advances in Cement Research 1(4), pp. 195-206.

Douglas, R. P., (2004). Properties of Self-Consolidating Concrete Containing Type F Fly Ash, M.Sc. Thesis, Northwestern University.Evanston, Illinois, SN. 2619.

Dransfield, J., (2003). Admixtures for concrete, mortar and grout. In: Newman, J. and Choo, B. S. (eds.). Advanced Concrete Technology: Constituent Materials. Oxford: Elsevier, pp. 162-195.

Dufour, F., Pijaudier-Cabot, G., (2005). Numerical modelling of concrete flow: homogeneous approach. International Journal for Numerical and Analytical Methods in Geomechanics, 29(4), pp. 395–416.

Duval, R., Kadri, E., (1998). Influence of Silica Fume on the Workability and the Compressive Strength of High-Performance Concretes. Cement and Concrete Research 28(4), pp. 533–547.

EFNRC, (2005). The European Guidelines for Self-Compacting, Specification, Production and Use. [Online] Available at: www.efnarc.org [Accessed 07/12/2012]

Emborg, M. , Gurnewald, S. , Hedin, C., Carlsward , J., (2003). Test methods for filling ability of SCC. In: 3rd International Symposium on Self-Compacting Concrete. pp. 323–334, (editor) (O. Wallevik and I. Nlssoien), RILEM Publications SARL, France.

Ferraris, C.F., (1999). Measurement of the rheological properties of high performance concrete: State of the art report, Journal of Research of the National Institute of Standards and Technology 104(5), pp. 461- 477.

Feys, D., Verhoeven, R., De Schutter, G., (2007). Evaluation of time independent rheological models applicable to fresh self-compacting concrete. Applied Rheology 17(5), pp. 1–10.

Frédéric, D. and Gilles, P.-C. (2005). Numerical modelling of concrete flow: homogeneous approach. International Journal for Numerical and Analytical Methods in Geomechanics 29(4), pp. 395–416.

Gaimster, R., Dixon, N., (2003). Self-compacting concrete, in Advanced concrete technology, Newman, J., Choo, B. S. (eds), Oxford, Elsevier, 3, pp. 202-223.

Gao, J., Fourie, A., (2015). Spread is better: An investigation of the mini-slump test. Minerals Engineering, 71, pp. 120–132.

Gesoğlu, M., Güneyisi, E., Özbay, E., (2009). Properties of self-compacting concretes made with binary, ternary, and quaternary cementitious blends of fly ash, blast furnace slag, and silica fume. Construction and Building Materials 23(5), pp. 1847–1854.

Ghanbari, A., (2011). Self-compacting high and ultra-high performance concretes, PhD Thesis, Cardiff University, UK.

Ghanbari, A., Karihaloo, B.L., (2009). Prediction of the plastic viscosity of self-compacting steel fibre reinforced concrete. Cement and Concrete Research 39(12), pp. 1209–1216.

Gingold, R.A., Monaghan, J. J., (1977). Smoothed particle hydrodynamics: theory and application to non-spherical stars. Monthly Notices of the Royal Astronomical Society 181(3), pp. 375–389.

Gram, A., (2009). Numerical Modelling of Self-Compacting concrete flow-Discrete and Continuous Approach, PhD Thesis, Royal Institute of Technology, Sweden.

Grünewald, S., (2004). Performance-based design of self-compacting fibre reinforced concrete, Ph.D. Thesis, Delft university, Netherlands.

Heirman, G., Vandewalle, L., Van Gemert, D. , Wallevik, Ó. ,(2008). Integration approach of the Couette inverse problem of powder type self-compacting concrete in a wide-gap concentric cylinder rheometer. Journal of non-Newtonian Fluid Mechanics 150(2), pp. 93–103.

Jadiri, G., F., K., Rand, S. Al 2010. New Method for Proportioning Self-Consolidating Concrete Based on Compressive Strength Requirements. ACI Materials Journal 107(5).

Ji, J., Zhao, Q., Yan, G., Li, H. (2008). BP network based mix proportion design of self-compacting concrete. Second International Conference on Innovative Computing, Information and Control, ICICIC 2007, IEEE CONFERENCE PUBLICATIONS doi10.1109/ICICIC.2007.201

Karihaloo, B. L., Ghanbari, A., (2012). Mix proportioning of self- compacting high- and ultra- high-performance concretes with and without steel fibres. Magazine of Concrete Research 64(12), pp. 1089–1100.

Kelecy, F.J., Pletcher, R. H., (1997). The development of a free surface capturing approach for multidimensional free surface flows in closed containers. Journal of Computational Physics 138(2), pp. 939–980.

Kennedy, C.T. 1940. The Design of Concrete Mixes, American Concrete Institute 36, pp. 373–400.

Khayat, K. H., (1995). Effects of Antiwashout Admixtures on Fresh Concrete Properties. ACI Materials Journal, 92(2), pp. 164-171.

Khayat, K. H., (1998). Use of viscosity-modifying admixture to reduce top-bar effect of anchored bars cast with fluid concrete. ACI Materials Journal 95(2), pp. 158–167.

Khayat, K. H., (2000). Workability , Testing , and Performance of Self-Consolidating Concrete. ACI Materials Journal, 96, pp. 346–354.

Khayat, K. H., Ghezal, A., Hadriche, M. S., (1999). Factorial design model for proportioning self-consolidating concrete. Materials and Structures 32(9), pp. 679–686.

Kitaoji, H., Tanigawa, Y., Mori, H. , Kurokawa, Y. , Urano, S. , 1997. Flow simulation of fresh concrete cast into wall structure by viscoplastic divided space element method. Transactions of the Japan Concrete Institute 18, pp. 45–52.

Koehler, E. P., Fowler, D. W., (2007a). Aggregates in Self-Consolidating Concrete. ProQuest, PhD Thesis, University of Texas at Austin, pp. 1–18.

Koehler, E. P., Fowler, D. W., (2007b). Proportioning SCC Based on Aggregate Characteristics. 5th International RILEM Symposium on Self-Compacting Concrete 3-5 September 2007, Ghent, Belgium,pp. 67–72.

Koehler, E. P., Fowler, D. W., Foley, E. H., Rogers, G. J., Watanachet, S., Jung, M. J., (2007). Self-Consolidating Concrete for Precast Structural Applications: Mixture Proportions, Workability, and Early-Age Hardened Properties, Aggregates Foundation for Technology: Research and Education, University of Texas, Austin, CTR Technical Report: 0-5134-1, pp.348.

Kong, H. J., Bike, S. G., Li, V., C., (2003). Development of a self-consolidating engineered cementitious composite employing electrosteric dispersion/stabilization. Cement and Concrete Composites 25(3), pp. 301–309.

Koshizuka, S., Nobe, A., Oka, Y., (1998). Numerical analysis of breaking waves using moving particle semi- implicit method. International Journal for Numerical Methods in Fluids, 26(7), pp. 751-769.

Koshizuka, S., Oka, Y., Tamako, H., (1995). A particle method for calculating splashing of incompressible viscous fluid. Proc. Int: International Conference on Mathematics and Computations, Reactor Physics and Environmental Analysis, 2, American Nuclear Society, Inc., La Grange Park, IL (United States), pp. 1514-1521.

Krieger, I. M., Dougherty, T. G., (1959). A mechanism for non-Newtonian flow in suspensions of rigid spheres. Journal of Rheology, 3(1), pp. 137-152.

Kulasegaram, S., Karihaloo, B. L., (2013). Fibre-reinforced, self-compacting concrete flow modelled by smooth particle hydrodynamics. Proceedings of the ICE-Engineering and Computational Mechanics 166(1), pp. 22–31.

Kulasegaram, S., Karihaloo, B. L., Ghanbari, A., (2011). Modelling the flow of self-compacting concrete. International Journal for Numerical and Analytical Methods in Geomechanics, 35(6), pp. 713-723.

Kurokawa, Y., Tanigawa, Y., Mori, H., Nishinosono, Y., (1997). Analytical study on effect of volume fraction of coarse aggregate on Bingham's constants of fresh concrete. Transactions of the Japan Concrete Institute, 18, pp. 37-44.

Kwan, A. K. H., Ng, I. Y. T., (2010). Improving Performance and Robustness of SCC by Adding Supplementary Cementitious Materials. Construction and Building Materials, 24(11), pp. 2260–2266.

Lee, E. S. E. S., Moulinec, C., Xu, R., Violeau , D., Laurence , D., Stansby, P. , (2008). Comparisons of weakly compressible and truly incompressible algorithms for the SPH mesh free particle method. Journal of Computational Physics 227(18), pp. 8417–8436.

Lewis, R., Sear, L., Wainwright, P., Ryle, R., (2003). Advanced Concrete Technology-Constituent Materials, Cementitious additions. Newman, J. and Choo, B.S. (Eds). Oxford: Elsevier Ltd, pp. 96-159.

Li, S. F., Liu, W. K., (1996). Moving least square kernel Galerkin method (II) fourier analysis. Computer Methods in Applied Mechanics and Engineering, 139(4), pp. 159-193.

Li, S. F., Liu, W. K., (2002). Meshfree and particle methods and their applications, American Society of Mechanical Engineers, 55(1), pp. 1-34.

Li, C. Z., Feng, N., Li, Y. D., Chen, R. J., (2005). Effects of polyethylene oxide side chains on the performance of polycarboxylate-type water reducers. Cement and Concrete Research, 35(5), pp. 867-873.

Liu, G. R., Liu, M. B., (2003). Smooth particle hydrodynamics. Singapore: World Scientific Publishing CO. Pte. Ltd. ISBN 981-238-456-1.

Liu , M. B., Liu, G. R., (2010). Smoothed Particle Hydrodynamics (SPH): an Overview and Recent Developments. Archives of Computational Methods in Engineering, 17, pp. 25-76.

Long, Wu-J., Khayat, K., Lemieux, G., Hwang, S., Han, Nng, X., (2014). Performance-Based Specifications of Workability Characteristics of Prestressed, Precast Self-Consolidating Concrete—A North American Prospective. Materials 7(4), pp. 2474–2489.

Looney, T. J., Arezoumandi, M., Volz, J. S., Myers, J. J., (2012). An Experimental Study on Bond Strength of Reinforcing Steel in Self-Consolidating Concrete. International Journal of Concrete Structures and Materials 6(3), pp. 187–197.

Lucy, L. B., (1977). A numerical approach to the testing of the fission hypothesis. Astronomical Journal, 82(12), pp. 1013–1024.

Martys, N. S., (2005). Study of a dissipative particle dynamics based approach for modeling suspensions. Journal of Rheology 49(2), pp. 401-424.

Mehta, P.K., (1986). Concrete. Structure, properties and materials (Book), Availability: Prentice-Hall, Incorporated Route 9W Englewood Cliffs, NJ 07632 USA ,pp. 450.

Monaghan, J.J., (1994). Simulating Free Surface Flows with SPH. Journal of Computational Physics, 110(2), pp. 399–406.

Monaghan, J.J., (1996). Gravity currents and solitary waves. Physica D: Nonlinear Phenomena 98(2-4), pp. 523–533.

Monaghan, J. J., Gingold, R. A, (1983). Shock simulation by the particle method SPH. Journal of Computational Physics, 52(2), pp. 374-389.

Monaghan, J. J., Kocharyan, A., (1995). SPH simulation of multi-phase flow. Computer Physics Communications, 87(1/2), pp. 225-235.

Monaghan, J. J., Lattanzio, J. C., (1985). A refined particle method for astrophysical problems. Astronomy and Astrophysics, 149(1), pp. 135-143.

Mori, H., Tanigawa, Y., (1992). Simulation methods for fluidity of fresh concrete. Nagoya University, Memoirs of the school of engineering, pp. 71-133.

Morris, J. P., Fox, P. J., Zhu, Y., (1997). Modelling low Reynolds number incompressible flows using SPH. Journal of Computational Physics, 136(1), pp. 214-226.

Naik, T. R., Chun, Y. M., Kumar, R., Bruce, W. R., (2004). Development of high-strength self-consolidation concrete, Center of by- products utilization, Report No. CBU-2003-14, Department of Civil Engineering and Mechanics College of Engineering and Applied Science THE UNIVERSITY OF WISCONSIN – MILWAUKEE ,pp. 1-27.

Nehdi, M., Rahman, M., (2004). Estimating rheological properties of cement pastes using various rheological models for different test geometry, gap and surface friction. Cement and Concrete Research, 34(11), pp. 1993-2007.

Nguyen, T. L. H., Roussel, N., Coussot, P., (2006). Correlation between L-box test and rheological parameters of a homogeneous yield stress fluid. Cement and Concrete Research 36(10), pp. 1789–1796.

Obla, K. H. H. R. H., Thomas, M., Shashiprakash, S. G., Perebatova, O., (2003). Properties of Concrete Containing Ultra-Fine Fly Ash. ACI Materials Journal, 100(5), pp. 426-433.

Oh, S. G., Noguchi, T., Tomosawa, F., (1997). Evaluation of pass ability of self-compacting concrete by visualization mode.In proceeding of Japan concrete institute, 19(1), pp. 37-42.

Okamura, H., Ouchi, M., (1999). Self-compacting concrete. Development, present use and future. In 1st International RILEM Symposium on Self-Compacting Concrete, Skarendahl, Å. and Petersson, Ö. , (eds). Stockholm, Sweden, RILEM Publications SARL, France pp. 3-14.

Okamura, H., Ouchi, M., (2003), Self-compacting concrete, Journal of Advanced Concrete Technology, 1(1), pp. 5-15.

Okamura, H., Ouchi, M., Hibino, M., Ozawa, K., (1998). A rational mix-design method for mortar in self-compacting concrete. In the 6th East Asia-Pacific Conference on Structural Engineering and Construction, Taipei, ROC, 2, RILEM Publications SARL, France pp. 1307-1312.

Okamura, H., Ozawa, K., (1995). Mix design for self-compacting concrete. Concrete Library of JSCE, 25, pp. 107-120.

Oner, A., Akyuz, S., (2007). An Experimental Study on optimum usage of GGBS for the compressive strength of concrete. Cement and Concrete Composites, 29(6), pp. 505-514.

Ouchi, M., Nakamura, S., Osterson, T., Hallberg, S., Lwin, M., (2003). Applications of self-compacting concrete in Japan, Europe and the United States. In: International Symposium on High Performance Computing (ISHPC). pp. 1–20. avalable at:
https://www.fhwa.dot.gov/bridge/scc.pdf

Papadakis, V. G., (1999). Experimental investigation and theoretical modeling of silica fume activity in concrete. Cement and Concrete Research 29(1), pp. 79–86.

Papanastasiou, T. C., (1987). Flows of Materials with Yield. Journal of Rheology 31(5),pp. 385-404.

Park, C. K., Noh, M. H., Park, T. H., (2005). Rheological Properties of Cementitious Materials Containing Mineral Admixtures. Cement and Concrete Research, 35(5), pp. 842-849.

Patzák, B., Bittnar, Z., (2009). Modeling of fresh concrete flow. Computers and Structures, 87(15), pp. 962-969.

PCI (Precast/Prestressed Concrete Institute**)**, (2003). Interim Guidelines for the Use of Self-Consolidating Concrete in Precast/Prestressed Concrete Institute. [Online] Available at: www.pci.org [Accessed 05 12 2012].

Rahman, M. K., Baluch, M. H., Malik, M. A., (2014). Thixotropic behavior of self compacting concrete with different mineral admixtures. Construction and Building Materials 50, pp. 710–717.

Ramachandran, V. S., Beaudoin, J. J., (2001). Techniques in concrete science and technology. Principles, techniques and applications, William Andrew & Noyes Publications, USA. ISBN-13: 978-0815514374.

Ramachandran, V. S., Feldman, R. F., Beaudoin, J. J., (1981). Concrete Science, Heyden and Son Ltd, ISBN: 0855017031.

Rao, G. A., (2003). Investigations on the performance of silica fume-incorporated cement pastes and mortars. Cement and Concrete Research 33(11), pp. 1765–1770.

Richard, P., Cheyrezy, M., (1995). Composition of reactive powder concretes. Cement and Concrete Research 25(7), pp. 1501–1511.

Roussel, N., (2006). Correlation between yield stress and slump: Comparison between numerical simulations and concrete rheometers results. Materials and Structures, 39(4), pp. 501-509.

Roussel, N., (2007). A Theoretical Frame to Study Stability of Fresh Concrete. Materials and Structures, 39(1), pp. 81–91.

Roussel, N., Coussot, P., (2005). Fifty-cent rheometers for yield stress measurements: from slump to spreading flow. Journal of Rheology, 49(3), pp. 705–718.

Roussel, N., Geiker, M. R., Dufour, F., Thrane, L. N., Szabo, P., (2007). Computational modeling of concrete flow: General overview. Cement and Concrete Research 37(9), pp. 1298–1307.

Roussel, N., Nguyen, T., Yazoghli, O., Coussot, P., (2009). Passing ability of fresh concrete: A probabilistic approach. Cement and Concrete Research, 39(3), pp. 227-232.

Roziere, E., Granger, S., Turcry, P., Loukili, A., (2007). Influence of Paste Volume on Shrinkage Cracking and Fracture Properties of Self Compacting Concrete. Cement and Concrete Composites, 29(8), pp. 626-636.

Şahmaran, M., Christianto, H. A., Yaman, I. O., (2006). The effect of chemical admixtures and mineral additives on the properties of self-compacting mortars. Cement and Concrete Composites 28(5), pp. 432–440.

Shah, U. N., Modhera, C. D., (2014). Study on fresh properties of self-compactingconcrete with processed fly ash, International Journal of Research in Engineering & Technology 2(5), pp. 271–274.

Shao, S., Lo, E. Y. M., (2003). Incompressible SPH method for simulating Newtonian and non-Newtonian flows with a free surface, Advances in Water Resources 26(7), pp. 787–800.

Siddique, R., Khan, M. I., (2011). Supplementary Cementing Materials: Silica Fume. Engineering Materials, Ch:2. Springer-Verlag Berlin Heidelberg, , pp. 67-119. ISBN: 978-3-642-17865-8.

Solenthaler, B., Pajarola,R., (2009). Predictive-Corrective Incompressible SPH, ACM Transactions on Graphics, 28(3), pp. 1-6.

Sonebi, M., (2004). Medium Strength Self-Compacting Concrete Containing Fly Ash: Modeling Using Statistical Factorial Plans. Cement and Concrete Research, 34(7), pp. 1199-1208.

Struble, L., Sun, G. K., (1995). Viscosity of Portland cement paste as a function of concentration. Advanced Cement Based Materials, 2(2), pp. 62-69.

Su, N., Miao, B., (2003). A new method for the mix design of medium strength flowing concrete with low cement content. Cement and Concrete Composites, 25(2), pp. 215-222.

Surabhi, C. S., Soman, M., Prakash, V. S., (2009). Influence of Limestone Powder on Properties of Self-Compacting Concrete. 10th National Conference on Technological Trends (NCTT09), (Kerala, India), pp. 159-164.

Svec, O., Skocek, J., Stang, H., Geiker, M. R., Roussel, N., (2012). Free surface flow of a suspension of rigid particles in a non-Newtonian fluid: A lattice Boltzmann approach. Journal of Non-Newtonian Fluid Mechanics, 179/180, pp. 32-42.

Takeda, H., Miyama, S. M., Sekiya, M., (1994). Numerical Simulation of Viscous Flow by Smoothed Particle Hydrodynamics. Progress of Theoretical Physics, 92(5), pp. 939-960.

Tattersall, G. H., (2003). Workability and quality control of concrete. CRC Press, ISBN 0-203-47314-0.

Taylor, M., (1997). Characterisation of normal and high-strength plain and fibre-reinforced concretes by means of strength fracture and combined fracture/relaxation tests, PhD Thesis, Cardiff University.UK.

Thrane, L., Pade, C., Svensson, T., (2007). Estimation of Bingham rheological parameters of SCC from slump flow measurement. 5th International RILEM Symposium on self compacting concrete (3-5 September), Ghent, Belgium, G. De Schutter and V. Boel, RILEM Publications SARL, France, pp. 353–358.

Thrane, L., Szabo, P., Geiker, M., Glavind, M. and Stang, H., (2004), Simulation of the test method “L-box” for self-compacting concrete, Annual Transactions of the Nordic Rheology Society, 12, pp. 47-54.

Tregger, N., Ferrara, L. and Shah, S. P., (2007), Empirical relationships between viscosity and flow time measurements from mini-slump tests for cement pastes formulated from SCC, Proceedings of the 5th International RILEM Symposium-SCC 2007, pp. 273-278. Ghent, Belgium.

Tviksta, L. G., (2000). Guidlines- Task 9-End product, Brite EuRam Proposal No. BE96-3801.

Utsi, S., Emborg, M and Carlsward, J., (2003), Relation between workability and rheological parameters, In: Proceedings of the 3rd International RILEM Symposium, Pro 33, Wallevik, O., Nielsson, I. (eds). RILEM: Cachan, pp. 154-164.

Uysal, M., Yilmaz, K., (2011). Effect of mineral admixtures on properties of self-compacting concrete, Cement and Concrete Composites 33(7), pp. 771–776.

Vasilic, K., Meng, B., Kühne, H. C., Roussel, N., (2011). Flow of fresh concrete through steel bars: A porous medium analogy. Cement and Concrete Research 41(5), pp. 496–503.

Vesenjak, M., Ren, Z., (2007). Application Aspects of the Meshless SPH Method. Journal of the Serbian Society for Computational Mechanics, 1(1), pp. 74-86.

Welton, W., (1998). Two-dimensional PDF/SPH simulation of compressible turbulent flows. Journal of Computational Physics, 139(2), pp. 410-443.

Wilson, H.K., Stowe, R.L. (1971). Effect of Rate of Lifting of Slump Cone on Indicated Slump of Concrete, Miscellaneous paper C-71-7, US Army Engineer Waterways Experiment Station, Vicksburge, Mississippi, pp.6

Wróblewski, P., Kopeć, M., Boryczko, K., (2007). SPH – a comparison of neighbor search methods based on constant number of neighbors and constant cut-off radius. Task Quarterly, 11(3), pp. 273-283.

Xiong, S., Liu, W. K., Cao, J., Li, C. S., Rodrigues, J. M. C., Martins, P. A. F., (2005). Simulation of bulk metal forming processes using the reproducing kernel particle method. Computers & Structures, 83(8/9), pp. 574–587.

Yahia, A., Tanimura, M., Shimoyama, Y., (2005). Rheological properties of highly flowable mortar containing limestone filler-effect of powder content and w/c ratio. Cement and Concrete Research, 35(3), pp. 532-539.

Youjun, X. I. E., Yunhua, L., I., U.,Guangcheng, L., (2007). a Mix Design Method for Self-Compacting Concrete. Symposium, International Rilem Concrete, Self-compacting (September), pp. 189–195.

Zhu, Y. et al. 1999. A Pore-Scale Numerical Model for Flow through Porous Media. Int. J. Numer. Anal. Methods Geomech. 23(July 1998), pp. 881–904.